

Contents lists available at ScienceDirect

Journal of Solid State Chemistry

journal homepage: www.elsevier.com/locate/jssc



The development of strategies for nanoparticle synthesis: Considerations for deepening understanding of inherently complex systems[★]



Jennifer M. Lee¹, Rebecca C. Miller¹, Lily J. Moloney, Amy L. Prieto*

Department of Chemistry, Colorado State University, Fort Collins, CO 80523, United States

ABSTRACT

The last fifty years of solid-state chemistry have produced a wealth of compounds with complex structures, exciting properties, and from those discoveries, an explosion of new technologies. We continue to strive to understand structure-property relationships as well as develop expedient methods to discover and control new materials. Nanoparticle synthesis is one area of synthetic solid-state chemistry that is currently experiencing a significant growth of deepening understanding and increasing sophistication. Herein, we review examples from the literature where insight about a synthesis can be built from to catalyze new discoveries. The focus is on synthetic reports of nanoparticles of increasing complexity.

Contents

1.	Introd	duction		244		
2.	Connecting parameters of nanoparticle syntheses to reaction mechanism and pathway					
	2.1. Investigating the formation of anionic, chalcogenide species					
		2.1.1.	Tertiary phosphine chalcogenides: mechanism of chalcogen delivery and reactivity trends.	246		
		2.1.2.	Diorganyl dichalcogenides: reactivity trends and extrapolation from binary to ternary systems	247		
		2.1.3.	Alkylamine-chalcogenides: chalcogen dissolution and reduction			
		2.1.4.	Multiple roles of 1-dodecanethiol (DDT): sulfur precursor, stabilizing ligand, and solvent			
		2.1.5.	Thiourea and selenourea: chemical decomposition.	249		
		2.1.6.	In situ evolution of gaseous chalcogenide species from elemental chalcogen interaction with 1-octadecene (ODE)			
		2.1.7.	Perspective			
	2.2.	Underst	tanding cationic speciation of NP precursors: a case study on metal amides.			
		2.2.1.	The hard-soft acid-base principle	253		
		2.2.2.	Evolution of proposed reaction mechanisms for metal amides in NP synthesis	253		
		2.2.3.	Noteworthy amide-assisted NP synthetic studies	256		
		2.2.4.	Metal amide NP syntheses of interest for further mechanistic studies	260		
		2.2.5.	Outlook on cationic precursors and use of metal amides in NP syntheses			
	2.3.	Underst	anding reaction pathways			
		2.3.1.	Reaction pathway studies in bulk solid-state synthesis.	262		
		2.3.2.	Reaction pathway studies in NP synthesis	263		
		2.3.3.	Outlook for solution-based NP reaction pathways	268		
		2.3.4.	Conclusion for understanding reaction pathways.	269		
3.	Characterization of NP syntheses					
	3.1. Characterization for elucidating reaction mechanisms					

^{*} Nanoparticle synthesis, reaction mechanisms, reaction pathways.

^{*} Corresponding author.

E-mail address: Amy.prieto@colostate.edu (A.L. Prieto).

¹ Equal contribution first authors.

	3.1.2.	Infrared (IR) spectroscopy for solution composition and NP ligand identification	271
	3.1.3.	Mass spectrometry to support the presence of reaction species interactions	272
	3.1.4.	UV–Vis spectroscopy	273
3.2.	Characte	erization for elucidating reaction pathway	273
	3.2.1.	X-ray diffraction (XRD)	273
	3.2.2.	Raman spectroscopy	275
	3.2.3.	Thermal analysis.	278
	3.2.4.	X-ray photoelectron spectroscopy and X-ray absorption spectroscopy	279
	3.2.5.	Ex situ transmission electron microscopy (TEM)	280
3.3.	Prospect	ts in NP reaction characterization: understanding the complexity of NP syntheses	281
	3.3.1.	Using mass conservation to rationalize NC growth via in situ FTIR and UV-Vis spectroscopy	281
	3.3.2.	In situ synchrotron X-ray scattering studies	282
	3.3.3.	Outlook of in situ X-ray diffraction for NP synthesis	282
3.4.	Characte	erization summary and perspective	284
Acknowle	edgements .		285

Glossary

BDE: Bond dissociation energy

DDT: 1-Dodecanethiol

E: Chalcogen

EBSD: Electron backscatter diffraction

EDS: Energy-dispersive X-ray spectroscopy

EI: Electron ionization

EM, TEM, HRTEM, STEM, SEM: Electron microscopy, Transmission EM,

High-resolution TEM, Scanning TEM, Scanning EM EXAFS: Extended X-ray absorption fine structure

FTIR: Fourier transform infrared spectroscopy

FWHM: Full width half maximum

HDA: Hexadecylamine

HSAB: Hard-soft acid-base

HSQC: Heteronuclear single quantum coherence spectroscopy

ICP-MS: Inductively coupled plasma mass spectrometry

IR and NIR: Infrared and near infrared

LA: Lauric acid

m/z: Mass-to-charge ratio

MALDI: Matrix assisted laser desorption ionization

MS: Mass spectrometry MSC: Magic-sized cluster

NC: Nanocrystal NP: Nanoparticle

NMR: Nuclear magnetic resonance

NP: Nanoparticle

OA: Oleic acid

ODE: 1-Octadecene

OLA: Oleylamine

PL: Photoluminescence

PLE: Photoluminescence excitation

QD: Quantum dot

RT: Room temperature

SAED: Selected area electron diffraction

SAXS, WAXS: Small-angle X-ray scattering, wide-angle X-ray scattering

SLS: Solution-liquid-solid

THF: Tetrahydrofuran

TOF: Time of flight

TOP: Trioctylphosphine

TOPO: Trioctylphosphine oxide

UV-Vis: Ultraviolet-visible

WANDA: Workstation for Automated Nanomaterials Discovery and Analysis

XAS: X-ray absorption spectroscopy

XPS: X-ray photoelectron spectroscopy

XRD, PXRD: X-ray diffraction, Powder XRD

1. Introduction

The last fifty years of solid-state chemistry have produced a wealth of new compounds with complex structures, exciting properties, and from those discoveries, an explosion of new technologies. Although the field is still struggling to develop strategies to 'predict' new compounds with desired physical properties as well as the precise synthetic conditions required to synthesize those compounds, dramatic strides have been achieved in all areas that are of interest to solid state

chemists: theory, synthesis (over a range of temperatures, pressures, and states of matter in terms of reactants used) and characterization methods. We continue to strive to understand structure-property relationships as well as to develop expedient methods to discover and control new materials.

One sub-area of solid-state chemistry that we, the authors, are particularly excited about is the development of new synthetic methods for nanoparticles (NPs) of extended solids of increasing compositional complexity. Some of the techniques used in this field draw from where the solid-state community was nearly thirty years ago, in terms of efforts to lower reaction temperatures and expand the synthetic toolkit to enable access to both thermodynamic and kinetic phases [1]; the aim is still to predict, design, and understand reactions that ultimately achieve control over a wider phase space. The area of NP synthesis provides an exciting opportunity for elucidating understanding because its synthesis draws from the disciplines of solid state, organometallic, coordination, and organic chemistry. Here we discuss NPs that are solid-state compounds but with the added variable of size dependent properties and large surface area to volume ratios. The NP field has been motivated, ultimately, by an interest in novel physical properties, which is consistent with the history of solid-state chemistry. Exploratory synthesis and intellectually curious speculation will always be required to initiate discovery, but given the wealth of knowledge being collected now, themes, patterns, and the use of characterization tools from different fields can be combined. Our aim in this review is to highlight examples wherein new understanding or insight about a synthesis can be achieved and utilized to catalyze new discoveries. It is not possible to be exhaustive. Here we highlight examples of synthetic work focused on NPs with a range of stoichiometry (from elemental to multinary) with an eye toward future development and control over the synthesis of increasingly complex NPs. By complexity we mean either accessing multiple polymorphs in a single system or increasing complexity in composition or morphology. There are thorough reviews covering the conversion or assembly of NPs [2,3], the synthesis of core shell particles [4], and cation exchange [5], examples that we do not explicitly cover here.

Over the last thirty years, much has been discovered about how the components of a reaction can lead to the composition, size, and morphology of NPs. Building off of the knowledge gained by careful work on CdE (E = chalcogenide) systems [6,7], the field is striving to move past reports of cause and effect. Upon tuning the reaction variables, understanding is extrapolated from characterization of the final products. Identifying the pathways of a reaction may inform rational planning. It is currently very difficult to predict the results of a known targeted reaction if the reactants are new. Classic examples from the CdE literature over the years show how the evolution of precursors can lead to greater control over the rate of nucleation and

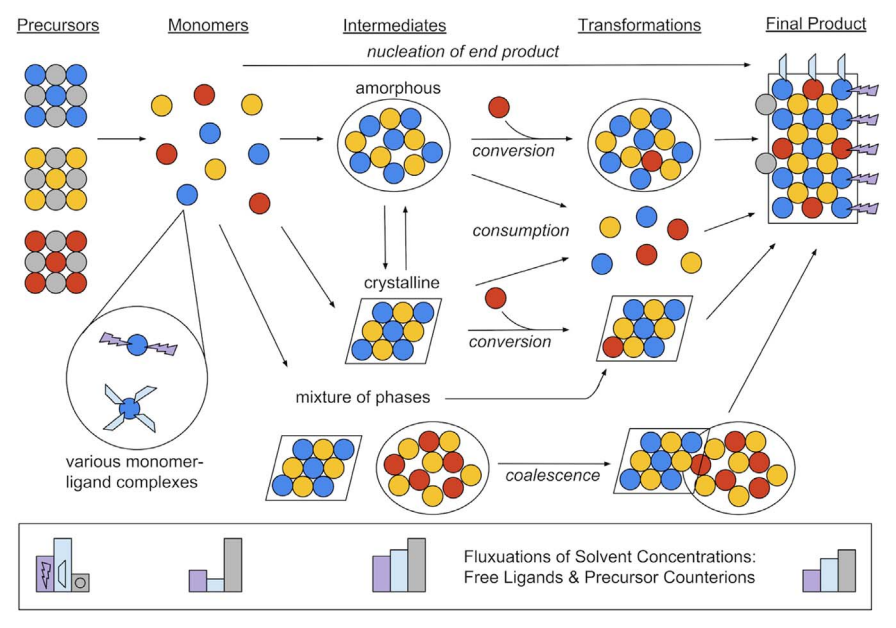
growth as well as how the subtle interplay between closely related structures can lead to control over morphology [8]. Even very simple cases of reactions focused on a single element, such as Co NPs, for example, highlight how complex these reactions can be [9]. Scheme 1 will be the general guide for this review, in terms of our perspective about strategies for NP synthesis and by understanding the processes by which starting materials, intermediates, and final products are formed.

We have depicted a simplistic overview of possible routes for the transformation of NP precursors to end products. These processes can be highly complex with many important, dynamic components and the possibility for multiple mechanisms and pathways to simultaneously exist. As viewed from left to right, we typically think of NP precursors being introduced into the solvent system and reacting or dissolving to form active species or monomers. The blue, yellow, and red-atom containing compounds are depicted to dissociate from their gray counterions. Moieties from the solvent system may complex the NP constituent element and alter their reactivity, as shown in the circular inset labeled "various monomer-ligand complexes" with purple lightning bolt and light blue trapezoid shapes on the darker blue atoms. Thus, due to dissociation or reaction of precursors and complexation by solvent molecules, the composition of the solvent system may change. Throughout the course of the reaction, these solvent concentrations are constantly in flux, depicted in an oversimplified manner by the purple, light blue, and gray bar graphs at the bottom of Scheme 1. The active species may then proceed along various routes to eventually precipitate the final product. These include the possibilities of direct multibody nucleation of the end product or the formation of any number of solidstate intermediates (crystalline or amorphous particles or clusters). Possible intermediates may then transform in different ways: (1) "consumption" as dissolution to produce elemental active species once more (though under different reaction conditions and possibly with different complexation), (2) "conversion" as incorporation of an active species into an intermediate, or (3) "coalescence" as attachment of solid intermediates prior to end product arrangement. The intricacy of this depiction also functions to highlight the convoluted impact each synthetic parameter may have.

The scope of this review aims to outline common synthetic considerations in terms of both parameter tuning and characterization of reaction mechanisms, pathways, and end products. We discuss what are, in our opinion, exemplary studies in which the understanding of NP synthesis has progressed. Often these discoveries result from the careful, systematic study of a single synthetic parameter and the careful characterization of all reaction components before, during, and after NP nucleation and growth. Aside from simply tuning synthetic knobs, observing end results, and speculating about reaction mechanisms and pathways, the studies we have chosen to highlight here have considered many alternative hypotheses. Characterization techniques become most powerful when complementary methods aim to identify signatures of possible routes (not proving their sole occurrence, necessarily) and explore control reactions and measurements to eliminate hypotheses. Due to the complex nature of NP syntheses, it is crucial to scrutinize synthetic parameters, controls, and measurements. It can be easy to overlook a secondary but more important change to reaction conditions due to the tuning of another parameter. Additionally, limitations in characterization techniques can pose challenges in ensuring that measurements and controls are truly representative of NP synthetic flask conditions.

We recognize the difficulty and exhaustive nature in the approach necessary for NP synthetic discovery as well as the possible limitations in terms of both material systems and resource availability. Understanding each process or component depicted in Scheme 1 requires extensive research over decades and from multiple scientific groups. As the NP community continues to make strides in understanding, we recommend careful attention when speculating or proposing reaction mechanisms, pathways, and the role of parameters. We would value an increased number and quality of hypotheses considered and careful diction utilized when describing what can be "known" about a studied system.

A large part of the challenge for understanding NP synthetic strategies and adapting knowledge to new material systems lies in their inherent complexity. However, common language may also play a role. General terms are sometimes used to imply differing meaning, depending on the context of the study. Thus, we wish to define a few terms we will use in our discussion of NP syntheses and characterization. They are as follows. Note: deconvolution of some of these terms is onerous; however, these descriptions are our best attempt at clarity of speech and meaning.



Scheme 1. A general scheme depicting the transformation of NP precursors to end products with possible reaction routes identified. Generally, syntheses follow the evolution of the underlined components but may involve multiple simultaneous processes and are inherently dynamic, complex systems. Constituent elements of the end product are depicted as red, yellow, and blue circles. Solvent molecules capable of complexation to the constituent elements (ligands) are depicted in purple lightning bolts and light blue trapezoids. Processes labeled between components are italicized. A simplistic description of the dynamic nature of the solvent system is shown in bar graphs at the bottom with exaggerated concentration changes of the two ligands and the precursor material counterions. (For interpretation of the references to color in this figure legend, the reader is referred to the web version of this

- "Nanoparticles (NPs)" as solid-phase particles with nanoscale dimensions. Specifically, the term nanocrystal (NC) should imply single crystallinity, but the term nanoparticle encompasses a wider range of nanostructures, including those which are polycrystalline.
- ◆ "Precursors" as the starting compounds for the constituent elements of the final NP
- "Active species" or "Monomers" as the compounds that undergo nucleation
- ◆ "Precursor Conversion" for the reaction(s) taking place during the transformation of precursors to active species
- *Solvent System" as the non-precursor components of the reaction solution. These are typically high boiling point solvents, but could include additive compounds. We won't use "surfactant" because it implies that this compound necessarily interacts with the surface of the NP, and this isn't always known.
- "Bound Ligand" and "Free Ligand" for describing molecular interactions with the NP surface. Bound ligands are at the NP interface whereas free ligands are molecules with potential for being ligated but are solubilized and unattached to NP surfaces.
- "Reaction Mechanism" refers to the chemical processes occurring between specific species within the reaction system. In Scheme 1, this could refer to the chemical equations that describe each of the arrows.
- "Reaction Pathway" refers to the route(s) taken by the reaction system from precursors to end products or the evolution of the solid phase components.
 - o "Conversion" pathway refers to the preservation of a solid-state intermediate followed by end product formation via incorporation or expulsion of elemental species. Note: the word "conversion" is also commonly used to describe the transformation of precursors to active species.
 - o "Consumption" pathway refers to the dissolution of a solid state intermediate, providing active monomers in solution, usually at different conditions (temperature, coordination, concentration, etc.) than the conditions during the intermediates' initial nucleation(s).
 - o "Coalescence" refers to the adhesion and/or merging of two solid state intermediates in solution followed by transformation to the end product.

Our review is organized, in general, by category of species in a reaction, followed by new advances in characterization methods. There are several areas where these topics overlap, and we have attempted to be clear about the connections.

2. Connecting parameters of nanoparticle syntheses to reaction mechanism and pathway

2.1. Investigating the formation of anionic, chalcogenide species

Selection of a chalcogen (E) precursor for solution-based NP synthesis is typically based on solubility, ease of use, and desired reactivity. However, this often becomes a game of trial-and-error in order to balance the reactivities of all species in the desired end compound and to avoid unintended byproducts. Discussed herein are some of the considerations we believe to be important not only when selecting a chalcogen precursor, but also in understanding its role and behavior when investigating the reaction system as a whole. While selection of the chalcogen precursor is a parameter that can be tuned, it may affect the identity of the active chalcogenide monomers, the interactions of the dissolved chalcogen monomers with all other components (including the often overlooked headspace), the reaction mechanism for chalcogenide species evolution and subsequent delivery, and the reaction pathway in which solid phase components are formed. For example, octadecene (ODE) is typically touted as a non-

coordinating and "innocent" bystander as motivation for its selection and use with chalcogen powders. A contradicting and surprising discovery is found in a report from Bullen et al. in which the transformation of ODE as a result of Se presence as well as the presence of Se-ODE coordinated species suggest ODE to be an active participant in the reaction system and may play an unexpected role after its transformation [10]. This underscores the importance of understanding the role of all participants and not discounting alternative considerations without the appropriate experimental data.

The value of the studies highlighted henceforth with respect to this review is their specificity in studying the transformation of precursor to monomer (Scheme 1) exhaustively, emphasizing how even understanding one process of the inherently complicated NP synthesis warrants its own body of literature. This allows elucidation of reactivity trends or prediction of how a precursor might interact in a reaction system as a whole (e.g. precursor reactivity, decomposition, activation, species evolved, etc.). In other words, these studies can be used as initial resources for rational chalcogen precursor selection as well as subsequent systematic changes in chalcogen precursors to balance the parameters required for a specific reaction system.

2.1.1. Tertiary phosphine chalcogenides: mechanism of chalcogen delivery and reactivity trends

In general, basic structural properties, the mechanism of delivery, and reactivity trends of tertiary phosphine chalcogenides are well-reviewed by García-Rodríguez et al. [11], Reiss et al. [12], and Alvarado et al. [13] Here, we briefly summarize a few key points. For the phosphine chalcogenide series, the reactivity order via bond dissociation energies (BDEs) of the phosphine chalcogenides follows S < Se < Te. Although Te will not be compared in this section, it is reviewed by García-Rodríguez et al. [11] and Reiss et al. [12]

However, we would like to highlight work by Yarema et al. published in 2016 in which they demonstrated the controlled reactions of Cu-In-Te and Ag-In-Te ternary NPs from TOPTe despite its unstable nature as it is able to equilibrate with its dissociated counterparts within hours [14]. Although this would suggest a greater difficulty in balancing with other constituent elements, the authors synthesized two I-III-VI ternaries with impressive size and composition control.

Determination of mechanistic details on the delivery of the chalcogen (E) from a tertiary phosphine chalcogenide (R₃PE) was pioneered by the Bawendi and Alivisatos groups using nuclear magnetic resonance (NMR) (see Section 3.1.1.1) [15,16]. For phosphine chalcogenides, chalcogen atoms can be cleaved by two mechanisms [11]: (1) an acid/base reaction in which the chalcogen transfers as reduced E2- and (2) a redox reaction in which it transfers as E°. Both mechanisms are known to be important in metal chalcogenide NP syntheses depending on the reaction conditions. In 2017, mechanism 1 was further probed by Frenette et al. who characterized the expected anhydride and tertiary phosphine oxide byproducts but additionally observed H₂Se generated by phosphine selenide decomposition [17]. The headspace was collected into carbon disulfide (CS2) by cannula transfer and analyzed via 77Se NMR. Interestingly, the authors discovered that binary quantum dots (QDs) could be synthesized by cannula transfer of this gaseous Se species into a separate flask of cadmium carboxylate, suggesting that phosphine selenide activation by a metal complex was not solely necessary for phosphine-chalcogenide bond cleavage. However, the authors acknowledged this observation did not necessarily disprove the previously proposed mechanism but provided it as an alternative route to QD formation. This highlights the difficulty in pinpointing an active precursor and identifying all interactions in even binary, but still complicated, NP systems.

The Vela Group has made significant strides toward understanding the reactivity trends of tertiary phosphine chalcogenide families as they performed thorough work in which empirical evidence complemented their theoretical calculations [13,18]. From DFT calculations, they rationalized that the BDE of the phosphorus-chalcogen (P=E) bond in

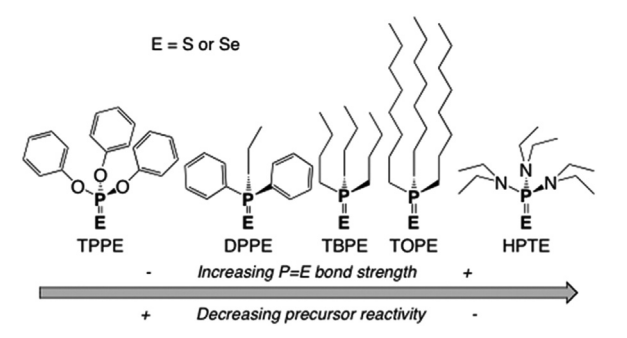


Fig. 1. Reactivity trend of tertiary phosphine chalcogenides: triphenylphosphite (TPP), diphenylpropylphosphine (DPP), tributylphopshine (TBP), trioctylphosphine (TOP), hexaethylphosphorustriamide (HPT). Reprinted with permission from Ref. [18]. Copyright 2012 American Chemical Society.

tertiary phosphine chalcogenides determined its reactivity such that an increasing P=E BDE gave rise to lower reactivity of the phosphine chalcogenide precursor. For any given phosphine, the Se reactivity is greater than that of S because S is smaller, more electronegative, and therefore, forms stronger bonds. Moreover, P=E bond strength increases with increasing electron-donating ability of the R functional groups as this helps stabilize the partial positive charge on the P atom. This theoretical model was supported by empirical CdS and CdSe syntheses in which the aspect ratios of the nanorods were tuned by the reactivity of the P=E bond (Fig. 1) [18]. Here, they saw the production of low aspect ratio NPs with diphenylpropylphosphine chalcogenide (DPPE), where the functional group was electron-withdrawing. When trioctylphosphine chalcogenide (TOPE) with a more electron-donating group was used, high aspect ratio particles formed. The general trend followed that as the P=E BDE decreased, thereby increasing reactivity, the aspect ratio and length of the NPs also decreased, meaning shorter and wider nanorods (Fig. 2). This trend was explained by the heightened reactivity of the phosphine chalcogenide, initiating faster and more uncontrollable reaction with the cadmium precursor, which led to lower selectivity for anisotropic 1D growth. The authors hypothesized this outcome was a nucleationdominated phenomenon because more reactive precursors are known to nucleate more rapidly and in greater concentration, leading to less precursor for growth. Further, high precursor concentrations were also reported to favor anisotropic growth, so the rate of chalcogen release during growth may have also contributed.

The strength of this report lies in establishing reactivity trends for the different series of tertiary phosphine chalcogenides. This enables selection of a chalcogen precursor due to the assignment of a quantitative value, e.g. BDE, instead of arbitrarily selecting a chalcogen precursor because it is common in the literature. This can be viewed as analogous to tuning a reaction with temperature and time parameters as they can be treated as "continuous" parameters (as in, there are no gaps in identifying a quantifiable value). As our knowledge of reactivity trends of tertiary phosphine chalcogenides expands, instead of these trends looking "step-wise," we are now filling in gaps so that a precursor can be strategically selected along a continuous plot. For example, in the first attempts of a ternary synthesis, one could select tertiary phosphine chalcogenides that possess BDEs at extreme ends; then, depending on the reaction products, one could rationalize a precursor with a BDE more suitable for the reaction system and conditions. This would hopefully lead to predictive control of the reaction outcome as we are now equipped with a standard base knowledge of how we might use this class of precursors.

2.1.2. Diorganyl dichalcogenides: reactivity trends and extrapolation from binary to ternary systems

The Vela group was also able to apply the same methodology from tertiary phosphine chalcogenides to diorganyl dichalcogenide precursors [13,19]. A DFT study predicted that between the C-E bond and the E-E bond, the bond with the greater influence on dichalcogenide reactivity was that of the C-E bond (Fig. 3). The E-E bond strength remains relatively constant within the disulfide or diselenide series. However, it should be noted that all bonds of both types must be broken to enable delivery of the chalcogen. These predictions were supported empirically by the following size and morphology observations of CdS NPs produced from dichalcogenides of varying C-E bond strengths. Dichalcogenides with very weak C-E bonds were found to be very reactive and led to rapid formation of large CdS NPs, while intermediate C-E bonds exhibited slower reactivity and produced smaller QDs. Strong C-E bond dichalcogenides reacted slowly and selectively to form anisotropic structures, and continuing the trend, dichalcogenides of very strong C-E bonds tended to be unreactive.

A 2018 report from the Brutchey group corroborated and extrapolated these findings to a ternary system, CuInSe₂, synthesized from diorganyl diselenide precursors [20]. The group also demonstrated that the kinetics of diselenide precursor conversion were dependent on the

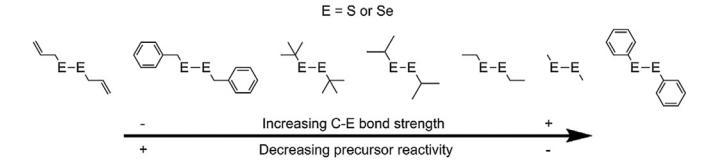


Fig. 3. Reactivity scale of diorganyl dichalcogenides based on C–E bond strength. Reprinted with permission from Ref. [13]. Copyright 2014 Elsevier.

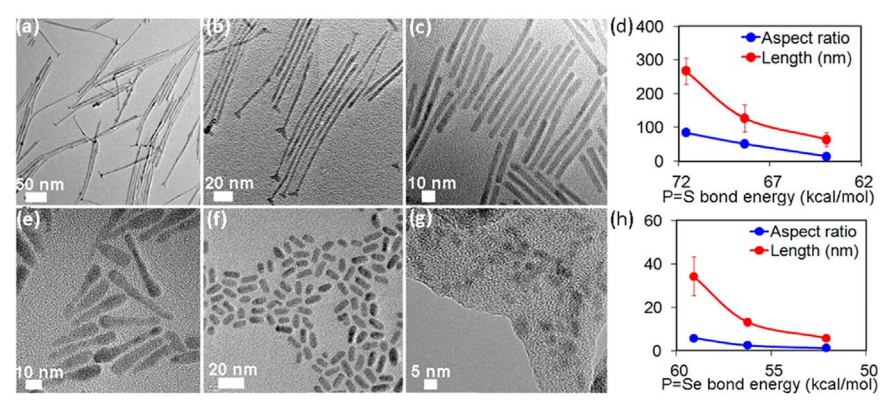


Fig. 2. Change in nanorod aspect ratio as a function of precursor reactivity. CdS nanorods made with (a, b, c) TOPS, TBPS, and DPPS, respectively. (d) Plot of CdS nanorod length (nm) and aspect ratio as a function of calculated P=S bond strength. CdSe nanorods made with (e, f, g) TOPSe, TBPSe, and DPPSe, respectively. (h) Plot of CdSe nanorod length (nm) and aspect ratio as a function of calculated P=Se bond strength. Reprinted with permission from Ref. [18]. Copyright 2012 American Chemical Society.

C-Se BDEs and that, interestingly, the strength of this bond was phase directing (Fig. 4). It was found that the chalcopyrite phase formed from precursors with weaker C-Se bonds via a fast-nucleating Cu2-xSe NP intermediate, while the metastable wurtzite-like phase formed from precursors with stronger C-Se bonds through a slow-nucleating umangite Cu₃Se₂ phase. While a range of dichalcogenides were tested en route to the formation of thermodynamically stable chalcopyrite and metastable wurtzite phases of CuInSe2, more mechanistic insight is required for the general use of dichalcogenides for ternaries. While ex situ X-ray diffraction (XRD) enabled the discovery of these respective reaction pathways, rigorous studies analogous to those presented in Section 2.1.1 would be useful to apply dichalcogenides to rational synthesis principles. However, tertiary phosphine chalcogenides have the advantage of being monitored by the P nuclei. NMR spectroscopies such as ¹H, ¹³C, and most importantly, ⁷⁷Se could be used in addition although we acknowledge this is not always an accessible technique.

$2.1.3. \ Alkylamine-chalcogenides: \quad chalcogen \quad dissolution \quad and \\ reduction$

Generally, the simplest method to prepare a chalcogen precursor is mixing elemental powders of S or Se, which can exist respectively as S₈ and Se₈ rings as well as polymeric chains, with a high boiling point organic solvent. Solvents such as primary alkylamines or phosphines are common and versatile because they are reducing and have the dual capability of acting as a surface ligand, coordinating to the surfaces of NPs to stabilize the surface. Specifically, oleylamine (OLA) is desirable and widely used due to its multiple roles: (1) as a reducing agent from either its olefin or amine functional groups; (2) as a neutral, labile coordinating ligand group through the lone pair on the amine; and (3) as a long chain alkylamine affording controlled NP growth and a high boiling point synthetic parameter [21]. However, delivery of the chalcogen in these cases is not straightforward as the possible identities of active and non-active species are difficult to detect and categorize. Efforts to achieve mechanistic insight into these intermediate species and potential side products exist with the aim to uncover how these might affect the reaction pathway of NP formation.

While several mechanisms have been proposed for the case of sulfur, seminal work from the Ozin group proposed that sulfur solubilized in octylamine (via sonication at 80 °C), existed mainly as alkylammonium polysulfides [22]. Octylamine was studied as a model compound for other common primary alkylamines because it can be bought commercially at a higher purity. OLA is typically used at 70% tech grade purity, for reference. Upon heating (2 h at 130 °C), the polysulfide ions reacted with excess alkylamine to liberate H₂S,

indicated indirectly by the transformation of PbO-coated paper to PbS in the presence of the reaction flask headspace. Byproducts of the $\rm H_2S$ liberation reaction, such as thioamides, reacted further to continue evolving $\rm H_2S$ although it remained unclear how and if these species contributed to the reaction pathway. Although studying octylamine instead of OLA afforded simplification of data, OLA has further functionality in the C-9 alkene [21] that we suspect could contribute to the identity of the reaction byproducts. Moreover, the composition and grade of OLA can influence the outcome of a reaction. While this study is a valuable resource for initial understanding of the potential reaction mechanisms in which S could interact with a primary alkylamine, it cannot account for all the unexpected side reactions that might occur as a result of OLA's impurities.

Regarding selenium dissolution in alkylamines, early reports of directly dissolved Se powder in OLA often exhibited uncontrolled reactivity of NPs [23]. An alternative route was developed in 2010 in which Wei et al. demonstrated sodium borohydride, NaBH4, was key in balancing the reactivities of many constituent elements, synthesizing not only binary but also ternary NPs (Fig. 5) [24]. In the presence of OLA, the authors speculated that NaBH₄ reduced Se to generate some general alkylammonium selenide species in situ. Although the exact speciation was not well characterized, Se powder was dissolved with ease at RT. In a report from our group by Riha et al., the authors were able to achieve the balanced reactivities of five different constituent elements through the use of NaBH4 to dissolve both S and Se in OLA which resulted in compositionally controlled CZTS_{1-x}Se_x NPs [25]. Keeping the precursors separate in OLA resulted in either a Se-rich composition or phase separation of CZTS and CZTSe NPs, which the authors speculated was due to the variations in relative chalcogenide speciation at nucleation. Despite the lack of true understanding of the actual speciation, the versatility of using NaBH₄ in the presence of OLA to dissolve Se and somewhat balance reactivities demonstrates the value of its extrapolated use to other systems.

In summary, while ease of dissolution is motivation for any use of a chalcogen precursor, this rarely results in simplicity of active precursor identity. It is still important to understand the mechanism of chalcogenide precursor evolution and delivery to aid in understanding the reaction pathway. This can be accomplished by careful characterization of all components as exemplified by the Ozin group's detection of $\rm H_2S$ by reaction of the captured headspace [22]. However, the report highlights the caution necessary to ensure the legitimacy of a control reaction. While it may be tempting to compare OLA by replacing its role with a cleaner alkylamine to narrow the scope of possible reaction mechanisms, care should be taken to truly determine that the final

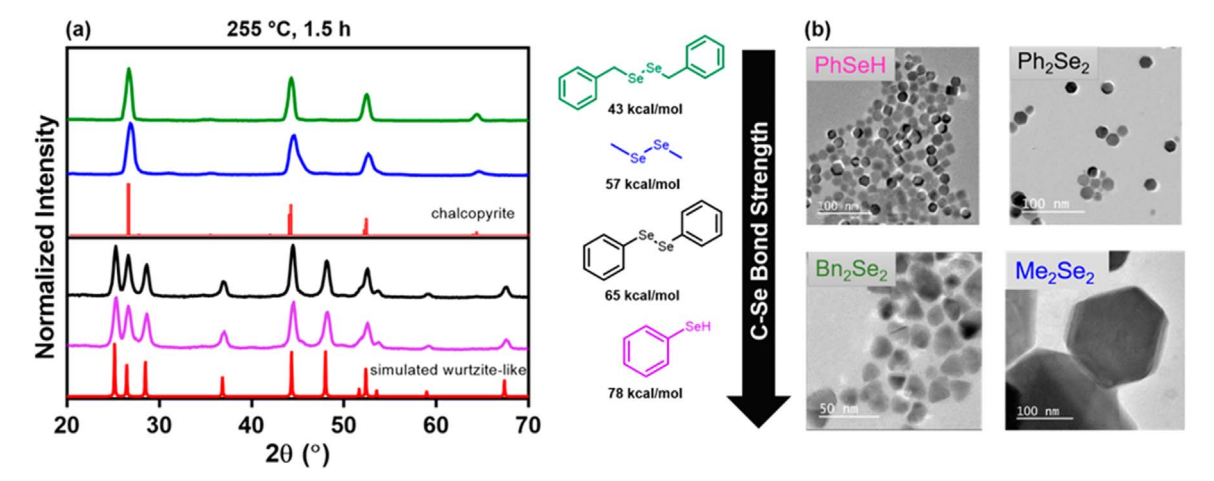


Fig. 4. (a) Powder X-ray diffraction (PXRD) patterns of CuInSe₂ NPs derived from the corresponding diselenide and benzeneselenol (PhSeH) precursors, and the reactivity scale of DFT calculated BDEs of C–E bonds. (b) TEM of the resulting NPs synthesized by the corresponding diselenide. Reprinted with permission from Ref. [20]. Copyright 2018 American Chemical Society.

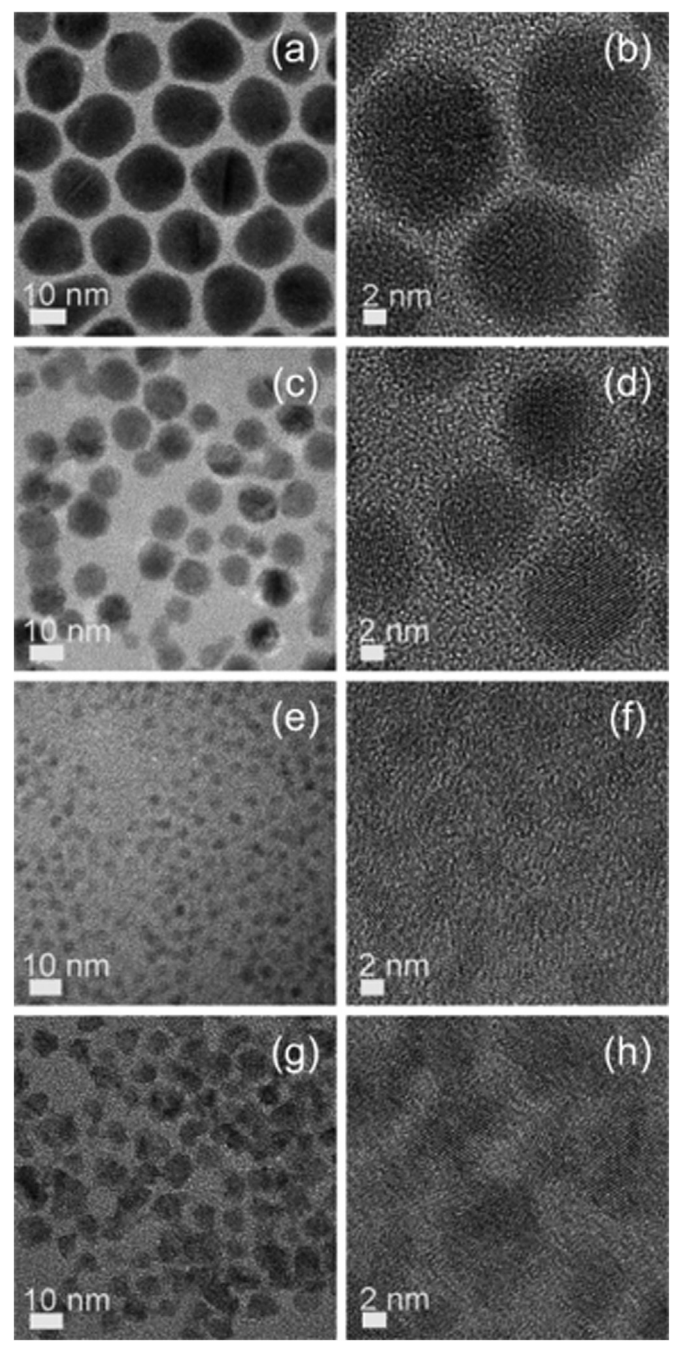


Fig. 5. Versatility of Se-OLA precursor in the presence of NaBH₄. (a, c, e, g) Transmission electron microscopy (TEM) and (b, d, f, h) high-resolution TEM (HRTEM) images of (a, b) Ag₂Se, (c, d) PbSe, (e, f) ZnSe, and (g, h) CuInSe₂ NPs synthesized with the Se-OLA-NaBH₄ precursor. Reprinted with permission from Ref. [24]. Copyright 2010 American Chemical Society.

products and reaction pathway are unaffected. Further, unlike tertiary phosphine chalcogenides, S and Se may not possess analogous reactivities to one another in the presence of alkylamines. Further mechanistic insight into the speciation of Se in OLA is required, so it should be treated separately.

2.1.4. Multiple roles of 1-dodecanethiol (DDT): sulfur precursor, stabilizing ligand, and solvent

It is well-reported that DDT can be used not only as a sulfur source via thermal decomposition but also as a stabilizing ligand and/or solvent [12,26]. Thermal decomposition of DDT is reported to be initiated by the formation of a metal thiolate by reaction of the thiol

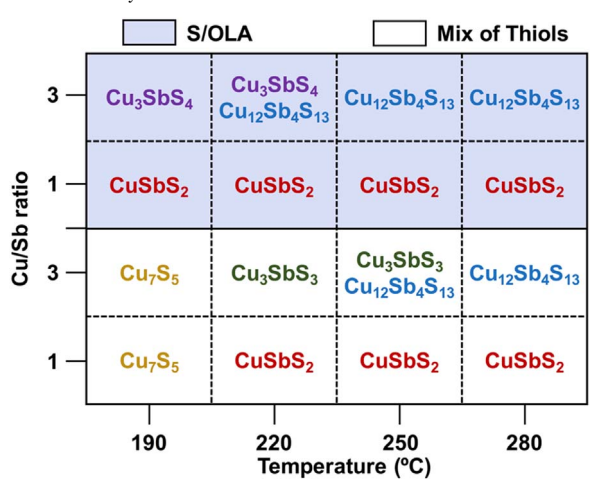
group with the metal of interest and is dependent on the hard-soft acidbase (HSAB) principle (Section 2.2.1) [12]. Softer Lewis acids interact more strongly with the thiolate group, weakening the adjacent C-S bond, which results in lower temperatures of decomposition as opposed to harder Lewis acids which exhibit the opposite trend. DDT can also influence the reaction pathway as exemplified by Ramasamy et al. [27] The authors synthesized a family of four Cu-Sb-S NPs including CuSbS₂ (chalcostibite), Cu₁₂Sb₄S₁₃ (tetrahedrite), Cu₃SbS₃ (skinnerite), and Cu₃SbS₄ (fematinite) by varying the Cu:Sb ratio, sulfur precursor identity (S/OLA vs 1-DDT/t-DDT), and temperature (Table 1). The differences in products as a result of sulfur precursor suggests the differences in reaction pathway. Because the authors focused on the characterization of optoelectronic properties such as bandgaps and absorption spectra, there was limited discussion and analysis on the compiled effects of tuning several synthetic knobs for this system. Although how DDT affects the reaction pathway remains unclear, its interactions in the reaction system differ from other sulfur precursors, thereby creating an interesting future study to examine the distinct speciation of the sulfur precursors.

Although DDT can be used as a S source, motivation for its use with elemental Se as a Se source is varied. While TOP readily dissolves Se powder to form TOPSe at RT with sonication or stirring, OLA requires heating to effectively dissolve Se powder. However, by including DDT with OLA, Se can be readily dissolved at RT [28]. Walker et al. proposed that this dissolution happens through a thiol-disulfide redox couple, formed by the reaction of two thiol molecules, that consequently reduces Se and protonates the amine, resulting in a (Se₈²⁻)(R₂-NH₃⁺)₂ complex. After the solution was formed, the authors demonstrated the ability to remove the thiol and disulfide compounds under vacuum, forming a selenide precursor free of other chalcogenides. This required the use of the short-chain ethylthiol for its difference in volatility relative to OLA. However, the sulfur compounds can be left in solution with the aim of forming mixed chalcogenide compounds.

2.1.5. Thiourea and selenourea: chemical decomposition

The use of thiourea and selenourea decomposition products as chalcogen precursors for NP syntheses is covered comprehensively in several reviews [11,12] as well as reports from the Owen group on a library of substituted thiourea and selenourea compounds [29,30]. The Owen group was able to achieve a wide range of reactivities and conversion rates by adjusting the organic substituents, thereby contributing to a continuous reactivity scale of quantifiable assignments as

Table 1Phases of Cu-Sb-S synthesized by systematic changes of parameters. Adapted with permission from Ref. [27]. Copyright 2014 American Chemical Society.



opposed to step-wise (discussed in Section 2.1.1). We highlight one specific use of thiourea in the formation of ternary NPs. In work from Sheets et al., Cu_3PS_4 NPs were prepared by reacting Cu_3P NPs with decomposed thiourea [31]. The authors suggested that thiourea isomerized to ammonium thiocyanate followed by decomposition into gaseous products, including H_2S and CS_2 . The success of this synthesis is curious because of the necessity for complete rearrangement of all Cu-P bonds to form the Cu-S bonds and S-P bonds that exist exclusively in the ternary material. While the paper does not describe any failed synthetic attempts or mechanistic insights, which would be useful for extrapolation to other systems, it stands as a relatively unique example of using an ex situ-prepared binary NP as a precursor to form a ternary compound.

2.1.6. In situ evolution of gaseous chalcogenide species from elemental chalcogen interaction with 1-octadecene (ODE)

Several studies outline the dissolution of chalcogen (S or Se) powder in ODE as an in situ source of hydrogen chalcogenide, H2E, which is hypothesized to be the active precursor in these NP syntheses [10,32-35]. Generally, the generation of H₂E has been characterized indirectly via two methods: by bubbling the reaction flask headspace into a metal cation solution in which subsequent observation of MxEv precipitate indicated transfer of a gaseous chalcogenide species and by the identification of a transformed ODE solvent (e.g. oxidization products, isomerization, etc.) as a result of its interaction with a chalcogen. While general mechanisms for the evolution of gaseous H₂E and expected byproducts have been proposed, there is still some uncertainty in pinpointing an exact reaction mechanism. These indirect characterization methods confirm the presence of a reactive gaseous chalcogenide species, but they are unable to conclusively confirm that the species is H₂E and/or that this gaseous species is the active monomer for NP production. These attempts have been further complicated by the observation of different interactions of S and Se with ODE [10,33]. While many efforts have been made in utilizing complementary techniques, ideally, we would be able to directly characterize gaseous species in situ simultaneously with the reaction solvent for a complete understanding of the interaction. Moreover, there exists a lack of understanding in the subsequent influence of the chalcogen-ODE precursor and byproducts on the reaction pathway for NP formation. This is likely due to the fact that these studies focus on the syntheses of binaries, which usually are thermodynamically favorable products and less frequently encounter some of the compositional and phase control difficulties of many multinary NP systems. Beyond a more direct observation of the active chalcogenide species, mechanistic exploration of the interactions between these species and metal cations is required. For example, in the case of H₂E truly being the resultant active chalcogenide species for both S- and Se-ODE systems, these compounds are not guaranteed to react to form NPs equivalently. Hopefully, through discussion of these results, we hope to emphasize the importance of understanding chalcogen powder dissolution in a presumably non-coordinating, "innocent" solvent and studying all interactions, especially among overlooked gaseous species and within the reaction headspace. Further, we hope to highlight that S and Se in ODE do not undergo analogous reaction mechanisms and, thus, do not provide the same reaction pathways when interacting with cationic species in a reaction system. Careful characterization is required to understand all the participants in a specific system without bias.

Yordanov et al. expanded the library of potential solvents that could be used to produce both $\rm H_2S$ and $\rm H_2Se$ [32]. However, only Se powder in paraffin was reported whereas S powder was studied in paraffin, hexadecylamine (HDA), stearic acid, trioctylphosphine oxide (TOPO), oleic acid (OA), sunflower-seed oil, and ODE. The effectiveness of a solvent was ordered by $\rm H_2S$ yield which was determined by gravimetric analysis of CdS precipitate (Table 2). The precipitate was generated by cannula transfer of the gaseous species into a solution of Cd (Fig. 6). While this study stands as a diverse list for choosing chalcogen-solvent

Table 2Yield of H₂S from reaction between sulfur and various organic solvents at 250 °C for 1 h. Reprinted with permission from Ref. [32]. Copyright 2008 Springer Nature.

Compound	Yield, %
Liquid paraffin	79
Hexadecylamine	73
Stearic acid	64
Trioctylphosphine oxide	54
Oleic acid	10
Sunflower-seed oil	9
1-Octadecene	6

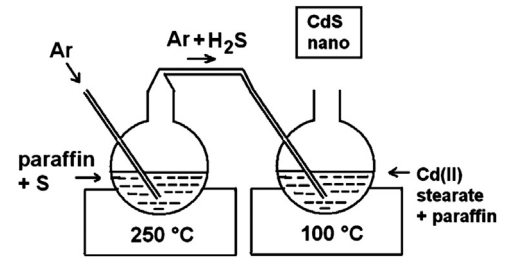


Fig. 6. Schematic representation of CdS NP synthesis by cannula transfer of gaseous headspace of S-paraffin flask to Cd stearate. Reprinted with permission from Ref. [32]. Copyright 2008 Springer Nature.

systems that yield different concentrations of gaseous chalcogen species, it would be strengthened by further characterization. Drawing conclusions from a single metric ignores the possibility of the explored systems exhibiting chemical differences in the composition of the gaseous chalcogenide species. Additionally, variations in the solvent systems explored (in terms of starting compounds, impurities, and transformed products) could likely affect subsequent NP formation. Thus, for greater understanding of the role of chalcogen-ODE solutions in NP syntheses and extension to more complicated, multinary systems, more detailed studies of the reaction mechanisms and pathways would be beneficial. This would involve characterization of monomer speciation and the influence on end products. From empirical evidence of attempts to synthesize ternary NPs, we observed that Se dissolved in HDA, TOPO, or ODE under the same reaction conditions (1 h at 250 °C) all resulted in different reaction products. This suggests that perhaps the dominant factor may not be the quantity of an active precursor but how the speciation of this precursor influences the reaction pathway, although we acknowledge that our results are not the most comparable because solvent interactions with Se may not be analogous to those of S.

A 2011 report from Li et al. attempted to understand the reaction products of sulfur and ODE and how the sulfur precursor is formed and delivered in ODE [33]. In the Peng group's previous study, published in 2009, Xie et al. studied the formation of CdS and discovered that it required a low activation energy, hinting that the reaction temperature could be lowered below typical reaction temperatures (> 250 °C) and that the rate-limiting step was the activation of a S-containing precursor [36]. In their 2011 study, Li et al. tested this hypothesis by performing the CdS reaction (cadmium octanoate/S = 2:1 in excess ODE) at the thermally activated reaction temperature (180 °C) or, more specifically, the lowest temperature at which H2S generation and corresponding CdS formation were detected in control experiments [33]. While no precursors self-reacted in control reactions at elevated temperatures (100-220 °C), ODE oxidized upon addition of S to form H₂S and byproducts. The detection of H₂S was performed by two tests: introduction of Pb(Ac)₂ testing paper to the S-ODE solution headspace and cannula transfer of the reaction gas phase bubbled into silver nitrate and zinc acetate solutions separately which formed black silver sulfide and white zinc sulfide, respectively. To test that the correlation

of CdS formation and H2S generation was indicative of S activation as the rate-determining step, the same synthetic procedure was carried out but with equimolar cadmium octanoate, ODE, and S (cadmium octanoate/S/ODE = 1:1:1) to bias for quantifiable side products. Otherwise, 125,000× magnification was required to observe relevant peaks in NMR spectra. While this raised concern that changing the precursor concentrations affected the equilibria in various chemical reactions, the authors compared this data set with that of the original syntheses. Although unable to directly detect H2S gas by the outlined method, the group indirectly characterized its presence by the identification of the expected fatty acid side product by Fourier transform infrared spectroscopy (FTIR), and the oxidation of ODE by an α-H NMR peak of its alkene group. The ultimate yield of S in the form of CdS only accounted for 3/3 of the initial elemental sulfur, indicating the likely formation of side products. The authors detected that the oxidation product of ODE in the organic phase consisted of 2-tetradecylthiophene and an unidentifiable, insoluble black mass. The exact structure was identified by NMR (Fig. 7), gas chromatography-mass spectrometry (GC-MS), and 2D-correlated NMR. Interestingly, these techniques did not show any sign of thiol or disulfide during the synthesis of CdS although their Se-containing analogous counterparts were observed in the formation of CdSe using a similar reaction system by Bullen et al. [10] discussed below. This further suggests the different speciation of S and Se dissolved in ODE. More so than other studies, this work by the Peng group extensively characterized all interactions of the reaction system in the formation of CdS binary NPs. Not only was the speciation of S dissolved in ODE elucidated, but the reaction pathway was also partially revealed by determination of the rate-limiting step of CdS NP formation.

Alternatively, the interactions of Se powder in alkane solution were studied by Deng et al. [34] The authors proposed that n-hexadecane oxidizes to an alkene in the presence of Se powder via a dehydrogenation mechanism which was rationalized by the detection of H_2Se through cannula transfer of the reaction headspace into a solution of $Cd(NO_3)_2$ and the detection of an alkene via FTIR. Discussion of the FTIR data is in Section 3.1.2.

Inspiration was drawn by Bullen et al. who extensively characterized Se as a chalcogen source in ODE to standardize and optimize its use [10]. Some broad comparisons can be drawn to the reaction studied by Deng et al. [34] However, we caution that the systems are not directly comparable because Deng et al. synthesized CdSe in n-hexadecane while Bullen et al. used ODE. The reaction mechanism of Se monomer(s) generation could be sensitive to the interaction differences between a primary alkene versus an alkane. The preparation

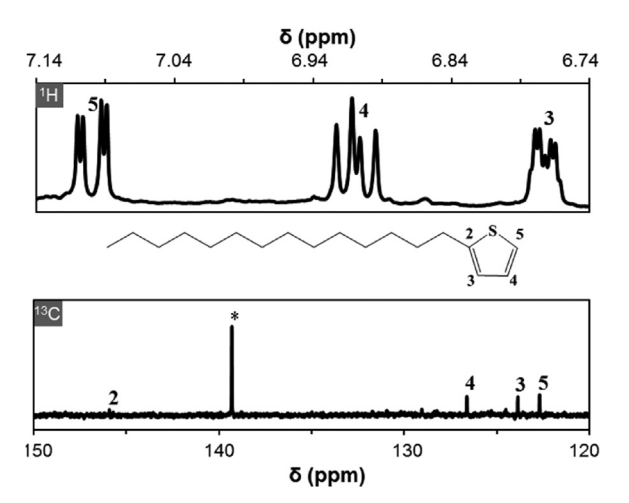


Fig. 7. NMR spectroscopy (¹H and ¹³C) detection of the ODE oxidation byproduct, 2-tetradecylthiophene, in the presence of sulfur. The ¹³C NMR peak marked by an askterisk comes from C-2 of ODE. Reprinted with permission from Ref. [33]. Copyright 2011 American Chemical Society.

of Se-ODE has varied through the literature in terms of time and temperature. Studies with its use have lacked close monitoring of the evolution of Se species, its mode of delivery in NP formation, and its efficacy as a Se precursor. The Bullen et al. report exhaustively measured efficacy by ultraviolet-visible (UV-Vis) spectroscopy, reaction yields of CdSe, inductively coupled plasma atomic emission spectroscopy (ICP-AES), photoluminescence excitation (PLE), X-ray absorption spectroscopy (XAS), NMR, and mass spectrometry (MS) (refer to Section 3 for an overview of characterization methods) [10]. These techniques demonstrated that the most effective use of Se-ODE required heating for 5 h at 180 °C as these were the minimum conditions required for complete Se dissolution. PLE was especially useful, in which the deepest color indicated the highest percentage of Se dissolution in ODE and thus activation. Prolonged heating at higher temperatures and/or longer times resulted in significant loss of Se in solution, hypothesized to be a competitive reaction forming gaseous H2Se. ICP-AES on active (5 h at 180 °C) and aged (48 h at 180 °C) samples confirmed some loss of solubilized Se. However, the authors had expected a greater decrease in Se concentration if H₂Se was the sole deactivation pathway due to literature precedence [32]. Complementary techniques including PLE and reaction yield for CdSe growth were therefore used. Changes in the absorbance profile at increased times or elevated temperature as well as a greatly reduced CdSe yield compared to Se concentration lost in solution suggested to the authors that loss in Se-ODE precursor efficacy could additionally be a result of a Se speciation change to a less active form.

Of note, 1-octadecene can isomerize over time to 2-octadecene in the presence of Se but not otherwise when applied to the same conditions (>5h at 180°C) as observed by 2D correlated NMR ¹H-¹³C heteronuclear single quantum coherence (HSQC) (see Section 3.1.1). While not directly comparable systems, we recall reaction mechanisms proposed from previous studies involving related components. In the combination of S and ODE, Li et al. also observed that precursors and solvents did not autonomously react, and the transformation of ODE required the presence of the chalcogen [33]. In contrast, the oxidation of ODE resulted in 2-tetradecylthiophene accompanied by an unidentifiable black substance. Deng et al. reported the production of H₂Se and a dehydrogenated alkene group from the combination of Se powder and long alkyl hydrocarbons (n-hexadecane and paraffin), reiterating the different speciations of long-chain alkyl hydrocarbons versus long-chain monoolefins [34]. Beyond the observation of this isomerization, the authors were unable to identify the role of H₂Se in its production. Based on empirical evidence of this work, we propose two hypotheses to target the understanding of ODE isomerization. One involves the in situ generation of H2Se resulting in the production of 2-octadecene. Alternatively, H2Se could possibly act as a significantly electrophilic species in order to thermodynamically shift to the isomerization product.

Regarding the effects on CdSe NP formation, Bullen et al. observed many different Se species in the reaction system but admitted the inability to differentiate between active and inactive Se species [10]. While the potential Se precursor structures of the Bullen study are detailed in Section 3.1.3, we would like to highlight the group's restraint in not speculating beyond what any of the data indicate. Interaction between Se and ODE was detected by a varied C-1 signal in ¹H-¹³C HSOC (see Section 3.1.1), indicative of Se bonding to C-1 in a variety of ways. No interaction would have, instead, been characterized by a uniform chemical environment. Positive electron ionization mass spectrometry (EI MS) of active (1 h at 200 °C) and inactive (48 h at 200 °C) Se-ODE samples were also studied. Five singly charged species were detected for the active sample, where m/z is mass-to-charge ratio: ODE (m/z = 252), ODE+Se (m/z = 331), ODE+2Se (m/z = 410), 2ODE +Se (m/z = 586), and 2ODE+2Se (m/z = 664). The same species with the exception of ODE+2Se and 2ODE+2Se were observed in the inactive sample. While these results neither elucidated the mechanism in which H₂Se is generated in situ nor suggested how these species contributed to the overall reaction pathway, the detection of these species does support the existence of multiple Se species and the difficulty in deconvolution between active and inactive precursors in the formation of CdSe. Another H₂Se study by Pu et al. acknowledged similar issues in identifying the exact reaction pathway in the formation of CdSe by Se-ODE [35]. Although the formation of H₂Se was supported by similar techniques mentioned above, it was difficult to determine whether H₂Se played a role in the formation of CdSe. Overall, this report suggests the importance of carefully considering the reaction precursor interactions with all solvents.

The literature for the colloidal nanoparticle community has typically cited ODE as a non-coordinating and innocent bystander in NP reactions as a motivation for its use. However, this is not the case in the presence of a chalcogen and may not be the case with other reaction components as well. This is true in cases outside of the scope of chalcogenide precursors. For example, a contradicting and surprising discovery is the coordination of ODE on synthesized phases of the Li-Zn-Sb family, specifically cubic MgAgAs-type and CaZn₂Sb-type LiZnSb crystallites [37].

2.1.7. Perspective

While we cannot expect that these chalcogenide precursors in a binary nanoparticle system will behave in an extrapolated manner to more complicated multinary systems, the body of literature demonstrates that the field is trending toward identifying reactivity trends of related chalcogenide precursors and that these scales can help direct NP synthesis and serve as strategies for rational precursor selection. Ideally, we would like to make direct, quantifiable reactivity comparisons between the different types of chalcogen precursors and between different solvent systems, but the property trends would be hard to define because there are often many processes occurring that involve transformations of both the chalcogen and solvent system into different and hard to identify species (precursor to monomer transformation in Scheme 1). While it could be argued that Se-ODE and Se-OLA are more reactive precursors than phosphine chalcogenides in terms of BDE (P=Se = 364 kJ/mol versus Se-Se = 172 kJ/mol and Se=Se = 272 kJ/mol, for fragmentation of cyclooctaselenium rings or selenium chains) [10], we see through the literature that the speciation is different for these chalcogen precursors. Thus, the use of BDE to singly assign reactivity for more complicated dissolution mechanism products would be severely overlooking the true interactions between chalcogen

However, more broad generalizations could be made. Precursors such as DDT and thiourea are motivated by decomposition mechanisms and easy handling. If interested in control and tunability, tertiary phosphine chalcogenides are well-understood in the literature and therefore result in more rational predictions on potential reaction outcomes. Moreover, there appears to still be a need for understanding the true active chalcogen species in E-ODE as characterizations have shown that the combination produces several Se species with possible additional undetected ones. Interesting observations in the case of phosphine chalcogenides are that S and Se precursor series will generally follow analogous reactivity trends respective to one another and that the reaction pathways of NP formation were also found to be similar. However, this does not appear to be the case for chalcogen powder dissolved in ODE or other long chain alkyl hydrocarbons compounds wherein the speciation of S and Se are different and therefore could result in different reaction pathways of NP formation. This emphasizes the importance of understanding these studies in order to provide careful considerations when designing one's own experimental methods.

Ultimately, herein we described reports in which the speciation and reactivity of chalcogen precursors for NP synthesis were examined, highlighting those with careful analysis in order to test the reaction mechanisms proposed. While describing NP reaction systems is difficult and designing a synthesis for one even more so, we hope to have described some useful methods in understanding the identities of

active chalcogen precursors alongside mindful characterization in the mechanism of chalcogen precursor delivery and subsequent formation of byproducts in a variety of solvent systems. Robust studies recognize unexpected interactions of the chalcogen precursor with reaction components and the resultant effects on the NP reaction pathway.

2.2. Understanding cationic speciation of NP precursors: a case study on metal amides

Considering cation precursors in NP syntheses, metal salts such as halides, oxides, and acetates, among others, are commonly used. Solubility of the starting materials plays an obvious role, but complexation in solution, whether to solvents or various other components, often underlies the key factor in tuning the reactivity of cationic components in NP syntheses. Traditionally in early NP syntheses, highly reactive precursors amenable to forming a supersaturation of active species in solution for inducing swift nucleation were targeted. In a landmark review on NP synthesis from 2005, Yin et al. described promising precursors were those with easily dissociating leaving groups [7]. Acknowledging the complexity of NP synthetic systems and its major differences with chemical vapor deposition (CVD) techniques, the authors suggested the adaptation of CVD precursors for early solution-based NP synthetic development. As understanding in the field has progressed, simpler metal salts have been more commonly employed. A major factor in this shift comes from a better identification of the active species, specifically how the metal atoms are complexed in solution immediately prior to nucleation. Often, some form of solvent molecules exists as the ultimate metal complexing agent(s) during reaction. Advances in cation precursor selection have occurred via achieving the active cation species from more benign starting precursors. This change usually accompanies additional benefits with the use of relatively safer (regarding both human use and environmental impact) and more economical precursors.

One specific example of this cation precursor evolution exists in the history of cadmium chalcogenides. Early work, including the influential study by Murray et al., employed the use of highly reactive dimethyl-cadmium, targeting swift nucleation for monodisperse particles via pyrolysis of this organometallic compound [6]. In following works, Cd was found to complex with strong ligands, such as hexylphosphonic acid, prior to NP formation [38]. This prompted skepticism of the need for the sensitive, reactive dimethylcadmium precursor. Indeed, syntheses with CdCl₂ and CdO were explored, identifying high quality NPs formed from CdO alongside the use of phosphonic acids [38]. Thus, the initial choice of a highly reactive compound targeting rapid nucleation was replaced by simpler, more stable precursors that afforded the same, or similar, important reactive species.

Another area of NP synthesis in which discoveries parallel this theme lies in the use of metal amides as reactive species, whether directly as precursors or formed in situ. Advantages for the use of metal-nitrogen bonded precursors lie in their increased reactivity and commercial availability or relatively straightforward, albeit typically air-sensitive, production. Historically, these compounds have been favored for thin film deposition methods due to the absence of oxygen and carbon, producing films with lower levels of carbonization compared to metal-carbon bonded precursors [39]. In the body of this section, we cover studies showing the development of understanding for the use of these precursors in conjunction with other important reaction parameters. While not intended to be an exhaustive compilation of all NP syntheses involving metal amides, this narrative seeks to illustrate the importance and utility of examining possible alternative hypotheses and the role of seemingly uninvolved components in NP reaction systems. The impact of each incremental discovery within these amide-assisted NP syntheses is exemplified in the breadth of material systems accessed by these versatile strategies.

2.2.1. The hard-soft acid-base principle

To preface a history of metal amide understanding in NP syntheses, the hard-soft acid-base (HSAB) principle provides a framework for interpreting some of the observations covered in the upcoming discussion. Introduced by Pearson in 1963, its ideas inform many aspects of NP systems: precursor decomposition or stability, reactive monomer complexation, surface-ligand interactions, cation-exchange mechanisms, ligand exchange mechanisms, etc. [40-42]. Within the HSAB principle, chemical groups are categorized as Lewis acids (electron acceptors) and Lewis bases (electron donors) each on a scale between hard and soft. Hard acids usually exhibit high positive charge and small size with paired valence electrons, while soft acids show the opposite: low positive charge, large size, and often unshared valence electron pairs. Hard bases have tightly held electrons, while soft bases' electron clouds are easily deformed and oxidation is less difficult. In general, polarizability of components underscores the main difference with low polarizability in hard acids and bases and high polarizability in soft ones. The key HSAB principle then follows that hard acids prefer to coordinate with hard bases and soft acids with soft bases. Common NP synthetic acids and bases are organized along a hard/soft scale in Fig. 8 [12].

Of course, solution-based NP synthetic systems are inherently complex with many interacting components. Relying on standard, quantitative properties of atoms and compounds may aid explanation of empirical synthetic observations, but syntheses are hardly carried out at standard conditions, and extrapolating to NP synthetic conditions degrades the standard properties' reliability for this use. Thus, the strength of relying on Pearson's HSAB principle may lie in its empirical basis. It suggests how components might interact, but it is not a quantitative law. Within the principle itself (outside of the world of NP synthesis), Pearson acknowledges there exist important chemical factors determining bond energies that must be taken into account beyond the HSAB principle, such as orbital overlap and steric repulsions. Nonetheless, scientists have benefited from NP synthetic explorations guided by the general trends of the HSAB principle which is featured in a few examples in this section. Additionally, without explicit referral to HSAB, results from some studies can be interpreted in the context of the HSAB principle.

2.2.2. Evolution of proposed reaction mechanisms for metal amides in NP sunthesis

Metal amide precursors and related in situ formed species have been used for the synthesis of metal, metalloid, binary, and multinary nanoparticles. Relative to common NP conditions (metal salts in high

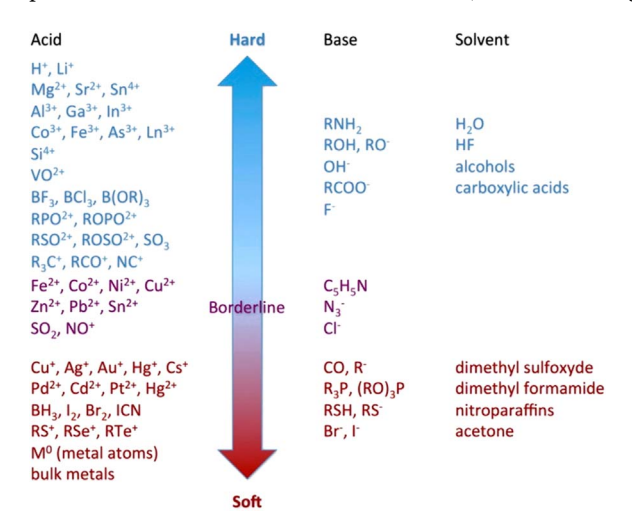


Fig. 8. Common NP synthetic components categorized as Lewis acids and bases on a qualitative scale of hard to soft, based on the Pearson HSAB principle. Reproduced with permission from Ref. [12]. Copyright 2016 American Chemical Society.

boiling point solvents), the introduction of a metal amide species often enhances reactivity of the involved components which can alter nucleation kinetics. Strategically, this has been used as a handle for forming smaller, more monodisperse NPs or for balancing the reactivity of multiple cationic components. This specific field highlights an interesting look into the evolution of scientists' understanding of NP synthetic parameters and its subsequent application to new material systems.

We also refer the reader to a 2013 review by Yarema et al. that tabulated NP syntheses derived from metal amide species and complemented the summary with a theoretical study of the thermal stability of various monomeric metal silvlamides [39]. In this section. we wish to narrate exemplary metal amide syntheses to emphasize the problematic appeal of suggesting a singular reaction parameter as the sole important factor or speculating a reaction mechanism without disproving alternative mechanisms. We acknowledge the difficulty in NP synthesis characterization and in the identification of short-lived intermediates that are crucial to reaction mechanisms, especially when certain facilities are not accessible or certain methodologies are useful only for certain systems (e.g. NMR being less useful for tracking non-NMR active nuclei). However, the evolution of understanding and increased knowledge of various reaction mechanisms in the field of metal amides for NP syntheses provide a hopeful outlook. This shows the connection of increased exploration of reaction mechanisms and identification of impactful reaction parameters with the optimization of new material systems. It is still difficult to directly apply insight to the development of new NP syntheses. However, the evolution of understanding in the metal amide synthetic field has uncovered various reaction dynamics, all of which may be considered as possible mechanistic hypotheses in the expansion to novel NP material systems.

2.2.2.1. Early use of metal amides for the synthesis of metal and metalloid nanostructures. Early work employing metal amide precursors for metal NPs was pioneered by Chaudret et al. in the late '90 s and early '00 s and by Buhro et al. in the early '00 s. Chaudret et al. formed nanostructures of many metals and metalloids (Fig. 9), including but not limited to Sn/SnO₂ [43], Ni [44], Ru [45], Fe [48], Fe-Co [47], and Co [46]. The synthetic approach generally involved the use of an organometallic precursor (e.g. metal silylamides) in the presence of ligand solvent molecules used to direct various morphologies. Reduction of the metal centers was commonly induced by reaction with hydrogen under temperature and pressure. Metal oxide nanostructures were formed either by a secondary oxidation reaction step or by direct hydrolysis of the organometallic precursors [49–52]. A perspective article from Amiens et al. depicts the breadth of materials the authors were able to form via this general scheme [53].

Buhro et al. developed syntheses for small, monodisperse Bi NPs via the reported thermal decomposition of $Bi[N(SiMe_3)_2]_3$ in the presence of NaN(SiMe₃)₃ and polymer stabilizers [54–56]. The authors found the Bi NPs to be useful for diameter-controlled solution-liquid-solid (SLS) growth of semiconductor nanowires. In 2010, the authors published an advancement of their Bi NP synthesis which avoided the meticulous and sensitive synthesis of $Bi[N(SiMe_3)_2]_3$, stating it formed in situ from $BiCl_3$ and $NaN(SiMe_3)_2$. However, direct characterization of the transient Bi silylamide was not presented [56].

2.2.2.2. Small, monodisperse IV-VI NPs via IV-[N(SiMe₃)₂]₂. In 2007, Kovalenko et al. first extended the use of the metal silylamide, Sn[N(SiMe₃)₂]₂, to the synthesis of small, monodisperse tin monochalcogenide NPs [57]. The precursor was chosen for its increased reactivity compared to previous Sn salts (oleate, acetate, and chloride) explored by the authors which did not produce small, monodisperse NPs. The synthesis of SnTe was reported specifically, but it was also stated the procedure could be adapted to form both SnSe and SnS. In 2008 and 2010, Hickey et al. [58] and Baumgardner et al. [59] extended the use of Sn[N(SiMe₃)₂]₂ to the formation of SnS and

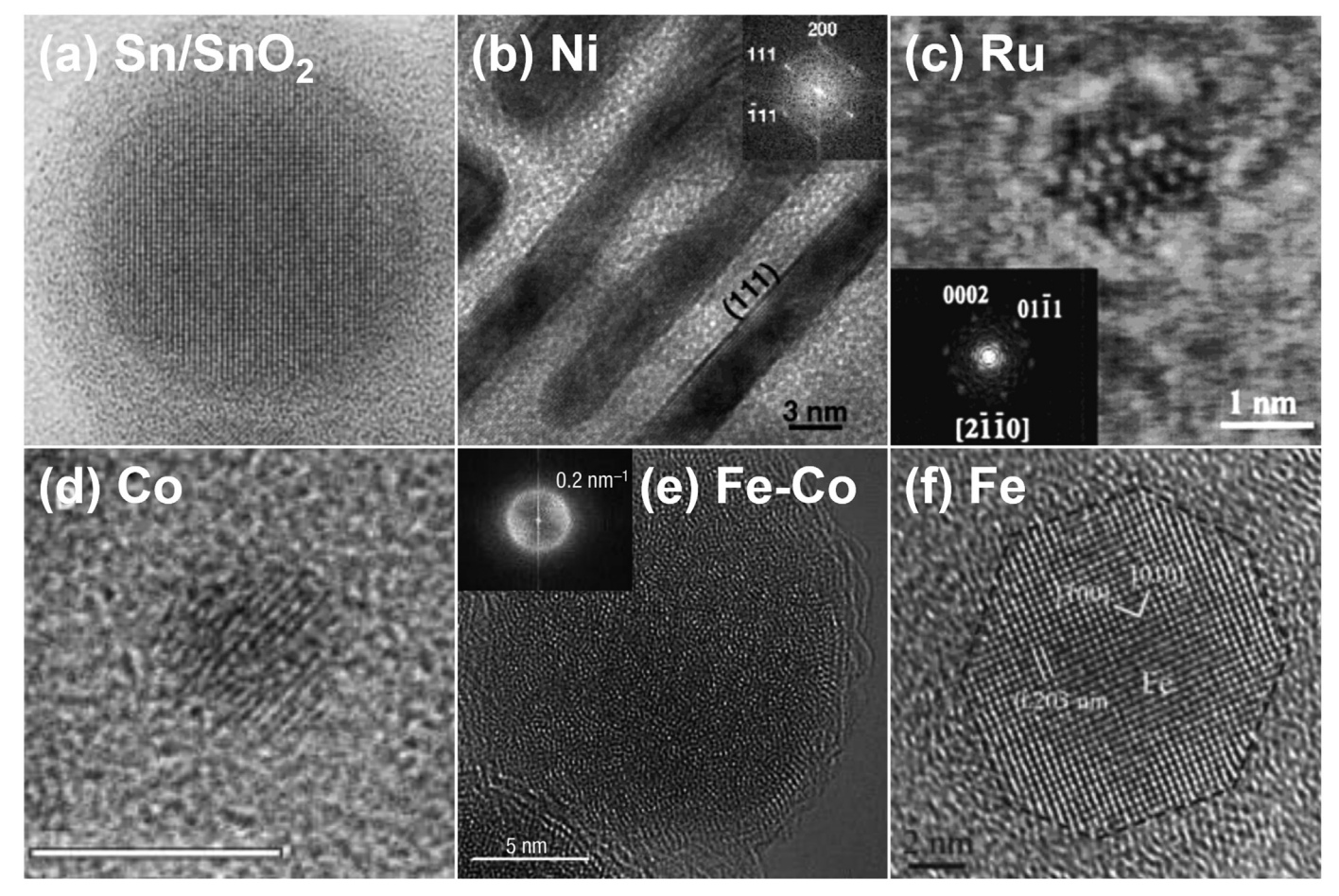


Fig. 9. Electron micrographs of various nanostructures formed by an organometallic approach from the group of Chaudret et al. Part (a) is Sn/SnO₂, adapted with permission from Ref. [43]. Copyright 1999 Wiley-VCH Verlag GmbH, Weinheim, Fed. Rep. of Germany. Part (b) is Ni nanorods, adapted with permission from Ref. [44]. Copyright 2001 American Chemical Society. Part (c) is Ru adapted with permission from Ref. [46]. Copyright 2002 Wiley-VCH Verlag GmbH & Co. KGaA, Weinheim. Part (e) is Fe—Co, adapted with permission from Ref. [47]. Copyright 2005 Springer Nature. Part (f) is Fe, adapted with permission from Ref. [48]. Copyright 2011 Royal Society of Chemistry.

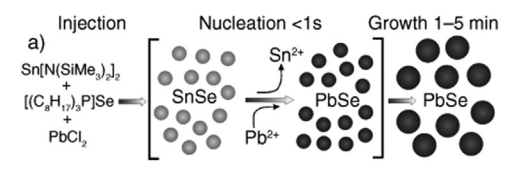
SnSe NPs, respectively. These studies observed dependencies of NP size and morphology on parameters such as reaction temperature and the amount of alkylamine solvent. Specifically, Hickey et al. found manipulation of the solvent system affected the morphology of the SnS NPs with a higher OLA amount resulting in smaller, spherical particles and a higher oleic acid (OA) amount giving larger, angular ones.

In 2011, GeTe NPs of different sizes (8, 17, and 100 nm) with the two smaller sizes relying on $\text{Ge[N(SiMe}_3)_2]_2$ as the germanium precursor were formed by Polking et al. [60] This Ge compound induced nucleation much faster than GeCl_2 -dioxane, which was used for 100 nm-sized NPs. The authors acknowledged the reaction mechanism was not fully understood but associated the reduced NP size with an increased reduction rate of Ge^{2^+} in the silylamide as opposed to the halide salt. For further discussion of Sn and Ge monochalcogenide nanostructures, we refer the reader to a review compiled by Antunez et al. in 2011 [61].

This sampling of IV-VI NP syntheses stands as one of the early examples of the versatility of a metal silylamide precursor for rapid development of small, monodisperse NPs in related material systems. In the next few sections, we highlight a cascade of publications reported to be inspired by each other sequentially, including each of their proposed synthetic explanations.

2.2.2.3. Proposed cation-exchange-mediated nucleation mechanism for PbSe NPs. An interesting early study from Kovalenko et al. in 2008 employed $Sn[N(SiMe_3)_2]_2$ for the formation of Pb chalcogenides and suggested a cation-exchange-mediated nucleation [62]. Inclusion of the

Sn silylamide compound with PbCl2, TOPSe, and OLA resulted in small, monodisperse PbSe NPs as opposed to the large, elongated particles observed without the Sn compound. Additionally, size tuning of the PbSe NPs was observed to be dependent on the concentration of the Sn silylamide compound. Via in situ infrared photoluminescence (IR PL) measurements, luminescent PbSe was detected within the first second after injection. The authors suggested the reaction scheme outlined in Scheme 2. Assuming the initial formation of SnSe, the system seemed to display "an unusually fast cation-exchange reaction." While the lattice free energies of PbSe and SnSe could not provide an explanation, two factors were offered in alignment with the suggested pathway. These included both the small size of the NPs, being comparable to solid state reaction widths (4-5 nm), and the favored interaction of the harder acid, Sn²⁺, with the solvent, OLA, relative to softer Pb²⁺. This study stands as an example in which the authors speculated a given reaction pathway based on empirical evidence of the starting materials and the observed end products. Standard properties,



Scheme 2. Proposed reaction mechanism for the formation of PbSe NPs via cation-exchange-mediated-nucleation and subsequent growth. Adapted with permission from Ref. [62]. Copyright 2008 Wiley-VCH Verlag GmbH & Co. KGaA, Weinheim.

such as lattice free energies, and characteristics based on the HSAB principle were discussed to offer explanation in their connection between reaction pathway speculation and observations. However, analytical techniques to detect intermediates and byproducts alongside control reactions to attempt to disprove possible alternative hypotheses were not employed.

2.2.2.4. Proposed silylamide metathesis reaction mechanism. The PbSe NP reaction mechanism above inspired Yarema et al. to adapt the synthesis for the formation of luminescent Ag₂Se NPs in 2011 [63]. Unlike the PbSe system, altering the Sn silylamide amount was not observed to induce Ag₂Se NP size tuning. Thus, LiN(SiMe₃)₂ was substituted for the Sn analogue, and improved NPs were formed with respect to colloidal stability, photoluminescence, quantum efficiency, and synthetic yield. Different from the quasi-seeded cation exchange mechanism proposed in the PbSe work, a metathesis-based reaction mechanism was offered. Illustrated in Scheme 3, a short-lived Ag silylamide complex was thought to form before decomposing to a Ag⁰ species and then reacting with the phosphine chalcogenide. To support this suggested route, the higher ionization potential of Ag relative to Li was cited as a driving force for their exchange. Additionally, a control experiment (synthesizing the Ag silylamide) was carried out in order to probe its solubility and decomposition in similar solvent systems. While it was found to be thermally robust up to 275 °C and not soluble in hydrocarbons, it underwent reduction to Ag0 in either hot tetrahydrofuran or pyridine, which was reported to exemplify its possible reactivity in the Ag₂Se formation.

The authors additionally carried out a synthesis identical to that of the Ag_2Se NPs but without Se, noting the formation of metallic Ag NPs and stating this proved the hypothesis of the reaction mechanism outlined in Scheme 3. Given the aforementioned Bi NP literature precedence that had cited the speculation of in situ formation of $Bi[N(SiMe_3)_2]_3$ from $BiCl_3$ and $NaN(SiMe_3)_2$ [56], the reaction mechanism proposed here seems natural. However, the control reactions of testing the solubility and reactivity of ex situ synthesized Ag silylamide alongside the results of the Ag_2Se reaction performed without Se only demonstrated the ability of Ag (however it might have been complexed) to react in those solvents and at those temperatures. This was already demonstrated to an extent by the formation of Ag_2Se in the original synthesis and, in our opinion, isn't conclusive evidence for the reaction mechanism.

We suggest a set of more convincing experiments might have been designed to identify either the presence or lack of byproduct compounds expected to form. Analysis of the reaction solution post nucleation and growth of the Ag_2Se NPs might afford more concrete evidence of the reaction mechanism. Attempting this could be exceedingly difficult, especially considering that one of the strengths of the amide-assisted synthesis lies in its swift nucleation, exacerbating the difficulty in detecting transient active species. However, we would encourage deeper questioning and characterization of the reaction mechanism proposed here.

Applying scrutiny to otherwise overlooked aspects of the system might be useful specifically in the case of understanding the dependence and independence of various parameters on Ag_2Se NP size. The authors described NP size to be independent of the silylamide salt concentration, reaction temperature, and growth time but dependent on the Ag:Se precursor molar ratio. This was offered with few synthetic details. The amounts of the lithium silylamide salt tested when varied were not reported, but it was stated the "amount of silylamide does not essentially

$$\begin{split} \mathsf{CF_3COOAg} + \mathsf{Li[N(SiMe_3)_2]} &\xrightarrow{\quad \quad } \{\mathsf{Ag[N(SiMe_3)_2]}\} + \mathsf{CF_3COOLi} \\ & \{\mathsf{Ag[N(SiMe_3)_2]}\} \xrightarrow{\text{in OLA}} [\mathsf{Ag^0}] \xrightarrow{\quad \quad \mathsf{TOPX} \quad } \mathsf{Ag_2X} \end{split}$$

Scheme 3. Proposed reaction mechanism for the formation of Ag_2E NPs via a metathesis exchange, reduction of Ag^+ , and reaction with phosphine chalcogenides. Reproduced with permission from Ref. [63]. Copyright 2011 American Chemical Society.

influence the final size of the NCs." Experimental amounts of the Ag and Se precursors for the Ag to Se ratios probed were absent; this information might be useful for considering the possible effect of the presumed innocent conjugate components of the precursors, TOP from TOPSe and trifluoroacetate from Ag trifluoroacetate. Based on the growing understanding of the solvent composition playing a larger role than expected in many NP systems, it would be of interest to more closely examine the possible effects of these unintended changes on the NP size variation reactions. A second area of interest would be the effect of reaction temperature and growth time on NP size and size dispersion. Despite the report of NP size independence from these parameters, these reactions required unspecified, varied temperatures (RT – 100 °C) with highly temperature-dependent growth times (2 min - several days) in order to attain optimal size dispersion. Overall, the odd nature of size tuning in the Ag₂Se NP system, requiring multiple changes to commonly important parameters, might be indicative of the proposed reaction mechanism being blind to unknown, important processes.

2.2.2.5. Metal-oleylamide intermediate detection & synthesis of metal & metalloid NPs. In 2013, pivotal work by Kravchyk et al. in the formation of Sn/SnO2 NPs was inspired by the success of these systems, employing the high reactivity of metal amide compounds to induce swift nucleation [64]. Indeed, the authors were able to produce small, monodisperse Sn NPs but, more importantly, gained a better understanding of the active Sn species, allowing a new reaction mechanism to be suggested. Key methodology to this work was $^{119}\mathrm{Sn}$ NMR, displaying the formation of a Sn-oleylamido complex upon the combination of a tin salt precursor, alkylamine solvent, and an organometallic base. Instead of the previously proposed metal silylamide metathesis reaction mechanism, a new role for the organometallic base was suggested. Upon introduction to the alkylamine solvent, it was thought to cause deprotonation, forming an olevlamide moiety, which could then complex with the metal cation. Instead of Sn[N(SiMe₃)₂]₂ as the active species for NP nucleation, Snoleylamido would then have been reduced to form Sn NPs.

Fig. 10 depicts the proposed reaction mechanism and shows the $^{119}{\rm Sn}$ NMR spectra for the listed combinations of Sn precursors, OLA, and Brønsted bases, each evidencing the formation of a single, equivalent Sn species. Based on the reaction mechanism proposed, the authors assigned this signal, $\delta(^{119}{\rm Sn})=62.5$ ppm, to the Snoleylamido species. In order to eliminate alternative hypotheses for the speciation of Sn in these solutions, various other Sn compounds were characterized. The pure liquid form of Sn[N(SiMe₃)₂]₂, the literature-predicted intermediate, gave signal at $\delta(^{119}{\rm Sn})=772$ ppm. Further, solvation effects were ruled out as a possible hypothesis for a shift to 62.5 ppm. The relatively non-coordinating solvent, squalene, with Sn[N(SiMe₃)₂]₂ gave signal at $\delta(^{119}{\rm Sn})=779$ ppm, while the

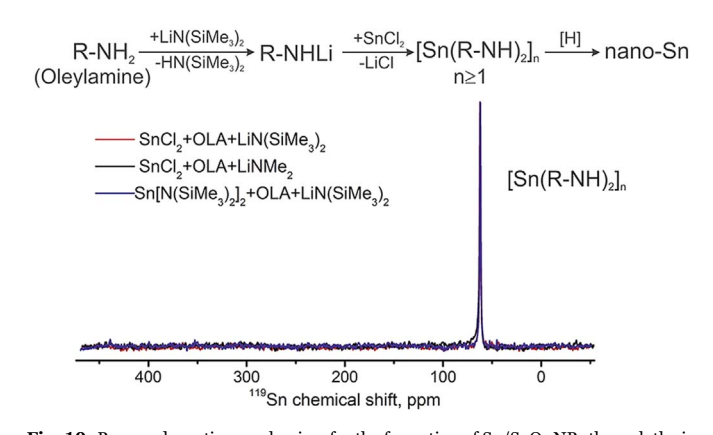


Fig. 10. Proposed reaction mechanism for the formation of Sn/SnO₂ NPs through the in situ formation of a Sn-oleylamido intermediate. Accompanying ¹¹⁹Sn NMR data for solutions combining Sn precursors, OLA, and Brønsted bases. Reproduced with permission from Ref. [64]. Copyright 2013 American Chemical Society.

combination of $Sn[N(SiMe_3)_2]_2$ and OLA gave signal at $\delta(^{119}Sn)=646$ ppm. A final control solution of $SnCl_2$ in OLA was ruled out with a characteristic peak at $\delta(^{119}Sn)=-420$ ppm. Lastly, the addition of a Brønsted base to either of the last two solutions, $Sn[N(SiMe_3)_2]_2/OLA$ or $SnCl_2/OLA$, resulted in conversion to the Sn-oleylamido complex, as observed by ^{119}Sn NMR. The strength of this work is demonstrated in the experimental evidence eliminating the possibility of the literature-predicted $Sn[N(SiMe_3)_2]_2$ intermediate and in the development of a new reaction mechanism possible for amide-assisted NP syntheses.

Understanding a step in the transformation of the reaction components prior to NP nucleation and growth aided the authors' abilities to extend this reaction scheme to the use of various other Sn salts, organometallic bases, and reducing agents [64]. Further, an impressive collection of metal and metalloid NP syntheses were developed and characterized by He et al., extending this general reaction scheme to materials including In, Bi, Sn, Sb, Cu, Zn, Ga, and some alloys such as ${\rm Bi}_x{\rm Sb}_{1-x}$, ${\rm Cu}_6{\rm Sn}_5$, and ${\rm Cu}_2{\rm Sb}$ (Scheme 4) [65]. The versatility of this NP synthetic strategy emphasizes the necessity for the consideration of this possible reaction mechanism, or a related process, in future studies of NPs developed with similar constituent reagents.

In summary, we found this collection of literature reports to provide an interesting evolution of characterization and understanding within these similarly composed reaction solutions. Initially, with the development of Sn and Ge monochalcogenides [57–61], the synthetic conditions for monodisperse, small NPs were presented alone. Extension of the system to PbSe NPs [62] accompanied a speculation for the reaction mechanism based on general solid-state knowledge and the HSAB principle without control experiments. Following, the Ag₂Se study [63] speculated a different reaction mechanism and carried out a few control reactions yielding further empirical evidence on the formation of solid-phase products but inconclusively provided evidence on the mechanism of formation itself. Finally, the Sn/SnO₂ NP study [64] and its subsequent extension to other metals and metalloids [65] offered yet another reaction mechanism and carried out careful

$$\begin{array}{c} \text{R-NH}_2 \xrightarrow{+ \text{ n-BuLi (base)}} \text{R-NHLi} \xrightarrow{+ \text{MCI}_n} \{\text{M(R-NH)}_n\} \xrightarrow{[H], \text{ T}} \text{nanoparticles} \\ (\text{Oleylamine}) \xrightarrow{-C_4H_{10}} \text{R-NHLi} \xrightarrow{+ \text{MCI}_n} \{\text{M(R-NH)}_n\} \xrightarrow{[n \ge 1]} \text{nanoparticles} \\ \text{base: } n\text{-BuLi, } \text{LiN(iPr)}_2, \text{LiN(SiMe}_3)_2 & \text{[H]: } (\text{i-Bu}_2\text{AIH})_2, \text{LiEt}_3\text{BH} \\ \text{pK} & \sim 50 & \sim 36 & \sim 30 \end{array}$$

Scheme 4. General synthetic route proposed by He et al. via the combination of metal and metalloid salts, alkylamines, and Brønsted bases. Metal-oleylamido intermediates are proposed to form which may then be reduced to metal and metalloid NPs. Reproduced with permission from Ref. [65]. Copyright 2015 American Chemical Society.

characterization of the reaction solution, aiming to identify the Sn complexation formed in situ. Insight attained within this system certainly benefited from the simplicity of the reduction of one NP constituent element (rather than formation of a binary, for example) and the utility of ¹¹⁹Sn NMR in the identification of the Sn intermediate. However, the general strategies regarding the consideration of alternative hypotheses and their elimination by careful characterization are valuable to adapt for the development of NPs of new material systems.

2.2.3. Noteworthy amide-assisted NP synthetic studies

Here, we highlight four amide-assisted NP synthetic studies in which careful discoveries on different aspects of these related systems have been made. While differences exist from one material system to the next, we hope the collection of these reports might spark ideas for possible alternative hypotheses in related systems. Additionally, the careful analysis and speculation presented in these studies could inform strategies for understanding NP syntheses beyond the amide-assisted scope.

2.2.3.1. Precursor addition rate affecting solvent system composition & NP morphology. One of the best examples of the connection between small, unexpectedly relevant changes in synthetic procedure and NP product outcome lies in the 2012 work of Liakakos et al. forming Co NPs of varying morphologies [9]. Immediately, the authors acknowledged the difficulty in controlling nanostructures at will. "NC synthesis is still largely empirical, and while several aspects can be explained a posteriori, it is nearly impossible to predict the results of a reaction that involves new reactants. Specific unexpected aspects inherent to each reaction can turn out to be dominant over general principles." Specifically, this study focused on understanding the reaction dynamics of one system due to observed irreproducible results. Nanostructures of Co were formed from a solution of [Co{N(SiMe₃)₂}₂(thf)], lauric acid (LA), and hexadecylamine (HDA) in the molar ratios of 1 to 2.04 to 0.36. The stock solution was held at 150 °C under 3 bar H₂, resulting in reduction of the Co species. Surprisingly, the addition rate of the Co precursor solution to the HDA/LA mixture was discovered to be instrumental in the varying Co morphology attained, as shown in Fig. 11.

Structural characterizations indicated the slow addition rate solution resulted in metallic Co material at an early stage of crystallization, lacking long-range order. The intermediate and fast addition rates gave rise to crystalline, metallic Co material with the majority phase being face-centered cubic (fcc) and hexagonal close-packed (hcp) phases, respectively. The core phase of the fast addition product was unidentifiable by HRTEM due to its large thickness, but the arms were identified

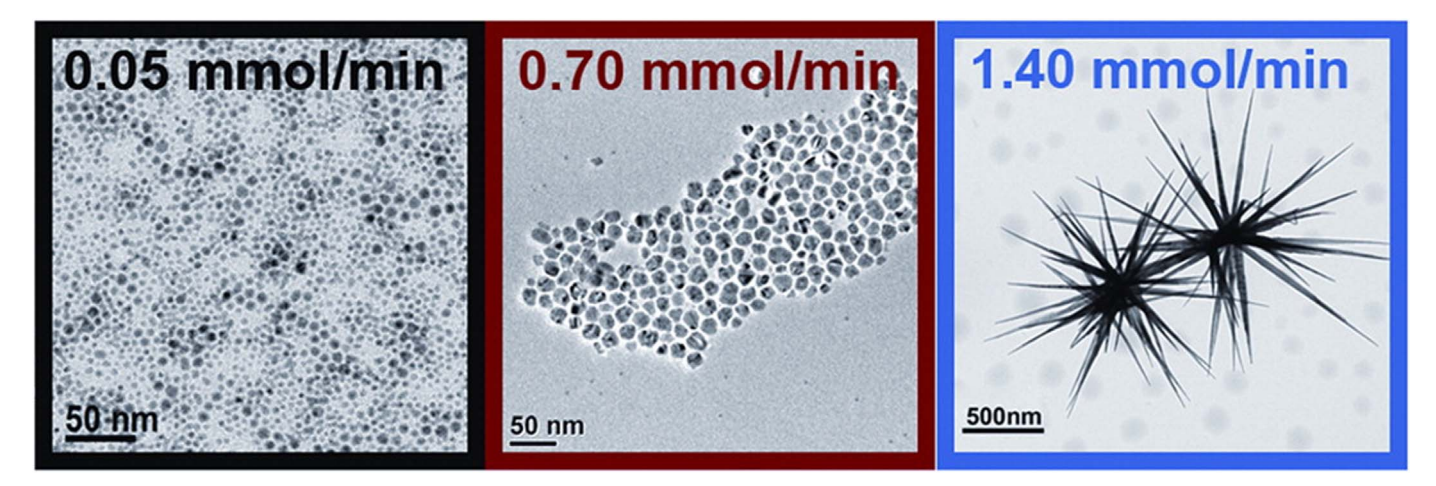


Fig. 11. TEM images of Co nanostructures formed from stock solutions of the same concentrations of [Co{N(SiMe₃)₂}₂(thf)], hexadecylamine, and lauric acid but prepared by different addition rates of the Co precursor. Note the differently-sized scale bars for the three images. Reproduced with permission from Ref. [9]. Copyright 2012 American Chemical Society.

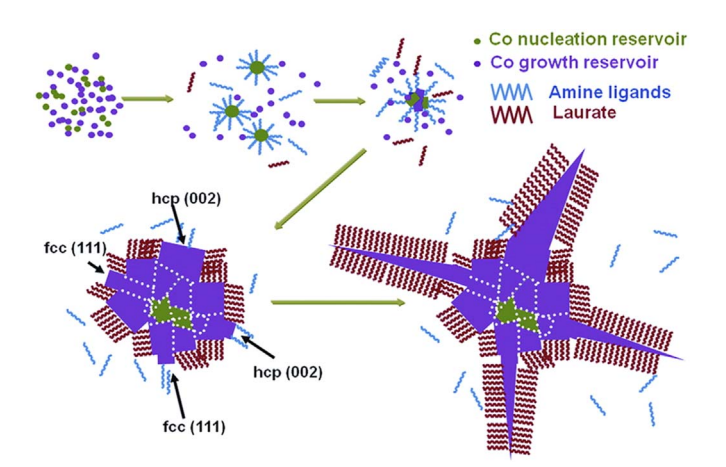
as *hcp* Co. Admirably, the authors clearly stated these structural and morphological characterizations allowed them to identify differences and speculate indications for their formation but did not give direct understanding of the precursor addition rate's effect. The slow addition rate was speculated to give rise to a higher amount of nucleation and therefore small particles, and oppositely, the fast addition was speculated to cause limited nucleation and form larger particles.

These observations inspired the authors to examine the reaction solution prior to reduction by H2. Initial observations from UV-Vis spectroscopy included the lack of a peak characteristic of the [Co{N(SiMe₃)₂}₂(thf)] precursor, indicating its rapid transformation in all cases. Three major peaks were observed in the UV-Vis spectra but in varying ratios of intensity for the different addition rate solutions, and these were observed to evolve over time. A key observation was the presence of a dominant peak in the slow addition solution that was almost absent from the fast addition spectra which, when aged, closely resembled that of independently synthesized Co[LA]2. The authors hypothesized the slow addition rate gave rise to an extended nucleation period, and this solution's dominant UV-Vis peak was suggested to correspond to an easily reduced Co species, forming non-crystalline, small Co particles. Correspondingly, fast addition products indicated to the authors a brief nucleation period; thus, Co[LA]2 was suggested to constitute part of the "growth reservoir," favoring slow growth of Co multipod structures. However, despite the observed UV-Vis spectra changes in both the fast and slow addition solutions over the course of time, aged solutions reacted under H2 gave Co morphologies consistent with their respective fresh solutions. The authors admitted this questioned the legitimacy of correlation between the UV-Vis solution spectra and the observed Co morphology.

Attempting to replicate the hypothesized composition of the fast addition rate solution, Co[LA]2 was put under H2 at 150 °C but was unable to be reduced. Upon the inclusion of HDA, Co multipods formed. The interaction of HDA and Co was investigated computationally and experimentally. Various HDA-containing Co complexes were calculated to be stable enough to exist in solution, and attempts to possible Co compounds from combinations [Co{N(SiMe₃)₂}₂(thf)], lauric acid (LA), and HDA were carried out. One Co complex for which a crystal structure could be determined was [Co[LA]₂(NH₃)₂]. The existence of ammonia indicated the possibility of following side reaction. Following deprotonation and coordination of the carboxylic acid moiety of LA with the Co precursor, HN(SiMe₃)₂ could be formed. Subsequently, two equivalents of excess LA and HN(SiMe₃)₂ could produce NH₃ and two silyl ester molecules. NMR (1H) spectra of the fast and slow addition solutions demonstrated the presence of HN(SiMe₃)₂ and the silyl ester. Interestingly, the slow addition solution revealed a much higher concentration of the silyl ester than the fast addition solution.

Altogether, the authors then correlated the importance of this side reaction to the Co reduction reactions. When the Co precursor was slowly added and reacted with LA, the generated HN(SiMe₃)₂ provided a competing reaction with LA, forming the silyl esters. A lesser amount of LA was left to complex with Co, and a smaller Co[LA]₂ growth reservoir existed relative to the fast addition solution. In that scenario, the majority of Co was complexed by LA, constituting a large "growth reservoir" and a smaller "nucleation reservoir." Further, the formation of the interesting multipod morphologies from this fast addition reaction solution was explained in the following way, depicted in Scheme 5.

A brief nucleation period resulted in a smaller amount of Co primary nuclei, which coalesced into polycrystalline cores. As this continued and the Co[LA]₂ growth reservoir was consumed, liberation of LA was suggested to become influential in the change of the growth mechanism. The competitive reaction of LA with HN(SiMe₃)₂ occurred, but as the LA concentration became significantly high, it began to selectively coordinate to the growing Co particles. The (002) *hcp* and



Scheme 5. Proposed reaction pathway for the formation of Co multipods from the fast addition stock solution under reduction by H₂. Reproduced with permission from Ref. [9]. Copyright 2012 American Chemical Society.

(111) fcc facets were suggested to be free, causing growth of the hcp multipod arms as the LA coordinated along the c axis of the growing arms. In all, the fast and slow additions of [Co{N(SiMe₃)₂}₂(thf)] into LA/HDA mixtures of identical initial compositions resulted in significantly different proportions of the nucleation and growth reservoirs, heavily influencing NP formation.

This study stands out as an eye-opening account of the possibility for apparently negligible details to employ great impact on a NP reaction system. The authors point out the need for scrutiny and consideration of many possible transformations of all components in NP reaction solutions, including those different from this silylamide/carboxylic acid/amine mixture. It may always be a possibility for unforeseen and changing side reactions to occur at any time during NP preparation and for their effects to impact the eventual products. The strengths of this study lie beyond the careful characterization of both solid-state and solution-based products, namely the authors' mindful interpretation of the data and direct discussion. This could inspire strategies for future NP synthetic developments.

2.2.3.2. First use of metal silylamides for ternary NPs and development of I-III-VI NPs. The first silvlamide-promoted synthesis for a ternary NP system was published by O. Yarema of the Wood group in the development of Cu-In-Se NP syntheses in 2013 [66]. Based on previous success in similar systems, OLA-based reactions were explored. While small Cu-In-Se NPs could be formed, they lacked photoluminescence. The authors attributed this to the alkylamine's reported role in catalyzing oxidation of NP surfaces [67]. Thus, altered reactions combined Cu and In halide salts in trioctylphosphine (TOP) and used an injection of LiN(SiMe3)2 and Se dissolved in TOP. Generally, as the silylamide amount was decreased, the NP size was found to increase with a lessened number of nucleation events offered as an explanation. This work was later extended to the Ag-In-Se system [68], utilizing an analogous reaction system; however, in the copperbased system, metal chlorides could be used while iodides were necessary in the silver-based system due to the observed decomposition of AgCl in TOP at > 100 °C. Within this reaction space, the manipulation of the amount of LiN(SiMe₃)₂ and the ratio of the metal precursors lent control over the NP composition (Fig. 12) while both the silylamide amount and the growth time were the key parameters for NP size control (Fig. 13).

Interestingly, the authors observed the dependence of the Ag:In composition in the NPs on the $LiN(SiMe_3)_2$ amount. When the molar amount of silylamide relative to iodide anions was in excess, the NPs displayed Ag:In molar ratios that reflected the molar ratios of the

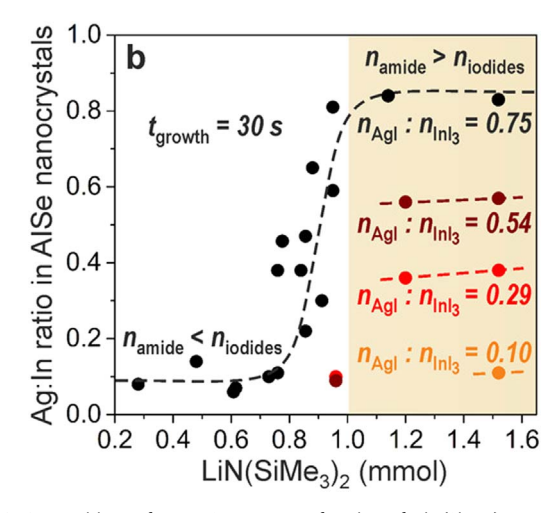


Fig. 12. Compositions of Ag-In-Se NPs as a function of LiN(SiMe₃)₂ amounts and AgI:InI₃ ratios while the growth time was maintained at 30 s. At high molar LiN(SiMe₃)₂ amounts relative to the counter Γ ions, the NP compositions reflected the starting metal stoichiometries. At low LiN(SiMe₃)₂ amounts, the NPs were In-rich. Adapted with permission from Ref. [68]. Copyright 2015 American Chemical Society.

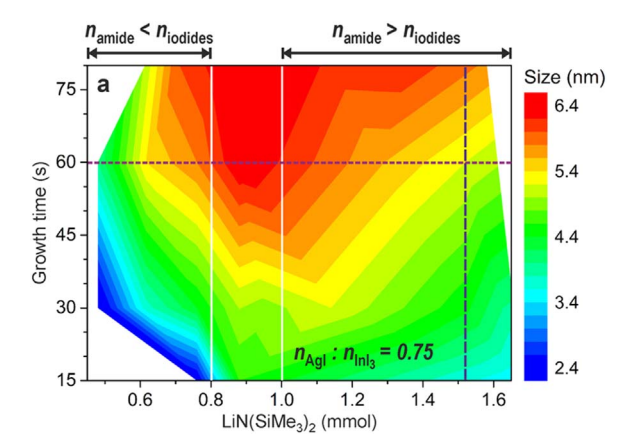


Fig. 13. Sizes of the Ag-In-Se NPs displayed as a function of the LiN(SiMe₃)₂ amount and growth time. The AgI:InI₃ molar ratio was held constant at 0.75. Adapted with permission from Ref. [68]. Copyright 2015 American Chemical Society.

starting metal precursors. Alternatively, when the silylamide molar amount was deficient relative to the iodide amount, the particles were In-rich, as shown in Fig. 12.

To explain this observation, the authors suggested the following reaction scheme, depicted in Scheme 6. Upon interaction of the metal iodide precursors with the Li silylamide, metal amide complexes form. These active species then react with TOPSe in order to form the Ag-In-Se NPs. The key factor was their suggestion that the In-amide had a much higher rate of formation than the Ag-amide $(r_{\rm In} >> r_{\rm Ag})$. When the silylamide amount was low, the difference between $r_{\rm Ag}$ and $r_{\rm In}$ was inferred by the In-rich NP compositions. When the silylamide was present in excess, the NP rate of formation was proposed to be the limiting step, and the NPs exhibited Ag:In ratios as supplied in the reaction solution.

The authors connected these observations with the HSAB principle as the hard base, $[N(SiMe_3)_2]^-$ should preferentially coordinate with

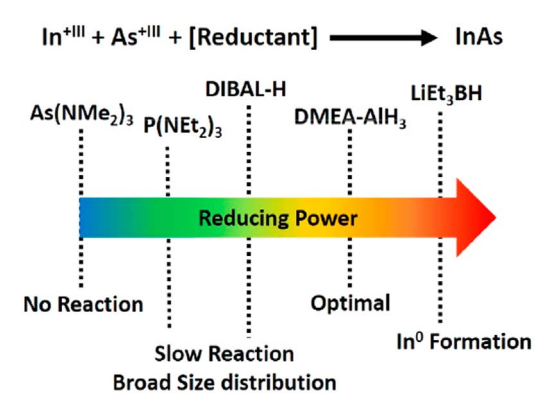
Scheme 6. Proposed reaction pathway for the formation of Ag-In-Se NPs. Reproduced with permission from Ref. [68]. Copyright 2015 American Chemical Society.

the hard acid, ${\rm In}^{3+}$ relative to the soft ${\rm Ag}^+$. Additionally, we offer support for this connection considering the metal precursors used were iodides. The soft base, iodide, would preferentially dissociate from ${\rm In}^{3+}$ over the ${\rm Ag}^+$ which could be an additional factor in the speculated differences in the metal amide rates of formation. This work exemplifies the potential for Li silylamide syntheses to not only be useful for forming smaller, more monodisperse NPs via enhanced nucleation but also as a possible handle for balancing the reactivities of multiple cations of varying HSAB character in a ternary compound.

Following, the amide-assisted approach was also applied to attain size and compositional control over the Cu-In-Te and Ag-In-Te NP systems in 2016 [14]. In translating the principles of the selenide system by substituting TOPTe for TOPSe, a difference in the reactivity of the two phosphine chalcogenides was found to be the major factor in the outcome of the reaction. Initially, a bimodal distribution of Cu-In-Te NPs was found to form which was attributed to TOPTe reacting with both metal amides and unconverted metal halides. The authors cited the higher reactivity of TOPTe relative to TOPSe. In order to promote the transformation of the metal halides to amides and push the NP formation to be the rate limiting step, the Li silylamide amount was increased. This demonstrated the utility of the proposed reaction mechanism from the Ag-In-Se study. Hypothesizing differences in the reaction rates based on the use of TOPTe, the authors were able to apply a straightforward adaptation and achieve size control over the Te-based NPs.

Additionally, these systems exemplify the sensitivity of controlling aspects such as composition and size dispersion. In the Cu-In-Te reactions, uncontrollable compositional control was observed at temperatures of 280 °C or greater; however, too low of a reaction temperature was also detrimental for the same parameter, as observed in the Ag-In-Te system. The inactivity of the In-amide complex below 220 °C resulted in Ag-rich ternary NPs as well as the side product, Ag₂Te. Compositional control was achieved in these syntheses by using slightly lower temperatures for the Cu system and by decreasing the initial amount of the Ag precursor for the Ag system. The reaction temperatures also influenced both systems in terms of size distribution. In the Cu system, temperatures at 240 °C or lower gave broad size distributions and featureless absorption spectra, while the NP nucleation rate in the Ag system was so swift that reducing the reaction temperatures narrowed size distributions. The variations in optimization of these parameters within these two highly related NP reaction systems displays the sensitivity and complex nature of rational design in NP synthesis. It can be highly difficult to tease out direct trends based on one synthetic parameter, and extrapolating the knowledge to other material systems does not often result in predictable effects. For a broader scope on the synthesis and compositional control of I-III-VI NPs, we refer the reader to the comprehensive review by Yarema et al. [69].

2.2.3.3. Role of the reducing agent for amide-assisted InAs OD synthesis. In amide-assisted syntheses, the strength of the metalamide bond may be large enough to require a reducing agent for optimized NP synthesis. A report in 2018 from the Talapin group focused on identifying the role of the reducing agent in the reaction of InCl₃ and As(NMe₂)₃ in OLA which produced more monodisperse InAs QDs [70]. Depending on the strength of the reductant, quantified by its hydride donating ability, varying QD products resulted. Outlined in Scheme 7, the weakest reducing power produced no reaction while slightly increasing the reductant's ability gave InAs products but with a broad size distribution. As the reducing ability of the reductant was increased and the precursor conversion rate increased, the size distribution narrowed which was explained within the LaMer model of nucleation and growth. The fast precursor conversion rate allowed a swift monomer supersaturation, causing a short nucleation burst. Shorter time scales of this nucleation period resulted in comparable growth times for the collection of particles and a smaller size



Scheme 7. General reaction equation for the formation of InAs QDs. Scaled description of reducing agents used in this work ranked in terms of reducing power alongside the observed effects on the NP reaction products. Adapted with permission from Ref. [70]. Copyright 2018 American Chemical Society.

distribution. Thus, increasing the power of the reductant exhibited a more monodisperse collection of InAs QDs. Using a reductant of greater strength than the optimal reductant identified in this study initiated an unwanted side reaction, reducing some In³⁺ to In⁰ NPs. Depending on the reactivities and stabilities of the metals involved, the reducing agent provided a handle for monodisperse NP formation.

The authors investigated the reducing ability of the compounds empirically by introduction to the precursor solution at RT and observed the solutions' color slowly change to red, proposed to be the formation of amorphous InAs clusters. The absorption spectra of the solutions were monitored over time, and a clear difference in precursor conversion rates could be identified, as depicted in Fig. 14.

This study stands as a good example of examining the role of one synthetic parameter, the reducing agent. Beyond simply connecting the synthetic variations with their respective reaction outcomes, the authors experimentally tested the hypothesis of the reductant strength affecting the precursor conversion kinetics. The authors discussed a standard property of the reductants, the hydride donor ability, but did not rely on it alone to explain the observed trends. Monitoring the evolution of precursor conversion via absorption spectroscopy provided some empirical evidence of how well the hydride donor ability stood as a predictive scale. An important strength of this test involved its inclusion of the NP reaction solvent system. Hopefully, in development of other NP syntheses involving reducing agents, the hydride donor

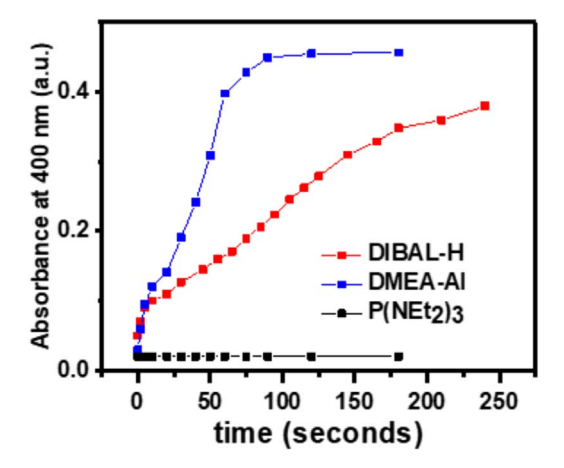


Fig. 14. The temporal evolution of absorption at 400 nm for solutions of various reducing agents following injection into the reaction mixture at RT. Reproduced with permission from Ref. [70]. Copyright 2018 American Chemical Society.

ability values could inform a mindful exploration of NP syntheses, accompanied with kinetic studies via spectroscopy. This study's system benefited from the precursor conversion kinetics existing on a suitably extended time scale when carried out at RT (as opposed to injection temperature) and from the signature red color of the conversion products. Beyond the scope of this specific example, it could be beneficial for NP synthetic studies to search for identifying, dynamic characteristics of precursor conversion and other processes during NP synthesis for empirical evidence of proposed reaction schemes.

2.2.3.4. Reaction mechanism of InN NP synthesis: in situ generation of $[NH_2]^-$ from alkylamides. In NP synthesis, alkylamides have also been extended to the synthesis of nitride materials, but an understanding of a reaction mechanism for nitrogen delivery has evaded the field. Previous studies found InN to form catalytically from metallic In core particles by the SLS mechanism [71-73], but the chemical mechanisms allowing the cleaving of the stable C–N bond have posed a significant question for the material's field.

In 2018, Chen et al. published a suggested reaction scheme for their synthesis of InN which involved injection of a Li alkylamide into an In halide/alkylamine solution [74]. Similar to the Co NP study by Liakakos et al. (see Section 2.2.3.1) [9], the authors studied the byproducts of the reaction mixture. Via ¹H NMR, secondary aldimines (R₁HC=NR₂) were detected which was supported by MS data identifying a m/z value corresponding to N-oleyl-oleylimine, the expected product from the condensation of two oleylamide compounds. This byproduct encouraged the authors to suggest the following reaction mechanism. Beginning with an oleylamide species (known to form from the combination of *n*-BuLi and OLA [65]) further oxidation would give the primary oleylimine. Due to the instability of these moieties, it was suggested to carry out condensation with another oleylamide forming the more stable secondary aldimine, the detected byproduct. The complete suggested reaction scheme is shown in Scheme 8 with the secondary aldimine formation depicted in steps 1a-b.

Two key points were raised related to the proposed mechanism for the aldimine formation: energy compensation of the C-N bond division and the formation of the amido group, [NH2]-. The breaking of one C-N bond was suggested to be compensated by the formation of one during condensation of the aldimine (step 1b). The amido group, [NH₂], was then hypothesized to be the active species for InN formation. Step 2 illustrates nitride formation from In³⁺, [NH₂], and two electron donors ([NH2]-, H-, or [RNH]- species). The observed side product In⁰ was described as likely stemming from reduction of In³⁺ by the hydride species, shown in steps R1 and R2. Supporting but not conclusive evidence resided in the detection of evolved H₂ during the reaction. The detrimental side reaction of the generation of NH₃ (S1) was also supported by its detection via gas chromatography. Additionally, the observation of higher In⁰:InN ratios than would be expected if all [NH₂] moieties were converted to InN suggested some of the active amido species were lost in the production of ammonia. The highest yield of InN relative to In⁰ was achieved with the use of a 3:1 alkylamide to In³⁺ ratio, as predicted by the scheme. All other precursor ratios resulted in lower yields of InN relative to In⁰. We point out this study as another detailed example in which byproducts of NP reactions were examined in order to backtrack a possible reaction mechanism with special consideration of many different reaction routes of the various interacting species present.

The authors noted the similarity in chemistry of this reaction mechanism with that of inorganic amides (NaNH₂) reacting with In salts, with the largest difference being an in situ formation of the [NH₂]⁻ species. Based on the findings of Kravchyk et al. on the in situ formation of oleylamide from *n*-BuLi and OLA [64], the important discovery of the generated [NH₂]⁻ in this reaction mechanism may

1/3
$$\ln^0 + 1/2 \frac{H_2}{R_1}$$

2/3 $\ln^0 + H^+$

R3

 H^+
 R
 NH
 NH

Scheme 8. Overall reaction scheme proposed for the transformation of alkylamide and In³⁺ precursors forming reduced In⁰ species and the desired product, InN. The in situ production of the proposed [NH₂]⁻ intermediate and active species for InN is outlined. Reproduced with permission from Ref. [74]. Copyright 2018 American Chemical Society.

inform future synthetic developments. Similar reaction conditions may allow synthesis of other nitride NPs. Additionally, the similarity in components and temperatures might spark questions regarding the ease of possibly forming metal nitride impurities in other metal NP syntheses. In exploring this possibility, it could be of use to employ the analytical techniques used in this study to identify the aldimine byproduct. If it were detected in other syntheses, the formation of $[NH_2]^-$ would be likely. While not guaranteed to react to form a metal nitride because it could completely convert to ammonia, these methods would provide some insight into this possible alternative hypothesis. This study points out the utility of adapting synthetic strategies to other material systems but emphasizes the need for continued critical examination and exploration of the new reaction mechanism without assuming the occurrence of exactly the same processes.

2.2.4. Metal amide NP syntheses of interest for further mechanistic studies

Next, we provide a non-exhaustive discussion highlighting a few metal amide studies in which further mechanistic exploration would be of interest. Considering the depth of knowledge gained in various NP material systems with similar reaction components outlined above, the following reports stand as intriguing examples to explore alternative hypotheses and reaction mechanisms.

2.2.4.1. Organoalkali compounds as proposed NP growth-directing agents. In 2008, Glaria et al. published a ZnO hydrolysis NP synthesis in which morphological differences were observed upon inclusion of different organoalkali compounds [50]. Generally, isotropic NPs formed upon the use of either LiNMe₂ or LiN(SiMe₃)₂, while

nanorods formed with the use of NaN(SiMe₃)₂ or in the absence of the organoalkali compounds (Fig. 15). Based on these three series of reaction conditions (varying the alkali compound from 1 to 10 mol% relative to Zn), the authors suggested Li ions were the key factor in mediating the NP growth. Two possible alternative hypotheses for the key factors in this reaction mechanism were considered, the generated amines (conjugate acids of the organoalkali compounds) and the tetrahydrofuran (THF) used to introduce the organoalkali compounds. Because of the volatility and likely early escape of HNMe₂, they ruled out the possible role of the amines. Also, since THF was used in each reaction and didn't appear to alter the morphology when the Na compound was used, its effect was dismissed.

Small differences were observed in NP size upon the use of the two different Li compounds with the particles being 0.6 nm larger on average when LiNMe₂ was used. To this, a possible variation in the hydrolysis rates of the two Li precursors was offered as explanation. In comparing the Li and Na silylamide compounds, the difference in ion size between the alkali metals was speculated to play a role because the size of Li is much more comparable to that of Zn than Na. While possible deposition of Li on the surface of the ZnO NPs may have played a role, possible differences in the reactivity of the Li and Na organoalkali compounds were not highly emphasized for morphological explanations. One could imagine altered acid-base chemistry of the mixture based on the use of either a Li or Na silylamide with effects extending to the hydrolysis reaction and nucleation of ZnO. This might affect NP morphology and size. Referring back to the Kravchyk et al. study, when different alkali silylamide compounds were used to form Sn/SnO₂, small differences in size and size dispersion were observed (see Section 2.2.2.5) [64]. This study reported simply the ability to

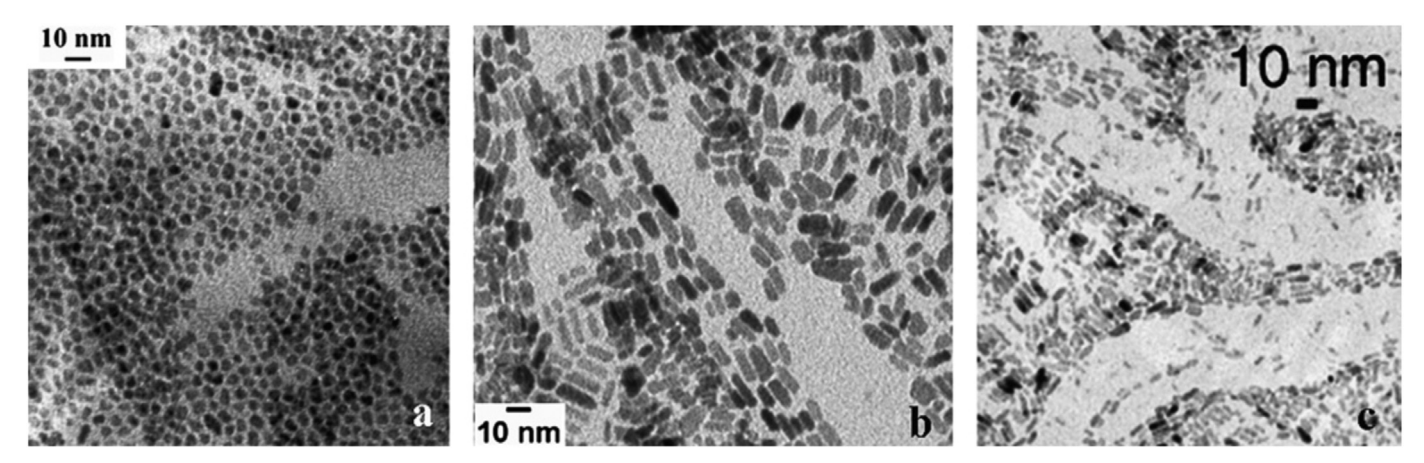


Fig. 15. TEM images of ZnO NPs formed from a hydrolysis reaction in the presence of (a) an organolithium compound, (b) an organosodium compound, and (c) the absence of an organoalkali compound. Reproduced with permission from Ref. [51]. Copyright 2009 Royal Society of Chemistry.

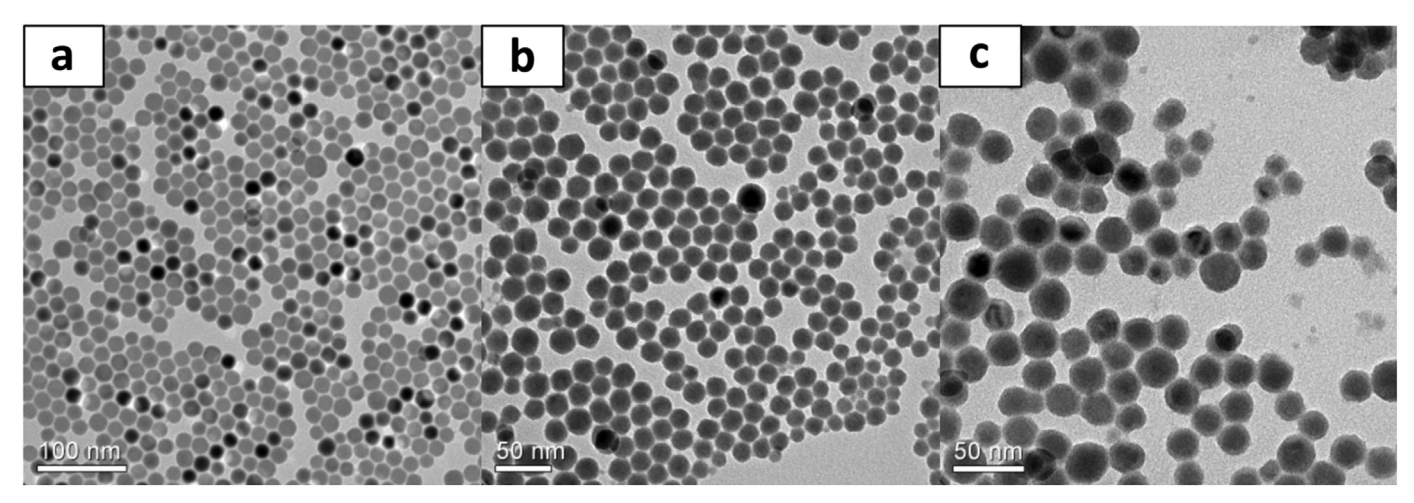


Fig. 16. TEM images of Sn/SnO₂ NPs synthesized by Kravchyk et al. using SnCl₂, diisobutylaluminum hydride, OLA, and a variable Brønsted base, specifically (a) LiNMe₂, (b) NaN(SiMe₃)₂, (c) KN(SiMe₃)₂. Reproduced with permission from Ref. [64]. Copyright 2013 American Chemical Society.

form small NPs from either LiN(SiMe₃)₂, NaN(SiMe₃)₂, or KN(SiMe₃)₂ (Fig. 16), but the size variations in Sn/SnO₂ seemed to be of similar magnitude to the size differences reported for ZnO. Additionally, because of the observed metal-oleylamide intermediates in the Kravchyk et al. study, it would be interesting to examine any possible role of the ZnO solvent, octylamine.

Based on the current understanding of amide-assisted syntheses, it could be of interest to examine the reaction mechanism for ZnO more closely. Gaining insight into possible solution pH changes based on variations of the organoalkali component might inform on the end product differences observed. Designing kinetic studies aimed at gaining knowledge on the nucleation of ZnO, perhaps by taking advantage of the luminescent properties of the end product, might advance the understanding of their formation. Additionally, characterization of the reaction solutions at different times might lend support or disprove certain hypotheses on possible reaction mechanisms. If a more conclusive role of the organoalkali compound could be identified, it would be interesting to explore the use of other analogous compounds.

2.2.4.2. Size tuning of Pb NPs by use of Sn and In silylamides. Lead NPs were formed by injection of Sn[N(SiMe₃)₂]₂ into a solution of Pb stearate by Zolotavin et al. in 2010 [75]. Two reaction mechanisms were suggested: a metathesis reaction forming a Pb[N(SiMe₃)₂]₂ intermediate for Pb⁰ as well as the decomposition of Sn-silylamide to Sn⁰ at a slower rate followed by electrochemical reduction of Pb²⁺ by metallic Sn. The second mechanism was explained by the 10 mV difference in chemical reduction potential between Sn²⁺ and Pb²⁺. Additionally, upon reduction of Pb stearate, Sn stearate was proposed to form which was then suggested to oxidize and form an amorphous lead-tin oxide shell. The authors proposed this mechanism based on literature, citing acceleration of this process by the presence of amines. This mechanism of shell oxidation was supported by a control reaction of alcohol reduction to Pb NPs and the observation of little to no oxide shell. In an attempt to eliminate the shell but still attain size control via silylamide synthesis, LiN(SiMe₃)₂ was used instead of Sn[N(SiMe₃)₂]₂. The formation of Pb[N(SiMe₃)₂]₂ was reported based on a yellow color observation followed by reduction to shell-less Pb⁰ but with low reaction yield and high size distribution.

Synthetic explorations for size control were carried out by attempting to manipulate the nucleation step and rate of shell growth. It was suggested that increasing the decomposition rate of the carboxylate salts would decrease the NP size. Based on the stated effect of amines facilitating the decomposition of Sn carboxylate salts, the authors introduced octadecylamine and indeed observed smaller NPs of ~4 nm

diameter compared to those previously made of ~11 nm. Manipulating the decomposition of the Sn and Pb silylamide compounds was also suggested to provide a handle for NP size control. An increase of the injection temperature and inclusion of $\text{LiN}(\text{SiMe}_3)_2$ in the $\text{Sn}[\text{N}(\text{SiMe}_3)_2]_2$ solution afforded NPs of diameters intermediate to the two sizes previously mentioned (7.7 nm). NPs of larger size, ~20 nm, could be attained by inclusion of indium acetylacetonate in the reaction mixture with the suggested explanation of a competitive side reaction in the formation of $\text{In}[\text{N}(\text{SiMe}_3)_2]_3$, resulting in a smaller number of nuclei and therefore bigger NPs. However, a smaller yield and a bimodal distribution with additional ~4 nm particles were observed. Simply lowering the Sn silylamide concentration did not provide larger NPs. Another explanation put forth was the possibility of the In compound affecting the shell formation.

Similar to the ZnO system [50], curious size tuning methods required for this synthesis might indicate higher complexity in the reaction mechanism(s) than originally thought. It would be interesting to explore the Pb NP formation with the use of LiN(SiMe₃)₂ to a greater extent because the reagent amounts weren't given. Taking the general synthetic strategy of He et al. [65], possibly using other Brønsted bases and/or including a reducing agent might allow a more straightforward and tunable reaction system. Additionally, because it is always possible for different material systems to exhibit unexpected reaction mechanisms, it would also benefit to examine the reaction solution analytically in order to identify intermediates and byproducts.

2.2.4.3. Pnictide silylamide precursors for ternary NPs. Nanoparticle syntheses of pnictide-containing ternary compounds using pnictide silylamide precursors have been developed by the Snee group in 2016 and 2017 [76,77]. Syntheses of Cu_3AsS_4 , InAs, and Cd_3As_2 NPs used the precursor [($Me_3Si)_2Nl_2AsCl$, As silylamide, which was promoted as safer and more stable relative to conventional arsenic precursors and was prepared in inert conditions from $LiN(SiMe_3)_2$ and $AsCl_3$ [76]. Following, a similar reaction strategy published by Das et al. allowed the formation of $AgSbSe_2$ and $AgBiSe_2$ through the use of metal silylamides ($M[N(SiMe_3)_2]_3$ where M = Sb, Bi), prepared from the metal halides and $LiN(SiMe_3)_2$ [77].

For the formation of InAs NPs, the authors discussed a proposed reaction mechanism beginning with the interaction of As silylamide and LiEt $_3$ BH (superhydride), suggesting the silylamide was reduced to [(Me $_3$ Si) $_2$ N] $_2$ AsH. This first step was investigated with 1 H NMR, and the following steps were investigated by computational modeling. In the NMR experimentation, As silylamide and superhydride were combined in toluene-d $_8$; however, this simplifies the reaction system by ignoring any role(s) of the solvents, ODE and OLA, or any possible

impurities therein. This appears to be especially important considering the As silylamide is dissolved in ODE and OLA prior to introduction of any other reaction components, including the reducing agent, superhydride. Considering the brevity of literature in which solvent components are considered innocent but in truth play large roles, these experiments seem a missed opportunity for elucidating a more complete reaction mechanism. While computational explorations would likely be hindered by taking such bulky solvent molecules into account, it would have been advantageous to explore their role in various analytical experiments, including NMR.

In the syntheses of AgSbSe2 and AgBiSe2, the use of reducing agents was found to be unnecessary to activate the pnictide silvlamide compounds. In fact, inclusion of a reducing agent in the synthesis of AgSbSe₂ resulted in a more polydisperse size distribution. Additionally, AgSbSe2 was formed via a hot injection NP synthesis while more monodisperse AgBiSe2 NPs resulted from a heat-up synthesis. For the AgSbSe2 NP synthesis, the choice of OLA and OA as solvents was discussed, identifying the amine as a softer coordinating moiety for the softer Ag⁺ cations and the harder oleate as a better coordinating base for the hard Sb³⁺ ions. An observation of the sensitivity of the system with respect to the combination order of precursors when preparing the metals injection solution was noted, stating the addition of AgNO3 followed by Sb[N(SiMe₃)₂]₃ into the solvent system, OLA and OA, was important for the product to show pure crystallinity. In order to understand their experimental observations, Das et al. carried out DFT calculations comparing the interactions of either SbCl3 or Sb[N(SiH₃)₂]₃ (a model compound for Sb silylamide) with a silveracetic acid complex. The calculations determined the halide salt formed a more tightly bound complex, indicating the significance of the amide ligands in enhancing the Sb reactivity with Ag. However, considered in vacuo from the surrounding solvent system, this interaction may not be accurately representative of the important reaction mechanisms taking place within the flask.

As seen in the Co NP system from Liakakos et al. [9], careful examination of reaction products (both solid phase and in solution) from seemingly unimportant procedural variations, such as order of precursor combination in this study or the rate of precursor addition in the Co study, can result in key findings to uncover influential chemical processes (see Section 2.2.3.1). Acknowledging the presence and possible transformations of the solvent system lends itself in identifying the effects that synthetic parameters have on the end products. Based on interactions between metal amide salts and OLA observed in the work by the Kovalenko group [64,65], the combination of these pnictide silylamide precursors with alkylamine solvents begs the question of whether the pnictides are complexed as suggested in the reaction mechanisms proposed. Additionally, because of the general success in this field of translating NP syntheses from the use of ex situ prepared metal silylamides to procedures combining metal halides, Brønsted bases, and solvent systems (often alkylamines), it would be interesting to explore whether these pnictide NP syntheses could be adapted similarly, eliminating the initial preparation of the pnictide silylamides. If the initial preparation of these pnictide silylamide precursors do appear to be necessary, then it would be compelling to characterize reaction solutions at all points throughout the procedure in order to gain better understanding about the formation of the end products. Identifying the active pnictide intermediates in these reaction systems might enable the choice of more direct synthetic routes to the same end. This would also provide insight advantageous for continuing the important work done in these studies: development of new, ternary material systems plagued by the lack of straightforward pnictide

2.2.5. Outlook on cationic precursors and use of metal amides in NP syntheses

This narrative highlighting the use of metal amides in NP syntheses, whether as precursors or possibly formed in situ, is not intended to be a

compendium of all amide-assisted syntheses but rather a demonstration of the impact that careful examination and characterization may have on NP synthesis. This has led to a rapid evolution in understanding the roles of constituent components in these reaction systems, including the cationic species, alkali bases, reducing agents, and the solvent system. While there are still questions to be answered, new mechanisms and pathways for consideration have been proposed. Because of the versatility shown for some of these synthetic schemes, it is important to consider how these processes might have an unintended effect on the development of new NP systems employing similar precursors and solvents. Further, strategies employed and limitations acknowledged are lessons that can be taken into account for the careful understanding and development of all solution-based NP systems.

2.3. Understanding reaction pathways

Studies exploring and manipulating reaction pathways widen the available qualitative kinetic and thermodynamic knowledge of a material system. This information can be utilized to access lower energy routes to desired phases, trap metastable phases, and attain novel products. Further, this knowledge can elucidate possible synthetic strategies for other systems, and as more reaction pathways are explored, patterns across systems could be revealed. Here we will discuss solution-based NP reaction pathways in reference to the evolution of amorphous and crystalline intermediates formed through the duration of a reaction toward an end product.

Reaction pathway studies are traditionally explored for bulk solid-state syntheses to understand the rate-limiting step, the diffusion of components, and finally the formation of the desired phase. Although bulk solid-state synthesis and solution-based NP synthesis differ in many ways, the desire to gain fundamental reaction pathway insights such as nucleation and growth exists in both fields. Here we draw parallels from bulk solid-state pathway studies with a non-exhaustive compilation of solution-based NP studies. These solution-based NP studies demonstrate the excitement but also difficulty in exploring reaction pathways due to the involvement of coinciding concepts drawn from different fields: solid-state chemistry, inorganic chemistry, coordination chemistry, and synthetic organic chemistry. Further, the studies discussed here exemplify the advances toward understanding reaction pathways and where the field can further grow.

2.3.1. Reaction pathway studies in bulk solid-state synthesis

Shoemaker et al. have studied reaction pathways of several different systems including K-Cu-S [78], K-Sn-S [78], Ba-Ru-S [79], and Fe-Si-S [80] using in situ XRD techniques. Specifically, Jiang et al. from the Shoemaker group employed in situ XRD to understand and manipulate the reaction pathway to Fe₂SiS₄ with the goal of producing Fe₂SiS₄ at a lower temperature [80]. Analysis of the in situ data for the reaction of the elemental compounds revealed the formation of Fe-S binaries and unreactive Si until the peritectic point of FeS2 which led to the formation of SiS2 and the desired ternary. The authors hypothesized that Si sulfurization was the slow step before the production of Fe₂SiS₄. They rationalized that combinations of pre-synthesized binaries with elemental compounds could aid in the navigation of kinetic pathways to bypass low Si reactivity and thus would require lower energy input for the end formation of Fe₂SiS₄. In support of this hypothesis, the evolution of Fe₂SiS₄ was observed at a lower temperature when presynthesized FeS and SiS2 were reacted, but ultimately they found the interaction between Fe₃Si and Fe₅Si₃ with elemental sulfur led to the lowest temperature formation of Fe₂SiS₄. Jiang et al. speculated the favorability of Fe sulfurization caused the dealloying of the Fe-Si binaries, leaving a defective Si network which allowed faster sulfuriza-

Jiang et al. established the value of characterizing reaction pathways both in their interpretation of the system's relative kinetics and

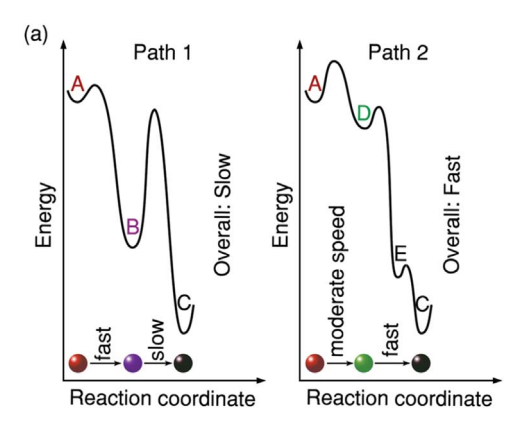
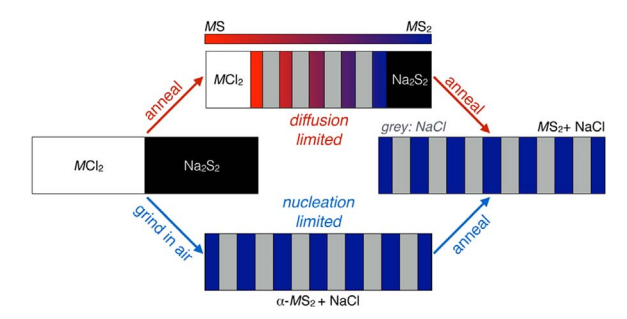


Fig. 17. Reaction coordinates comparing two Fe-Si-S reaction pathways for the reaction of Fe, Si, and S (A) to ultimately yield Fe_2SiS_4 (C). Following Path 1, the sulfurization of Fe leading to Fe-S binaries (B) was fast, but the sulfurization of Si to allow formation of Fe_2SiS_4 (C) was slow. Following Path 2, the synthesis of Fe-Si binaries (D) first allowed fast sulfurization of both Fe and Si to form Fe-S and Si-S binaries (E) and then Fe_2SiS_4 (C). Reprinted with permission from Ref. [80]. Copyright 2017 Royal Society of Chemistry.

thermodynamics and in their subsequent exploitation of this insight for targeted synthesis. In order to visualize these kinetic barriers and thermodynamic sinks en route to the desired product, coordinate plots were constructed (Fig. 17). Jiang et al. compared the coordinate plot of the reaction between elemental Fe, Si, and S (Path 1) with the coordinate plot of the reaction between pre-synthesized Fe-Si binaries and S (Path 2). In Path 1, the formation of the Fe-S binaries (B) acts as a thermodynamic sink, and the sulfurization of Si exists as a large kinetic barrier forming a trap state before the formation of Fe₂SiS₄ (C). Comparatively, in Path 2 the formation of the Fe-Si binaries (D) exploits the thermodynamic sink of Fe-S binary formation (E) to lower the kinetic barrier of the sulfurization of Si (E) and avoid a trap state. This study outlines a process to investigate reaction pathways and reveals a possible synthesis strategy. The general process of this study was the discovery of all solid-state intermediates followed by the manipulation of a parameter and the observation of the resultant intermediates. By investigating and manipulating the reaction pathway, Jiang et al. gained qualitative kinetic and thermodynamic insight and improved the low Si reactivity by pre-reacting it with Fe. In other words, they changed the precursor combination order to increase the reactivity of a specific precursor, a strategy that could be applied to other systems.

Martinolich et al. analyzed the reaction pathway of iron pyrite (FeS₂) using a process similar to the one outlined above [81]. A solidstate method, metathesis, was employed which couples a favorable, low enthalpy of formation product with a less stable product. In this case, Na₂S₂ was reacted with FeCl₂ to form NaCl, a favorable product, and FeS2, the desired though less favorable product. The FeS2 reaction pathway was analyzed using in situ XRD and determined to be diffusion limited, where an initial production of NaCl was fast but the diffusion of the resulting Fe and S systems was slow. In an effort to increase diffusion, Martinolich et al. tried mixing the precursors, Na₂S₂ and FeCl₂, by grinding. This was carried out in ambient conditions, and a black powder was formed but was indistinguishable by powder X-ray diffraction (PXRD) with the exception of NaCl. The powder was annealed at low temperatures (100-200 °C) resulting in the desired iron sulfide material. Analysis by PDF of the ground powder before annealing revealed the presence of metal-sulfur bonds but without long-range order. Subsequent annealing of the amorphous Fe-S intermediate to form the crystalline FeS2 product required a lower temperature than that for the air-free reaction because bonds did not need to be broken and formed, simply rearranged and crystallized. Martinolich et al. concluded this new pathway was limited by nucleation.



Scheme 9. Schematic of two accessible metathesis reaction pathways toward the same end products, FeS_2 (labeled here as MS_2) and NaCl. The top approach, heating precursors Na_2S_2 and $FeCl_2$ (MCl_2) in a sealed quartz tube under vacuum, was diffusion limited. The bottom approach, grinding the same precursors in ambient air followed by annealing, was nucleation limited. Reprinted with permission from Ref. [82]. Copyright 2017 American Chemical Society.

Similar to the Jiang et al. study, Martinolich et al. gained qualitative kinetic and thermodynamic insight through the investigation of intermediates accessed and the exploration of alternative pathways. Although reaction coordinates were not constructed, they observed a change in the rate-limiting step when the appropriate reaction conditions were altered (Scheme 9). Moreover, this pathway understanding was applied in the formation of CuSe₂, both the thermodynamically stable marcasite and the metastable pyrite phase, by reacting Na₂Se₂ with CuCl through the diffusion-limited and nucleation-limited pathways, respectively [82].

From these solid-state studies, a process to analyze the reaction pathway of a system stands out, and some of the advantages of studying reaction pathways become clear. The studies demonstrate that identification of intermediates along the reaction pathway can allow for strategic variation for targeted synthesis. The value of reaction pathway studies lies in this ability for reaction pathway manipulation. Targeted syntheses could include producing the same product but at a lower temperature (Jiang et al. [80]), forming a metastable product (Martinolich et al. [82]), accessing different products in a system of elements or a desired morphology, etc. As more reaction pathway information is uncovered by the general approach outlined in these solid-state examples, more synthetic strategies and cross system patterns can be discovered.

2.3.2. Reaction pathway studies in NP synthesis

The bulk solid-state examples above outline the parameter manipulation and the study of intermediate crystalline and amorphous phases as key steps in investigating reaction pathways. These steps are also explored in solution-based NP syntheses, but limitations (primarily in characterization methods readily available) and holes exist within these studies, presenting an exciting area for further exploration. The NP pathway studies we focus on use heatup and hot injection methods and change the reaction pathway through parameters such as precursor order combination and precursor ratios. We acknowledge that these are not the only approaches toward manipulation of NP synthesis pathways, but for the scope of this review, we hope these examples can highlight the importance of careful reaction pathway investigation and possible future strategies.

Heat-up and hot injection methods are common for solution-based NP synthesis due to their ability to produce uniform particles, though the nucleation steps for each method differ. Nucleation in NP syntheses is understood through the LaMer model that describes these two methods [83–85]. In both hot injection and heat-up reactions, historically, the "start" of the reaction is often thought to be nucleation. Specifically, nucleation is perceived as the direct formation of the desired phase. After nucleation, the growth of the desired product is described by the addition of monomers. This commonly used classical nucleation model often does not describe the entirety of solution-based

NP synthesis well. This is due to possible interactions, transformations, or reactions occurring before and/or after the nucleation event of the desired phase (Scheme 1). We believe a wider range of possible interactions and transformations should be included in standard NP synthetic models. This is not to say traditional models cannot be used to describe any NP synthesis. Traditional models could be applicable for individual reaction pathway steps (e.g. the formation of an intermediate phase), but models describing full reactions must further consider all mechanisms and pathways. For expansion of these models, first NP mechanisms and pathways must be investigated. We will discuss NP pathway studies in a fashion that mirrors the previously discussed solid-state studies. Some NP studies that explored the phase space of a system of elements to reach various end products, which inherently alters the reaction pathway, are highlighted. Pathway insight is gained when NP studies identify intermediates. Ultimately, a more comprehensive understanding of NP syntheses is achieved when pathway insight is investigated through both exploration of phase space and characterization of intermediates.

2.3.2.1. Exploring reaction phase space by altering synthetic parameters. In NP synthesis, a common strategy for understanding a material system is to vary parameters and then characterize the end products. These investigations acknowledge that the reaction pathway is altered due to different end products achieved, but the identification of possible solid-phase intermediates is left unknown. Rather, these studies discover the appropriate reaction conditions to achieve various targeted phases and thus elucidate the phase space available for a system of elements.

A study by Ramasamy et al. explored the Cu-Sb-S family by keeping the synthesis method, injection order, and cationic precursor identities constant but varying the Cu:Sb ratio, anionic precursor identity, and temperature [27]. The synthetic parameter changes and the product outcomes were compiled into a table (Table 1 in Section 2.1.4). illuminating trends. As long as the temperature was over 190 °C, the evolution of CuSbS2 was only dependent on the Cu:Sb ratio (1:1). Conversely, synthesis of Cu₁₂Sb₄S₁₃ depended on both the Cu:Sb ratio (3:1) and temperature, which required 150 °C or higher. Finally, production of Cu₃SbS₄ or Cu₃SbS₃ was dependent on all three variables. The synthetic conditions for all four Cu-Sb-Se ternary phases were determined which allowed trends to be seen. For example, qualitative thermodynamic information was realized due to certain phases (e.g. Cu₁₂Sb₄S₁₃) requiring a higher reaction temperature compared to others (e.g. Cu₃SbS₄). Additionally, the observed product dependence on one, two, or all three variables illustrates the complexity in optimizing parameters for a desired product. By changing the Cu:Sb ratio, anionic precursor identity, and reaction temperature, Ramasamy et al. determined the phase space of the Cu-Sb-S system. Additionally, synthesizing different desired products inherently allowed the authors to access various reaction pathways, but minimal pathway insight was gained. Further insight about how and why the pathway was altered when a parameter was changed could have been established by characterizing intermediates for the different reactions.

Some solution-based NP phase space investigations use general chemistry concepts related to precursor reactivity and thermodynamics to rationalize why tuning certain reaction parameters results in different products. For example, Wang et al. probed the phase space of Cu₂SnSe₃ NPs [86]. Optimization of NP synthetic conditions for the cubic (R3) and the wurtzite (R1) phases aided in understanding the formation of polytype NPs. Linear (R2) and tetrapod (R4) heterostructures formed via seeded growth of one phase off a core particle of the other. Reaction solution temperature, precursor composition, and order of precursor introduction stood as the most influential parameters for optimizing NP growth; the details are listed in Table 3. The metastable wurtzite phase NPs required lower temperatures (220-280 °C) and a Se precursor of higher reactivity (diphenyl diselenide) than for the cubic phase NPs. These reaction conditions were rationalized by their alignment with faster reaction rates which should favor the dynamically stable wurtzite phase. In contrast, the thermodynamically stable cubic phase required higher reaction temperatures (255-310 °C) and a Se precursor of lower reactivity (elemental Se). Phase-pure cubic NPs additionally required further cation precursor tuning in order to balance reactivities of all components to avoid binary impurities. The optimization of the two polytype heterostructure NPs benefited from the correlation of these reaction conditions and the resulting preferential phases. The majority of the insight gained in this report was identified via manipulation of reaction parameters and careful analysis of the end NP products. The wurtzite NP synthesis was the only synthesis for which the role of an intermediate was mentioned; the NPs were reported to always form by Sn insertion into a Cu-Se binary. However, neither data characterizing this intermediate nor further analysis of this reaction pathway was presented. This report stands as an example of the wide phase space accessible via this strategy of NP synthetic exploration.

Establishing the available phase space of a system allows for control of reaction pathways because various pure products can be reached. However, without identifying solid-phase intermediates, the majority of the reaction pathway is left unknown. Further, by only characterizing the end products, results could easily be interpreted based on simple models of direct nucleation and growth or lead to non-evidence based predictions, neither of which should be assumed. Extended insight into material families should include more extensive investigation of the individual pathways to elucidate the evolution of possible intermediates en route to the end NP.

Table 3
Reaction parameters for the synthesis of wurtzite, cubic, and polytype heterostructures of Cu₂SnSe₃. Reproduced with permission from Ref. [86]. Copyright 2014 American Chemical Society.

Reaction	Phase	Precursors in Flask	Injected Precursors	Injection Temperature	Growth Temperature	Shape
R1	Wurtzite	Ph ₂ Se ₂ , Cu-Oleate	Sn(Ac) ₄	230 °C	240 °C for 30 min	
R2	Polytype 1	Ph ₂ Se ₂ , CuCl, SnCl ₂	No injection	njection No injection 310 °C fo 60 min		
R3	Cubic	Se	CuCl, SnCl ₂	300 °C	300 °C for 5 min	
R4	Polytype 2	CuCl	Ph ₂ Se ₂ , Sn(Ac) ₄	290 °C	280 °C for 15 min	4

2.3.2.2. The evolution of intermediates in NP reaction pathways: a complex multinary (CIGSe) system. Ahmadi et al. used ex situ PXRD plus ex situ transmission electron microscopy (TEM) to thoroughly investigate the evolution of solid-phase intermediates toward CIGSe formation [87]. In their synthesis, CuCl, InCl₃, and Ga(acac)₃ were mixed in hexadecylamine (HDA) and heated to 130 °C at which point Se in HDA was injected. Following Se injection, the authors initially observed crystalline CuSe and CuGaSe2 as well as amorphous Se and In₂Se₃ particles. With complementary ex situ TEM, Ahmadi et al. proposed a scheme for the production of CIGSe (Fig. 18). The TEM images showed CuSe, the major phase with the largest particle size, transformed into CIGSe as time and temperature increased. Expanding upon simply the observation of solid-phase components present, they reported the transformation occurring in the following way. Initially, CuSe formed due to the reported ability for Cu2+ to complex with two HDA molecules (instead of three, as In³⁺ and Ga³⁺ are suggested to do) making it more reactive. Moreover, in this system, Cu²⁺ and Se²⁻ are the most compatible HSAB pair. The observation of In₂Se₃ was also reasoned using HSAB. Since In³⁺ is less electronegative than Ga³⁺, it is considered softer than Ga³⁺ and would more readily react with Se²⁻. Hence, instead of the formation of a Ga-Se binary, they predicted Ga-HDA reacted with the evolved CuSe to produce CuGaSe₂. As the temperature rose, In₂Se₃ was said to dissociate while Se and CuSe dissolved to form two quaternary CuIn_xGa_{1-x}Se₂ phases with different In:Ga stoichiometries. Finally, after an additional 60 min at 230 °C, monophase CuIn_{0.5}Ga_{0.5}Se₂ was detected.

This study exemplifies the challenges that multinary systems possess in that intricate pathways do not always proceed by initial nucleation of the desired phase followed by growth. Initially, various crystalline or amorphous intermediate phases can evolve, and then consumption, conversion, coalescence, or a combination of these pathways can occur to finally nucleate the end phase (Scheme 1). Ahmadi et al. gave vague descriptor words (e.g. dissociate and dissolve) to describe chemical interactions occurring between intermediates to yield CIGSe but didn't specify whether these transformations occurred through conversion, coalescence, and/or consumption (Scheme 1). However, controllably ruling out one route versus another is difficult

due to current characterization techniques, nucleation and growth models, and understanding of complex nucleation events. Additionally, since these pathways could be occurring simultaneously, deconvoluting the collected data to isolate signatures of a single pathway would be ambitious, but these limitations demonstrate the vast opportunities to further understand reaction pathways. Moreover, to lend more information to this complex CIGSe system, parameters could be varied to alter the reaction pathway. This would elucidate accessible phase space, possible synthetic strategies, and provide evidence toward the possible qualitative kinetics and thermodynamics at play in this system.

2.3.2.3. Reaction pathway studies through the identification of intermediates and varying reaction parameters. Thus far, we have discussed NP studies that have either investigated a systems' phase space by manipulating reaction parameters to elucidate various possible end products or explored the evolution of intermediates. These studies highlight the importance of each in understanding reaction pathways but also the holes left if only one is investigated. Here, we discuss the possibility of expanded reaction pathway knowledge from reports that have studied intermediates and tuned reaction parameters as a result of the knowledge of the intermediates present. Further, we highlight the obstacles and limitations within these NP pathway studies.

2.3.2.3.1. Reaction pathway study of In_2O_3 . Hutfluss et al. studied a phase transformation for In_2O_3 NPs [88]. This binary system of constant stoichiometry is relatively simple, but the authors identify and study the complexity of the phase transformation reaction pathway. The In_2O_3 phase transformation proceeded from the metastable, rhombohedral phase $(rh\text{-}In_2O_3)$ to the thermodynamically stable, cubic phase $(bcc\text{-}In_2O_3)$ and was examined by ex situ PXRD, extended X-ray absorption fine structure (EXAFS), TEM, and modeling techniques. The phase transformation was observed in NPs prepared by the addition of $In(acac)_3$ to OLA at various molar ratios (1:20, 1:16, or 1:12) followed by heating to various temperatures over a 60 min time interval. Once the desired temperature was reached, aliquots were removed over time, and the phase content was

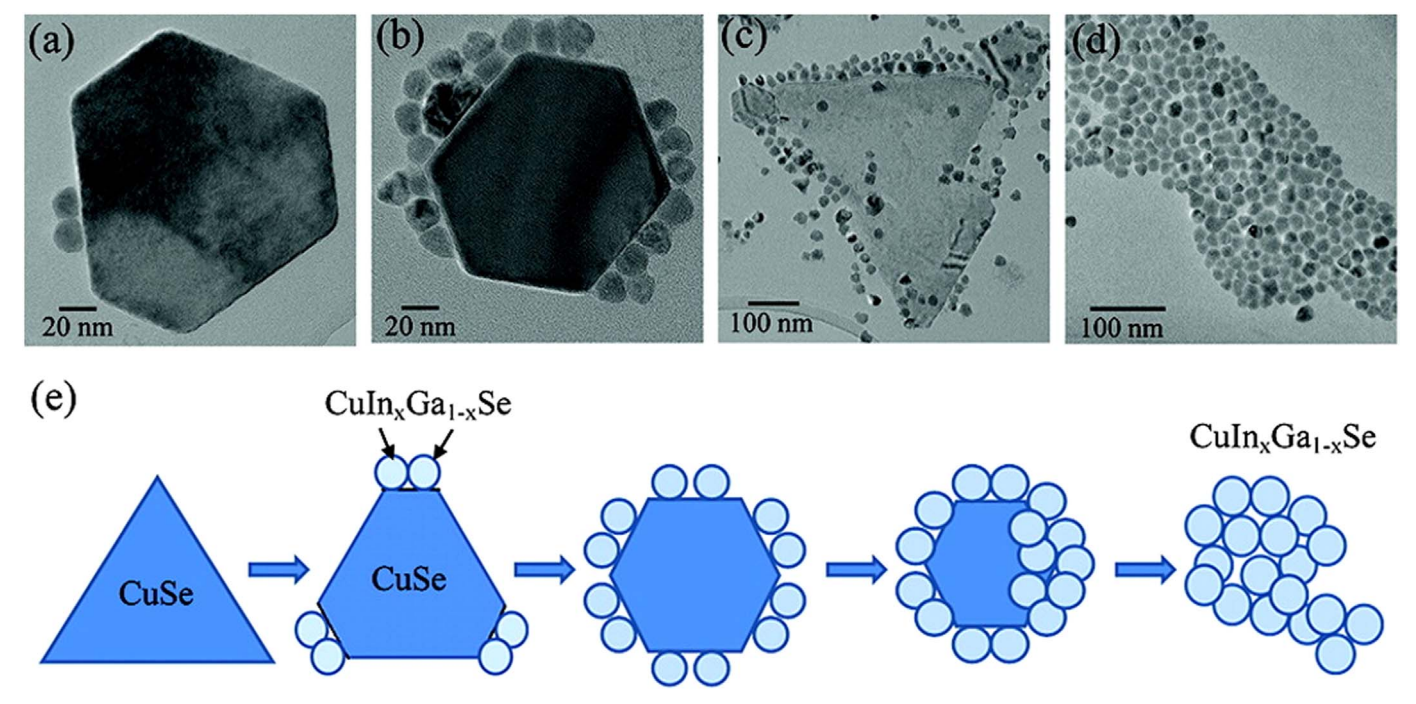
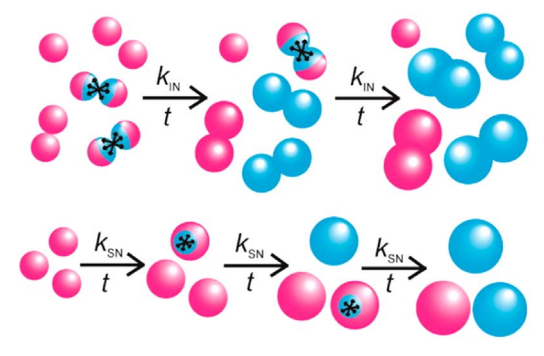


Fig. 18. TEM images of the reaction pathway evolution of CuIn_xGa_{1-x}Se at different time and temperature points, (a) 10 min at 130 °C, (b) 20 min at 160 °C, (c) 40 min at 200 °C, and (d) 60 min at 230 °C, which is represented by (e) the pictorial scheme. Reprinted with permission from Ref. [87]. Copyright 2012 American Chemical Society.

analyzed. The authors used a linear combination of reference diffraction patterns for pure rh-In2O3, bcc-In2O3, and InOOH (a known intermediate) samples to calculate the phase content. This was complemented by EXAFS. We want to bring attention to the use of linear combination over Rietveld refinement. Broadened XRD peaks as a result of smaller crystallite sizes in NPs can be troublesome for fitting data with Rietveld refinement. Hutfluss et al. attempted to account for various particle sizes by compiling reference patterns at various reaction temperatures, but only two temperature data sets were shown and further descriptions of the reference peaks were also limited. This reiterates the frequent limitations that occur in investigating the chemical interactions and transformations of solution-based NP systems. However, linear combination seemed to be successful in characterizing the phase transformation because the particle sizes determined by linear combination matched the particle sizes measured in TEM.

Values related to phase content and crystal size were extracted from the linear combinations of the XRD patterns and fitted to two nucleation models to investigate the phase transformation. These included: (1) interface nucleation where two particles must collide and form a nucleation site or (2) surface nucleation where nucleation sites form on individual particle surfaces (Scheme 10). From the modeled fits, they found the phase transformation occurred through two separate mechanisms depending on temperature and precursor concentration. At lower temperature and/or precursor concentration, the phase transformation occurred by surface nucleation, but at higher temperature and/or precursor concentration, the process occurred by interface nucleation which was attributed to an increased probability of collision. Additionally, the inspection and comparison of TEM images of aliquots taken during each reaction reinforced the hypothesis for the occurrence of the two different mechanisms (Fig. 19). Here, Hutfluss et al. noticed the high concentration sample consisted of dumbbellshaped particles compared to the presence of mostly spherical particles in the low concentration sample. The authors suggested this signified the dominance of interface or surface nucleation depending on high or low precursor concentration, respectively. Interestingly, they stated that a few small dumbbell-shaped, rh-In₂O₃ particles (Fig. 19d) were also observed in the low concentration sample. Because these particles were non-transformed, still rhombohedral, and smaller than the critical size at which phase transformation occurs for In2O3, they speculated these small dumbbell particles weren't evidence of interaction nucleation occurring at low precursor concentration.

In summary, Hutfluss et al. manipulated the phase transformation nucleation pathway of ${\rm In_2O_3}$ by controlling the precursor concentration and/or the temperature of the reaction. We want to highlight that, even when only one precursor is used and the same end product is formed,



Scheme 10. Cartoon indicating control over the nucleation pathway of the In₂O₃ phase transformation from rh-In₂O₃ (pink) to bcc-In₂O₃ (blue) depending on the concentration of In(acac)₃ in OLA. High concentration proceeds through interface nucleation (IN) and low concentration proceeds through surface nucleation (SN). Reprinted with permission from Ref. [88]. Copyright 2015 American Chemical Society. (For interpretation of the references to color in this figure legend, the reader is referred to the web version of this article.)

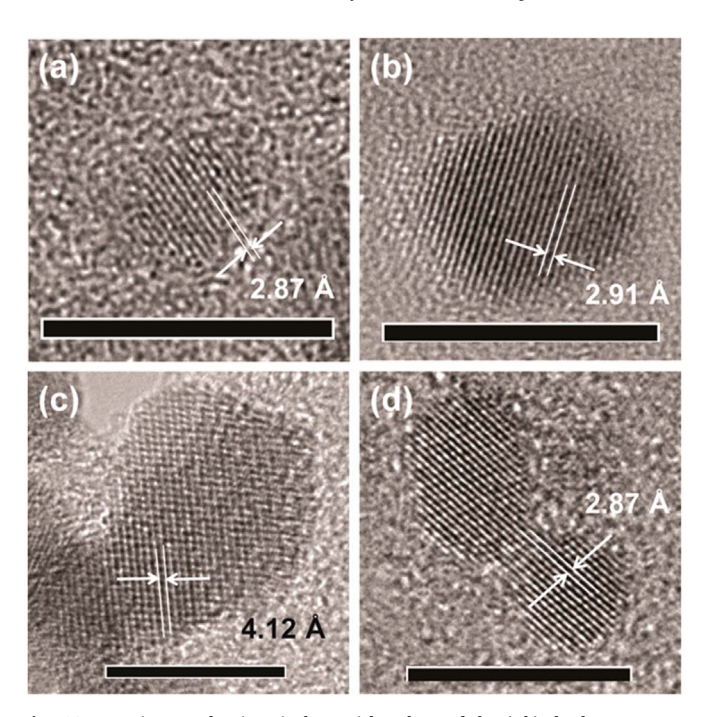


Fig. 19. TEM images showing single particles observed for (a,b) the low precursor concentration (In:OLA molar ratio = 1:20) reaction after 5 h at 200 °C and (c) the high precursor concentration (In:OLA molar ratio = 1:12) reaction after 2 h at 200 °C. Image (a) was identified as rh-In₂O₃ and (b) was identified as bcc-In₂O₃, supporting surface nucleation. Comparatively, (c) the dumbbell particle was identified as bcc-In₂O₃, supporting interface nucleation. Image (d) is an example of a dumbbell rh-In₂O₃ particle under the critical size in the low precursor sample. Reprinted with permission from Ref. [88]. Copyright 2015 American Chemical Society.

changing a common synthetic parameter can change the chemical interactions of the reaction components. This demonstrates the complexity of understanding the evolution of solid-state intermediates in a systems' pathway and the non-innocent impact small changes may have, similar to mechanistic studies. This is not to be a deterrent but rather to point out the vast opportunities for exploration in NP syntheses. Despite the challenging nature of these types of studies, the field of NP synthesis stands to benefit from the application of these characterization and synthetic strategies to other material systems.

2.3.2.3.2. Reaction pathway study of CuInSe₂. Kar et al. investigated the evolved solid-state intermediates in the formation of a ternary system, CuInSe₂, and the effect of precursor injection order on the pathway [89]. Precursors, CuCl, InCl₃, and Se, were individually dissolved in OLA and injected into a separate flask of OLA at 130 °C (original reaction (OR), Table 4). Then, as the reaction was heated to 275 °C, aliquots were removed and analyzed by ex situ PXRD and field effect scanning electron microscopy (FESEM). Immediately after addition of all three precursors, hexagonal γ -CuSe particles formed and grew, and at 195 °C cubic InSe and chalcopyrite CuInSe₂ particles were observed. The disappearance of the InSe and CuSe peaks correlated to the increase of the CuInSe₂ peaks above 210 °C which led the authors to the pathway hypothesis that the dissolution of the InSe and the CuSe particles yielded the ternary product.

In an attempt to support their reaction pathway hypothesis, Kar et al. reacted pre-synthesized CuSe and InSe particles in OLA at 275 °C (Control 1 (C1), Table 4). The reaction of the pre-synthesized binaries did lead to CuInSe₂, but interestingly, it led to the sphalerite CuInSe₂ instead of the chalcopyrite phase, as observed in the original reaction. The system's reaction pathway was more complex than the binary Cu and In selenides reacting, as originally proposed. The authors revised their hypothesis to the evolution of the sphalerite phase from an

Table 4

Reaction conditions and the resulting CuInSe₂ phase for the original reaction (OR) and the six control reactions (C1-6). Adapted with permission from Ref. [89]. Copyright 2011 American Chemical Society.

Reaction	Initial Flask Content	Injection 1	T_{1i}	Injection 2	T_{2i}	T_{f}	Product
OR	OLA	CuCl-OLA, lnCl ₃ -OLA, Se-OLA	130 °C	N/A	N/A	275 °C	Chalcopyrite
C1	OLA	CuSe, InSe	130 °C	N/A	N/A	275 °C	Sphalerite
C2	CuSe-OLA	lnCl ₃ -OLA	280 °C	N/A	N/A	280 °C	Chalcopyrite and Cu _{2-x} Se
C3	CuCl-OLA	lnCl ₃ -OLA	130 °C	Se-OLA	275 °C	275 °C	Sphalerite
C4	CuCl-OLA	Se-OLA	130 °C	lnCl ₃ -OLA	275 °C	275 °C	Chalcopyrite
C5	CuCl-OLA	lnCl ₃ -OLA, Se-OLA	275 °C	N/A	N/A	275 °C	Sphalerite
C6	CuCl-OLA	Se-OLA	275 °C	lnCl ₃ -OLA	275 °C (30 min later)	275 °C	Chalcopyrite

interaction between In and Cu selenide binaries and the evolution of the chalcopyrite phase from an interaction between CuSe and dissolved InCl₃ in OLA. The authors performed several control experiments (C2–6, Table 4) to support this new hypothesis and demonstrated the ability to switch reaction pathway by varying the precursor injection order to favor different end products. For example, when the In and Se precursors were added to CuCl-OLA together (C5), they believed copper and indium individually reacted with selenium to form binaries before resulting in the formation of the sphalerite phase. Comparatively, given a 30 min dwell time between the injection of the Se and In precursor (C6), Cu/Se binaries were suggested to form first and react with the dissolved InCl₃ precursor to form the chalcopyrite phase.

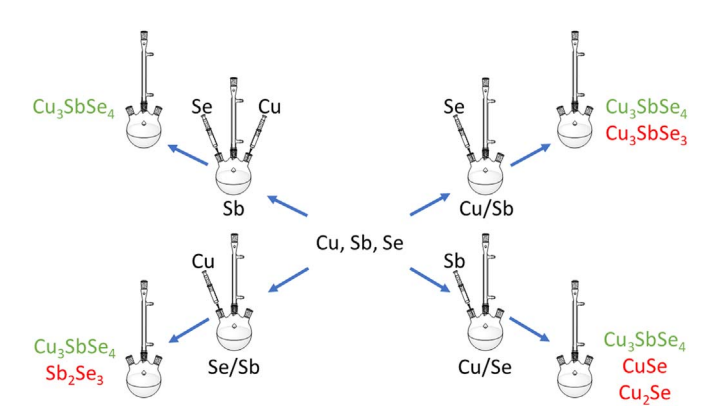
Similar to the Jiang et al. [80] and Martinolich et al. [81,82] solid-state pathway studies, this work first studied the evolution of intermediates and then altered a parameter to understand how the pathway was affected. Using this process, Kar et al. were able to demonstrate reaction pathway control [89]. By manipulating the precursor combination order, the majority phase could be switched between sphalerite and chalcopyrite. More importantly, Kar et al. demonstrated the necessity of control reactions and alternative hypotheses in reaction pathway studies. After initially identifying the evolution of intermediates and hypothesizing the interactions occurring to form chalcopyrite CuInSe₂, Kar et al. performed a control experiment (C1) that led them to suggest an alternative hypothesis and explore the effect of precursor injection order. Without performing this control reaction, Kar et al. might not have further explored the reaction pathway of CuInSe₂ and found that the pathway could be altered to favor either the chalcopyrite or sphalerite CuInSe₂.

However, we also want to call attention to areas where further studies could enhance the understanding of the reaction pathway. Kar et al. characterized intermediates only by PXRD and FESEM, which were inconclusive in confidently determining a truly phase-pure product because the diffraction patterns for these two CuInSe₂ phases are too similar, as will be discussed in further detail (Section 3.2.1). Additionally, in reference to the control experiments, the only reported evidence was the phase of the end CuInSe₂ product. The intermediates formed during these reaction variations were speculated in the explanation of their results, but it was not evident that aliquots were taken at various stages of the reaction to support the suggested transformations. Therefore, to strengthen their argument, possible future studies could include determination of the control reaction intermediates by ex situ TEM, XRD, and complementary characterization studies. These additional studies could lend support or potentially disallow the current reasoning for the observed pathways. Overall, Kar et al. found valuable information about the reaction pathway of CuInSe2 by carrying out a similar process as outlined in the solid-state examples. From this study, the importance of thoughtful, meticulous controls that explore alternative hypotheses is exhibited.

2.3.2.3.3. Reaction pathway study of the Cu-Sb-Se system. In submitted work from our group, Agocs et al. investigated reaction

pathways to Cu₃SbSe₄ NPs by both the evolution of intermediates and the order of precursor introduction [90]. Consequently, a swifter synthesis of smaller Cu₃SbSe₄ NPs was achieved. The procedure of the initial synthesis involved the injection of a CuCl₂/OLA solution into a Se/SbCl₃/OLA solution at 200 °C (Scheme 11). After at least a 4 h growth, the products were studied by ex situ XRD and TEM. Agocs et al. saw the presence of Sb₂Se₃ prior to and after Cu injection which initiated the formation of Cu₃SbSe₄ concurrent to the Sb₂Se₃ peaks slowly diminishing. This led to the hypothesis that the incorporation of Cu to form Cu₃SbSe₄ was slow. Similar to the Jiang et al. solid-state study [80], Agocs et al. explored variations in the precursor introduction order to avoid the formation of the Sb₂Se₃ binary and the slow transformation pathway [90]. A double injection of Cu and Se solutions into an Sb solution provided phase-pure Cu₃SbSe₄ NPs accessible in a 5 min growth rather than after at least a 4h growth (Scheme 11).

This report focused on the electronic measurements of the resulting NP films and, therefore, did not detail further investigations of the double injection pathway nor report on the other injection orders that led to impurities, which are summarized in Scheme 11. All possible single injection precursor additions were carried out while temperature and time were kept constant at 200 °C and 5 min. Similar to Ramasamy et al. [27], Agocs et al. explored the phase space of a system, but other than the initial reaction (Cu injection into the Sb and Se solution), the intermediates were not identified [90]. Although the results of these syntheses were not the desired product, their investigation may spark ideas for reaction pathway hypotheses. Evidence supporting possible interactions and transformations would result from a multi-faceted analytical approach. If these "failed attempts" were explored, the results could potentially uncover differing intermediate phases. These could then be used to establish a qualitative reaction landscape of this



Scheme 11. Schematic representation of the Cu-Sb-Se system demonstrating the effect of injection order on the reaction pathway by yielding different end products. All reactions were carried out with the same injection temperature and growth time. Green represents the desired phase and red represents the impurity phases observed. (For interpretation of the references to color in this figure legend, the reader is referred to the web version of this article.)

system that might aid in determining a synthetic strategy for other systems.

2.3.3. Outlook for solution-based NP reaction pathways

From the studies discussed in this section, the advantages, gaps in understanding, and limitations of exploring reaction pathways were illuminated. These present an exciting future for the solution-based NP synthetic field. Here, we discuss reports that represent the direction we think solution-based NP pathway studies are headed.

2.3.3.1. Pathway exploration of Li-Zn-Sb using WANDA. The Vela group explored the accessible pathways of the ternary Li-Zn-Sb system [37] using an automated, high throughput system called WANDA [91] (Workstation for Automated Nanomaterials Discovery and Analysis). White et al. were able to efficiently explore the effects of a wide range of injection and reaction temperature, time, precursor concentration, and precursor injection order as well as remove aliquots mid-reaction for analysis [37]. The information gained allowed them to produce a phase diagram that accesses five Li-Zn-Sb phases (metal, binary, and ternary) as a function of growth temperature and time (Fig. 20). This is an uncommon feat for the NP community but was achieved here due to WANDA providing an outlet for relatively rapid exploration of a wide range of reaction conditions and broad exploration of the material's phase space. Additionally, through this synthetic exploration, White et al. discovered a previously unobserved extended hexagonal LiZnSb structure (h*-LiZnSb). They delved into understanding the reaction pathway for the formation of this structure by characterizing aliquots with XRD, TEM, and X-ray photoelectron (XPS). Directly after the Sb spectroscopy (triphenylstibine) was injected into a solution of the Li and Zn precursors (n-butyllithium and diethylzinc in ODE and TOP), Zn seeds were observed. An amorphous Sb shell formed around the Zn seeds through interfacial solid-state diffusion. The authors hypothesized that through Li intercalation, h*-LiZnSb was formed. However, they were straightforward about the inability of the data collected to support this Li intercalation hypothesis. Overall, White et al. were able to use WANDA to probe various reaction conditions which enabled them to produce a phase diagram for the Li-Zn-Sb system and explore the pathway of the previously unobserved h*-LiZnSb phase. We want to point out that WANDA is a free and available technique to any researcher who intends to publish results. Proposals to use WANDA can be submitted to the Molecular Foundry research center, located in Lawrence Berkeley National Labs.

2.3.3.2. Reaction coordinate plot of InP QD synthesis. The Cossairt group attempted to control nucleation and growth of InP QDs to address poor size dispersity observed in past syntheses of InP [92]. By optimizing the reactivity of the phosphorus precursors, the authors

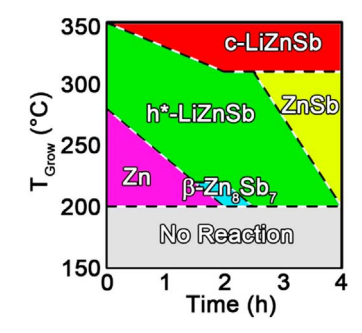


Fig. 20. The phase space of Li-Zn-Sb as a function of reaction conditions including time and growth temperature. Reproduced with permission from Ref. [37]. Copyright 2018 American Chemical Society.

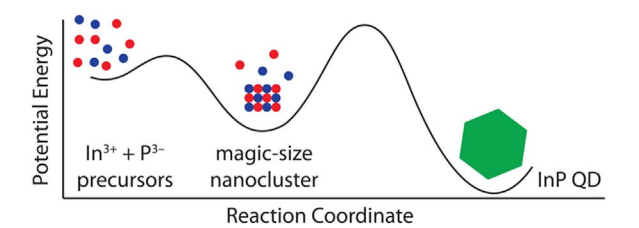
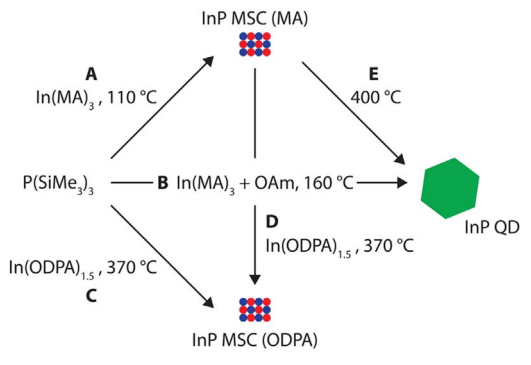


Fig. 21. General reaction coordinate plot of the two-step nucleation mechanism for the growth of InP QDs from In^{3+} and P^{3-} precursors, depicting the MSC as an isolable intermediate species. Reproduced with permission from Ref. [93]. Copyright 2015 American Chemical Society.

separated nucleation and growth but size distribution was not improved. The authors concluded, "These results are contrary to classical nucleation theory and suggest that control of precursor conversion rate alone is not sufficient to obtain a monodisperse sample of InP." [93] This led Gary et al. to investigate and map out the pathway for the formation of InP QDs (Fig. 21) [93]. The discrepancy of the InP system with classical nucleation theory was suggested to be due to the formation of magic-sized cluster (MSC) intermediates, which were detected via UV–Vis spectra with lowest energy electronic transition (LEET).

In order to understand the role MSCs played in nucleation and growth of InP, the authors observed the effects of varying the stability of the MSCs on the pathway. To do this, the authors attempted to synthesize and isolate InP MSCs terminated by carboxylate, amine, or phosphonate ligands (Scheme 12 Path A, B, and C, respectively). They found carboxylate-terminated MSCs (Path A) could be isolated and moved toward growth of polydisperse InP QDs. Amine ligands (Path B) bypassed the formation of MSCs to more uniform growth of InP QDs. Phosphonate-terminated MSCs could be isolated but did not move toward InP QDs (Section 3.1.4). Further, carboxylate-capped MSCs could be replaced by phosphonate ligands, but the opposite was not allowed (Path D). This analysis ranked MSC stability as amine-capped < carboxylate-capped < phosphonate-capped and illuminated a reaction landscape toward various products.

Additionally, Gary et al. investigated the transformation of MSCs to InP QDs by isolating the carboxylate-terminated MSCs and subsequently using them as a single-source precursor (SSP) toward InP QDs (Path E). This decoupled the formation of the MSCs from the subsequent nucleation and growth of InP. They observed uniform InP particle shape and InP QD size dependence on concentration. These observations followed classical nucleation theory. Thus, the authors predicted that the reaction pathway of MSCs to InP QDs occurred by monomers created from the dissolution of MSCs rather than an aggregative growth directly from MSCs. Gary et al. demon-



Scheme 12. Reaction pathways of molecular precursors, indium myristate $(In(MA)_3)$ and indium octadecylphosphonate $(In(ODPA)_{1.5})$, to InP MSCs and InP QDs in the solvent, octylamine (OAm). Pathways could be tuned by the capping ligands (A and C), carboxylate or phosphonate, as well as the addition of amine (B). Reproduced with permission from Ref. [93]. Copyright 2015 American Chemical Society.

strated that NP syntheses can not always be explained by classical nucleation models; this led them to conduct a thorough pathway investigation of the transformation of MSC intermediates to InP QDs. Moving forward, one could imagine that by exploring reaction pathways, a greater understanding of NP syntheses could be achieved and nucleation models could be updated. Moreover, Gary et al. produced a qualitative reaction coordinate plot, an infrequently used representation for NP syntheses, by studying intermediates and manipulating the stability of the MSCs, allowing them to access various pathways toward monodisperse InP QDs.

2.3.4. Conclusion for understanding reaction pathways

This section has outlined the process of studying reaction pathways, the possible advantages achieved from exploring reaction pathways, and possible future studies. Further, the importance of control reactions, alternative hypotheses, and the value in reporting failed routes in pathway investigations was demonstrated. The process of studying solution-based NP reaction pathways is progressing to parallel solidstate pathway studies (Jiang et al. [80] and Martinolich et al. [81,82]) where intermediates are characterized and the pathway is manipulated by rationally varying a parameter. Moving forward, White et al. illustrated the ability to efficiently and thoroughly investigate the reaction pathway for h*-LiZnSb and the phase space of the Li-Zn-Sb family using the high throughput system WANDA [37]. Additionally, Gary et al. demonstrated the InP QD pathway diverging from the classical nucleation model due to the important characterization of the MSC intermediate [92,93]. However, by isolating this intermediate and using it as a SSP, classical nucleation models could describe the transformation to InP QDs. Continuing the thorough investigation of solution-based NP syntheses will allow us to draw conclusions across similar systems, map qualitative thermodynamic and kinetic landscapes, expand nucleation models, as well as discover previously unobserved or metastable products.

3. Characterization of NP syntheses

This section is focused on characterization techniques used to garner information for understanding NP reaction mechanisms and pathways. Murphy and Buriak outlined a standard of best practices for reporting NP syntheses to which we refer the reader [94]. Beyond the careful characterization of end products, we also discuss methods aimed at identifying all components of the reaction systems before, during, and after NP nucleation and growth. We hope to show exemplary uses of different analytical techniques for this end, including what they offer for insight and their limitations, and we hope to suggest possible complementary tools.

This section is divided into two parts: characterization focused on understanding reaction mechanisms (often reactions involving organic species and precursors that lead to NP formation) and, secondly, characterization focused on understanding the reaction pathway (evolution of solid-phase components including phase, composition, and morphology of solid-state intermediates and NPs formed). At the end, some prospective NP characterization techniques and strategies for elucidating reaction mechanisms and pathways are highlighted.

3.1. Characterization for elucidating reaction mechanisms

A layer of complexity in NP systems lies in understanding the significant and multifaceted roles of the solvent. It is commonly understood that solvents frequently double as bound ligands but their possible role in chemical transformations, including but not limited to redox or coordination reactions, is often overlooked leaving the full mechanistic picture unknown. The main techniques currently utilized for unveiling the role solvents play in NP synthetic systems are NMR, FTIR, UV–Vis, and mass spectrometry.

3.1.1. Solution-based and prospective NMR spectroscopy techniques

3.1.1.1. Solution-based NMR spectroscopy. Solution-based NMR techniques are powerful for describing the organic portion of colloidal NP reaction systems. Often studies focus on the identity of the starting solvents and ligands coordinated to the surface of the NPs as well as their transformations as a result of temperature or interactions with precursors [11,12,95-98]. In particular, the value of ¹H NMR is not only the identification of these species but also their quantification by use of an internal standard as well as the nature of their possible coordination to the NP surface. In many of these solution-based experiments. NMR preparation is done with care to avoid the introduction of a compound (e.g. standard deuterated solvent) that may cause an altered reaction mechanism. Some studies measure the neat reaction solution [22] while others add deuterated chloroform (CDCl₃) only after the reaction has taken place [15]. Alternatively, Liu et al. took precaution by storing CDCl3 with relevant precursors at RT [16]. The solutions were subsequently studied after prolonged air exposure to ensure not only stability over time but to also ensure any instability phenomenon was deconvoluted from acquired NMR spectra. Although the reports described in this section are by no means an exhaustive list of every NMR study to characterize the organic portion of NPs, we simply wish to highlight some seminal examples.

Using solution-based NMR spectroscopies, Steckel et al. and Liu et al. proposed reaction mechanisms for Se delivery from a tertiary phosphine selenide to a metal precursor, Pb and Cd, respectively [15,16]. Steckel et al. made four equivalent reaction samples directly in NMR tubes and quenched the reaction progress at different times for ex situ ³¹P NMR and other complementary techniques; Liu et al. ran in situ NMR (1H, 13C, and 31P) in flamesealed NMR tubes under vacuum. Despite the different sample preparations, both proposed that the cleavage of the P=Se bond in tertiary phosphine selenides occurred by an acid/base reaction with metal oleates in which Se transferred as Se²⁻, resulting in metal selenide monomer, tertiary phosphine oxide, and an anhydride. To elucidate the mechanism involved, monitoring the growth of the oxidized tertiary phosphine and consumption of the tertiary phosphine selenide precursor by ³¹P NMR was key for both studies. Data from the study by Liu et al. is shown in Fig. 22 [16].

The Owen group has made significant contributions in the characterization of NP surface ligands by solution and solid-state NMR spectroscopies in order to ultimately tune the surface ligands for optoelectronic properties [99,100]. The work described here is significant because of the extensive experimental NMR spectroscopy protocols and thoughtful analysis of the resulting data. For example, Anderson et al. investigated the displacement of Z-type metal carbox-

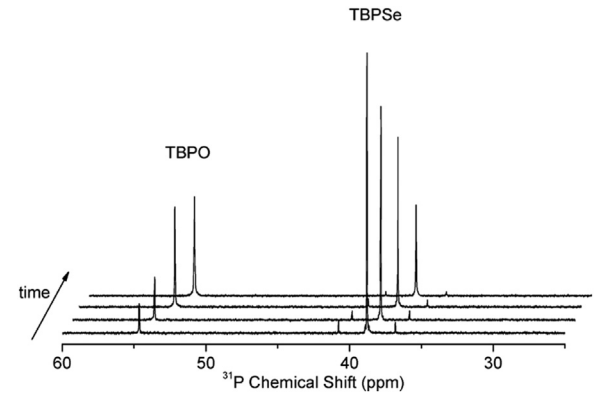


Fig. 22. Conversion of tertiary phosphine selenide (tri-*n*-butylphosphine selenide, TBPSe) and the subsequent growth of tertiary phosphine oxide (tri-*n*-butylphosphine oxide, TBPO) observed by ³¹P NMR. Reprinted with permission from Ref. [16]. Copyright 2007 American Chemical Society.

Scheme 13. Displacement of metal carboxylate ligands, L-M(O_2 CR)₂, by L-type ligands on metal chalcogenide NPs. Reprinted with permission from 100. Copyright 2013 American Chemical Society.

ylate ligands with various L-type Lewis base ligands (Scheme 13) [100]. In situ 1 H NMR spectroscopy was used to monitor the bound and free ligands from CdSe NPs by distinguishing NMR line widths as well as the concentration of free carboxylate ligands to measure relative displacement (Fig. 23a). Bound ligands tumble slowly causing broad signals while free ligands move freely in solution resulting in sharp signals. The authors targeted an isolated ppm range indicative of the vinylic hydrogens of oleyl chains and separate from the peaks of other solvent species. By increasing the concentration of L-type ligand N,N,'N,'N-tetramethylethylene-1,2-diamine (TMEDA), $Cd(O_2CR)_2$ was displaced from CdSe NPs, represented by the growth of a sharp peak and consequent decrease in the broad peak (Fig. 23).

Unfortunately, many NMR studies are limited to binary systems in which a reduced metal or metal cation directly reacts with the delivered chalcogenide. These systems are also typically focused on TOP-related surface compounds, probing common NMR-active nuclei such as $^1\mathrm{H}$ and $^{31}\mathrm{P}$. Because phosphorus species can be directly observed by NMR, gaining insight into the system is less prohibitive than, for example, amine-based systems [101]. Although $^{15}\mathrm{N}$ NMR does exist, it has low sensitivity as the natural abundance of $^{15}\mathrm{N}$ is 33% of $^{13}\mathrm{C}$. García-Rodríguez et al. tried to rectify this problem by utilizing 2D correlated NMR $^{1}\mathrm{H}^{-15}\mathrm{N}$ heteronuclear multiple bond correlation (HMBC) to investigate the role of alkylamine on the synthesis of CdSe NPs [102]. Another hurdle in NMR is that samples must be suspended for homogenous tumbling therefore limiting the types of samples to well-passivated NPs forming solutions without significant aggregation.

Examples of atoms other than ¹H and ³¹P that could be investigated in NP syntheses are ¹³C, ¹⁹F, ²⁹Si, ⁷⁷Se, ¹¹³Cd, ¹¹⁹Sn, and ¹²⁵Te but are discussed elsewhere [103]. For example, ¹³C NMR is useful in describing organic species when coupled with ¹H NMR as is the case

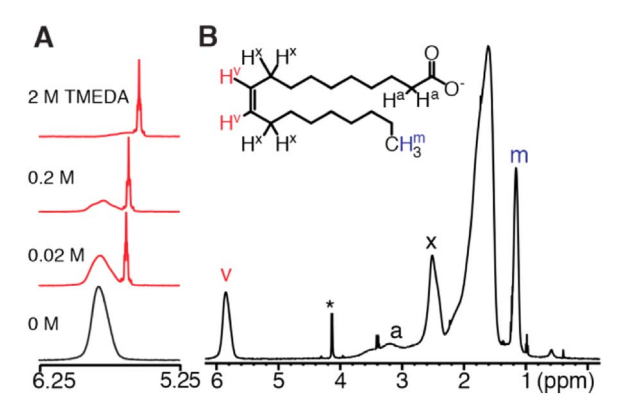


Fig. 23. (A) Vinyl region of oleic chain depicting NMR line widths of bound vs. free ligands. Bound ligands are observed through a broad peak while free ligands are observed through a sharp peak. The authors hypothesized that the changes to the chemical shifts with increasing TMEDA concentration were due to a change in dielectric of the solvent medium. (B) $^1\mathrm{H}$ NMR spectrum of purified CdSe NPs. The (*) ferrocene standard (δ = 4.1 ppm) used to measure oleyl concentrations. Reprinted with permission from Ref. [100]. Copyright 2013 American Chemical Society.

in a report by Bullen et al. [10]. The use of ⁷⁷Se is common in identifying chalcogenide species albeit prohibitively expensive to carry out numerous measurements [17]. An example of ¹¹⁹Sn NMR use can be found in Section 2.2.2.5 [64].

Additionally, one of the limitations of common NMR techniques is the inability to probe paramagnetic species. Electron paramagnetic resonance (EPR) has been used to characterize these species, especially targeting point defects in bulk and nanoparticle semiconductors. For example, this has been used to identify Mn^{2+} dopants in NP systems via hyperfine interactions of the ⁵⁵Mn nuclear spin (I = 5/2) [104].

We have split up these characterization techniques and are discussing them individually, but often data from different techniques are understood in conjunction to get a full picture of what transformations may be occurring. Thus, it is important to be careful in consideration of how reaction or sample conditions for one technique (NMR) might affect the material being studied for another technique. From a report by Anderson et al., ¹H NMR was used to elucidate bound ligand concentration which subsequently informed understanding on ligand exchange processes [100]. From these results, an important conclusion drawn was the contribution of ligand exchange processes on stoichiometry of the core NPs, an important factor in optoelectronic properties. While surface passivation and the identity of surface ligands to reduce recombination and boost quantum yield (QY) are important, optoelectronic properties are also sensitive to the concentration of free ligands in solution. This factor can affect the core NP stoichiometry because displacement or addition of ligands can remove or add core NP constituent atoms, respectively. For example, if the Cd(O2CR)2 ligand binds to the surface of the core NP, the Cd concentration would increase. Many reports prior to this one had focused solely on the identity of the bound ligands, unaware of stoichiometry changes consequently concluding in conflicting results. Instead, Anderson et al. made a direct correlation of PLOY measurements and Cd(O₂CR)₂ surface coverage to understand stoichiometry effects. Careful measurements such as these lead not only to deeper understanding of a system, compared to conventional hypotheses of prior literature, but can also provide standard practices for the use of NMR spectroscopy in investigating other NP systems.

3.1.1.2. Extended techniques: 2D NMR and solid-state NMR spectroscopies. Other examples of NMR spectroscopies include 2D NMR and solid-state NMR spectroscopies. While characterization techniques are already well established in other areas of chemistry, they are gaining more widespread and advanced use in the NP community, often providing unexpected insight. A 2018 paper from the Vela group used a combination of these techniques to characterize a series of Li-Zn-Sb phases that were synthesized via a high-throughput system, WANDA [37]. The compounds ODE and triphenylstibine (Ph₃Sb) were detected as surface passivating ligands by solid-state NMR spectroscopy and confirmed with 2D coupled NMR spectroscopy DQ-SQ which was used to study the spatial relationship of the surface ligands. Separately, Bullen et al. used 2D $^{1}H-^{13}C$ HSOC NMR spectroscopy to enable the correlation and appropriate peak assignment of the different Se and ODE chemical environments, elucidating the isomerization of 1-ODE to 2-ODE in the presence of Se at prolonged reaction temperature (Fig. 24) [10]. These results challenge the commonly held classification of ODE as a noncoordinating, innocent solvent. We believe mechanistic insight is strengthened by the use of NMR and further supported by the use of complementary techniques.

Further challenging convention, De Keukeleere et al. used ³¹P solidstate cross-polarization magic angle spinning (CP-MAS) NMR and solidstate ¹H-³¹P heteronuclear correlation spectroscopy to study the surface of TOPO-functionalized ZrO₂ NPs [101]. Literature prior to 2008 assumed TOPO alone was bound to NPs as L-type ligands, but findings by Wang et al. [105] in 2008 and Kopping et al. [106] discovered NPs, specifically

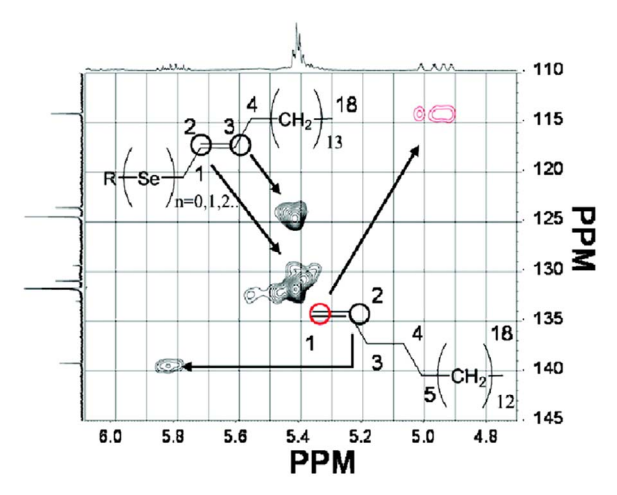


Fig. 24. Isomerization of 1-ODE to 2-ODE (here, a 48 h sample) observed by peak assignment of the alkene region in $^{1}H_{-}^{13}C$ HSQC. Adapted with permission from Ref. [10]. Copyright 2010 American Chemical Society.

CdSe NPs, were stabilized by phosphinic and/or phosphonic acid impurities in TOPO. In 2017, De Keukeleere et al. demonstrated that pure TOPO is neither inert nor a simple L-type ligand on ZrO2 NPs [101]. Under the acidic conditions used to synthesize ZrO2, pure TOPO underwent decomposition. Their results from both liquid and solid-state NMR corroborated the identification of three phosphorus-containing surface ligands, di-noctylphosphinic acid (DOPA), P,P'-(di-n-octyl) pyrophosphonate (PPA), and hydroxyl-tri-n-octylphosphonium ([HO-PR₃]⁺ where R = n-octyl), which were initially assigned by solution-based ³¹P NMR. The solid-state NMR techniques were further used to identify the extent to which the P-containing ligands were protonated. The authors found that DOPA adsorbed on the oxide surface and formed a hydrogen bond with surface hydroxyls, while PPA ligands did not participate in hydrogen bonding. The protonated TOPO, [HO-PR₃]⁺, was explained to be tightly associated with the NP surface due to electrostatic interactions and hydrogen bonding. Due to the high affinities of the byproducts for the NP surface, this potential speciation should be considered when using TOPO in other systems as it could likely occur undetected without careful characterization.

The ability of these studies to challenge conventional understanding (e.g. non-participating behavior of ODE) with the use of careful control experiments and considerable attention to the molecular portion of the NP demonstrates the viability of NMR methodologies for characterization of NP synthesis. Some of the explored portions of the NP synthesis include solvent transformations, the NP surface and its interactions with the reaction system, etc. However, in order to directly extrapolate these methods to multinary NP systems, the syntheses of more complicated systems should ideally be well-controlled (e.g. exhibiting suspension in solution) in order to minimize variables. The goal is to develop these characterization methods so that they can be used to inform and evolve multinary NP synthesis toward higher understanding and, therefore, higher control.

3.1.2. Infrared (IR) spectroscopy for solution composition and NP ligand identification

Fourier transform infrared spectroscopy (FTIR) is a simple technique that can answer similar questions to those answered by solution-based NMR techniques, especially in probing the composition of surface-bound ligands on NPs and the range of organic byproducts remaining in the supernatant. However, unlike NMR, FTIR is not used as a quantitative technique for NP studies; therefore, it is unable to provide the concentrations of species present. This does not discount FTIR from being a valuable technique because information about the reaction mechanism can be suggested. Deng et al. used FTIR to compare *n*-hexadecane before and after heating in the presence of Se powder [34]. The two spectra were the same with the exception of an absorption band at 1650 cm⁻¹ (Fig. 25),

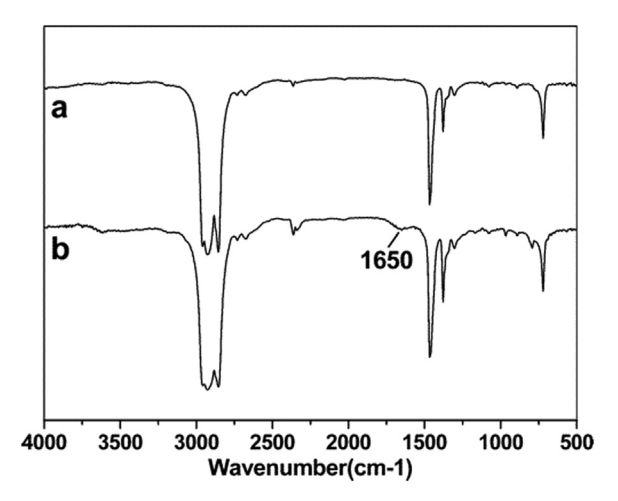


Fig. 25. FTIR spectrum of *n*-hexadecane (a) before and (b) after heating in the presence of Se. The presence of the stretch at 1650 cm⁻¹ indicated alkane dehydrogenation to an alkene. Reprinted with permission from 34. Copyright 2005 American Chemical Society.

characteristic of C=C stretching. The observation of this peak suggested to the authors the dehydrogenation of the long chain alkane to alkene and indirect confirmation of H2Se evolution. While not an unreasonable conclusion, the authors largely based these hypotheses on a broad shoulder absorption peak. Standard IR spectrum tables [107] suggest a medium intensity for a C=C sp² stretch. We offer the following reasons further supporting the existence of the low intensity peak. Weaker signals could likely appear due to an embedded trans-disubstituted alkene, but this would appear at slightly higher wavenumbers (1678-1668 cm⁻¹). While it could be that the broad shoulder peak at 1650 cm⁻¹ was due to an alkene stretch within a long hydrocarbon chain, effectively weakening the alkene stretch and shifting the corresponding peaks toward lower wavenumbers than predicted, the lack of this discussion and complementary characterizations weaken their hypotheses. Another reason that could have resulted in the same FTIR spectrum would have been the low concentration of alkene in solution, explained by Beer's law. Further, because FTIR is not quantitative, use of a complementary technique would have also been valuable to ensure the dehydrogenation of the alkane to alkene was the only solvent system reaction taking place. By overlooking potential alternative hypotheses, a misinterpretation of speciation could affect further speculation on reaction mechanism and pathway.

The Owen group used FTIR, complementing NMR spectroscopies, to study the nature of tightly bound carboxylates on CdSe NPs after the maximum displacement of 90–95% of these cadmium carboxylates by reaction with *n*-alkylamines [108]. Chen et al. hypothesized the incomplete displacement could be due to an adsorbed ammonium carboxylate ion pair ([O₂CR]⁻[H₃NR']⁺) formed from an amine and a carboxylic acid. The authors reasoned that addition of *n*-alkylamine to carboxylate-terminated CdSe NPs containing a carboxylic acid impurity (CdSe–Cd(O₂CR)₂/HO₂CR) could form *n*-alkylammonium and carboxylate ions that bind with the NPs (Scheme 14). In order to perform controlled measurements, NPs bound solely by *n*-alkylamines (CdSe-NH₂R') were isolated by completely displacing the carboxylate surface

$$O_{2CR}^{H} + RNH_{2} \longrightarrow O_{2CR}^{*}[O_{2}CR]^{-}[H_{3}NR]^{+}$$

$$+ M(O_{2}CR)_{2}(H_{2}NR)_{2}$$

Scheme 14. Addition of n-alkylamine (RNH $_2$) to carboxylate-terminated CdSe NPs containing a carboxylic acid impurity (CdSe–Cd(O $_2$ CR) $_2$ /HO $_2$ CR) formed an ammonium carboxylate ion pair ([O $_2$ CR] 1 [H $_3$ NR] 1) that binds to the NP surface. Here, white is stoichiometric metal chalcogenide NP, red is surface selenium, and green is surface cadmium. Reprinted with permission from Ref. [108]. Copyright 2017 American Chemical Society. (For interpretation of the references to color in this figure legend, the reader is referred to the web version of this article.)

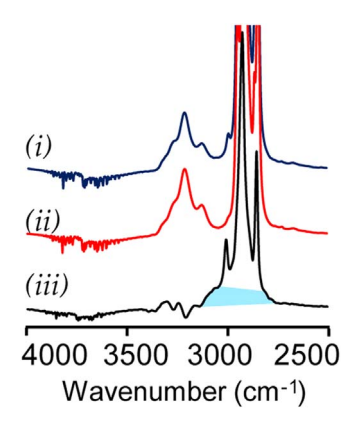


Fig. 26. FTIR spectrum of (i) CdSe–NH₂R'/ [O₂CR]⁻[H₃NR']⁺ (R = oleyl, R' = n-octyl) prepared from anhydrous oleic acid, (ii) CdSe–NH₂R' (R' = n-octyl), and (iii) their difference spectrum. Stretch characterizing [H₃N]⁺ (ν (N–H)) is highlighted in light blue. Adapted with permission from Ref. [108]. Copyright 2017 American Chemical Society. (For interpretation of the references to color in this figure legend, the reader is referred to the web version of this article.)

ligands from CdSe NPs using dimethylcadmium or diethylzinc. Upon addition of oleic acid (OA) to CdSe-NH2R', the authors observed in FTIR the proposed ammonium fragment ([H₃N-]⁺) via a broad N-H stretching band, highlighted by the light blue band (ν (N-H) = 2700-3100 cm⁻¹) in Fig. 26. This was separate from the expected surface bound amine (ν (N – H) = 3000–3400 cm⁻¹) and alkyl chains $(\nu(C-H) = 2700-3000 \text{ cm}^{-1})$. This is significant as the stretch was only visible after subtracting the spectrum of the control CdSe-NH₂R' from spectrum of the complexed ligand (CdSe-NH₂R'/ [O₂CR]⁻[H₃NR']⁺). The predicted carboxylate ion was observed through a carboxylate (-OOR) stretching band distinct from the expected bands of OA, a mixture of OA and CdSe-Cd(O2CR)2, and CdSe-NH₂R'. These two key observations supported the formation and tight binding of ammonium oleate to the NP surface which was formed by the addition of acidic molecules to CdSe-NH2R'. This finding is noteworthy as the subtlety of the FTIR signature for [H₃N-]⁺ could have been overlooked at first glance because the broad N-H band overlapped the alkyl chain stretching band.

Ultimately, these examples highlight the usefulness of FTIR as a qualitative technique. Extrapolating this characterization method to understand ternaries and other multinary systems would be straightforward as the method does not require the samples to be well-suspended, like in NMR, to gain qualitative information such as the possible identity of ligands or solvent species. Characterization of ligand identity and speciation could then inform on reaction mechanisms such as solvent (e.g. Deng et al. [34]) or ligand (e.g. Chen et al. [108]) transformations.

3.1.3. Mass spectrometry to support the presence of reaction species interactions

Mass spectrometry (MS) is used to analyze the role of solvents in NP reaction mechanisms. Kar et al. used matrix-assisted laser desorption ionization time of flight (MALDI-TOF) MS and FTIR to understand the solvent contributions of OLA in the synthesis of CuInSe₂ particles [89]. The use of a soft ionization MS method, such as MALDI, allows detection of species to be more representative of the reaction compared to a hard ionization source due to the lower chance of sample fragmentation. By comparing the reaction supernatant to the as-bought solvent, byproducts were identified, alluding to precursor solvent interactions and portions of the reaction mechanism. The authors drew three mechanistic conclusions from the MS data collected: (1) Cu became coordinated with OLA, (2) hydrocarbons in OLA became chlorinated, and (3) dioleylamine was formed. They complemented their hypotheses with FTIR, but their

suggested reaction mechanism could have been strengthened with alternative hypotheses either refuted or supported by additional characterization techniques and extensive controls. For example, possible roles of impurities in the solvent could have been considered. Lower purity, tech. grade OLA (normally 70%) is commonly used as a high boiling point solvent in NP syntheses, but specific impurities are rarely discussed. Kar et al. reported detection of shorter chain alkylamines in OLA, but did not address the ability of the OLA impurities to possibly interact similarly with reaction components in the supernatant. Moreover, Kar et al. observed significant peaks at 252, 254, and $266\,m/z$ which were labeled as $[C_{18}H_{35}-H^+]$, $[C_{18}H_{37}-H^+]$, and $[C_{18}H_{35}N-H^+]$, but these species were not discussed. These peaks could be important for understanding the reaction mechanism but could also be a result of OLA fragmentation due to MS being a harsher technique compared to other characterization methods.

Due to these uncertainties, we suggest control experiments that could have aided in their understanding of the reaction mechanism and ruled out other hypotheses discussed above. For instance, observing one precursor in OLA using the same heating profile as the reaction procedure could examine individual speciation. Additionally, it could be useful to heat OLA alone to identify the possibility of peaks originating from the self-reaction of OLA. Reacting simple, high purity alkane and alkene solvents with the precursors to see if similar interactions occur could also help clarify the data analysis of the complex OLA system. Overall, Kar et al. were able to come to mechanistic conclusions about the precursor solvent interactions en route to CuInSe₂ using MALDI-TOF MS and FTIR as a secondary technique, but exhaustive hypothesis speculations and control reactions could have further enlightened their study.

As described above, MS is a good complementary technique, but on its own, data analysis poses difficulty due to the breadth of possible species that could be identified, as further demonstrated in a report by Bullen et al. [10] Data from this technique could be used as evidence to support chemical processes that are hypothesized to occur in NP synthesis but does not necessarily distinguish between active and inactive components for NP formation. Specific to this study, the interaction of Se and ODE was uncovered via ¹H-¹³C HSQC NMR; thus, EI MS and ⁷⁷Se NMR were used to identify possible chalcogen species. When monoolefins are heated in the presence of sulfur or selenium, bridging chalcogenide chains form between the monoolefins by the vulcanization process. As this proceeds, the length of the chalcogenide chains decreases, resulting in further possible products. Therefore, in assigning MS data, it was worth considering all possible Se-ODE interactions. Positive EI mass spectra of Se-ODE samples were studied. Five singly charged species were detected: ODE (m/z = 252), ODE+Se (m/z = 331), ODE+ 2Se (m/z = 410), 2ODE+Se (m/z = 586), and 2ODE+ 2Se (m/z = 586)664). Moreover, a control reaction using gel permeation chromatography was performed to ensure that the individual contributions to the mass spectra were not arising purely from fragmentation. As the authors noted, only broad conclusions on the reaction mechanism of Se with ODE could be gathered from this data because both reactive and unreactive species are likely produced concurrently.

Mass spectrometry is a powerful technique in identifying a plethora of organic species because it is based on m/z ratio and samples are not restricted in requiring specific labeling of certain nuclei, as is the case for solution-based NMR. Moreover, sampling for MS is particularly facile and does not have too many constraints as both gas and liquid phases can be probed which could be advantageous for understanding the composition of the reaction headspace. However, MS is better suited as a complementary technique because its advantages present practical dilemmas. Because of the sensitivity of MS for nominal identification of all the species in the sample, analysis and labeling of the peaks are often difficult without adequate knowledge of what could exist in the sample. The high quantity of m/z peaks observed could

pose difficulty in identifying key species relevant for the reaction mechanism. This can be overcome as compounds typically have unique fragmentation patterns which can be matched with files in the standard NIST database. This is unfortunately limited to common compounds and does not contain all species of interest for the NP community. Further, it is difficult to discern whether detected species are evolved due to the harshness of the ion source or as a possible reaction intermediate. Therefore, MS can be used to support findings from other techniques, or the use of it could be strengthened when alternative hypotheses are also proposed and confirmation bias is avoided.

3.1.4. UV-Vis spectroscopu

UV—Vis spectroscopy is typically used to characterize optical properties of NPs and reaction solutions. This technique allows access to characterization of both reaction mechanisms and pathways, and its use demonstrates the difficulty in differentiating between the two processes. An example in which UV—Vis was used to understand reaction mechanism kinetics lies in the work of Srivastava et al., discussed in Section 2.2.3.3 [70]. The authors were able to experimentally rank reducing agents in order of reducing power by collecting the absorption spectra of reaction solutions held at room temperature. This lower temperature resulted in amorphous InAs clusters instead of QDs but was key in slowing down the reaction kinetics sufficiently for distinguishing the relative reaction rates.

One example expanding the use of UV-Vis to investigate the reaction pathway of InP was reported by Gary et al., described in Section 2.3.3.2 [93]. A lowest energy electronic transition (LEET) UV-Vis technique allowed the authors to observe the existence of magicsized cluster (MSC) intermediates and led them to propose a two-step nucleation and growth reaction of InP QDs. The technique allowed further investigation of the thermodynamic stability of InP MSCs, enabling the elucidation of different reaction pathways depending on the capping ligand, either carboxylate-terminated or phosphonateterminated. The authors observed different UV-Vis spectra for the differently-capped MSCs; carboxylate-termination gave rise to one peak while phosphonate-termination showed four. In order to test the thermal stability of MSCs based on capping, the MSCs were isolated and exposed to air over 24 h. This resulted in the observation of absorption broadening for the carboxylate clusters and an unchanged absorption profile for the phosphonate clusters. Thus, a higher stability of the phosphonate-terminated MSCs was rationalized which is reflected in the resultant reaction coordinate plot in Fig. 27.

In the field of quantum-confined NPs or quantum dots (QDs), the phenomenon of quantum confinement extends the use of UV-Vis spectroscopy to the characterization of physical properties. When the spatial dimensions of a material are confined to less than that of the material's Bohr exciton radius, the frontier electron orbitals exist at energy levels within the bands of the bulk semiconductor [109]. This

ties the size of QDs directly to the magnitude of the optical gap. Thus, UV-Vis spectroscopy is often used for size evaluation of well-known QDs. In conjunction, photoluminescence (PL) spectroscopy is used as a handle for understanding properties such as size dispersion because the PL spectral width is dictated by the size, shape, and composition distribution of a QD ensemble [109]. Measuring these properties can be accomplished both ex situ and in situ, discussed in the study of CdSe growth kinetics in a review by Kovalenko et al. [96].

The use of this technique continues to advance exemplified by combinatorial in situ methods. One example exists in a 2018 report by Li et al. which gathered IR and UV–Vis spectra to follow the growth mechanisms of QDs by mass conservation, discussed in Section 3.3.1 [110]. UV–Vis was used specifically to track QD size and concentration. Additionally, we propose this technique could progress understanding on NP reaction syntheses by the development of in situ fiber optic methods in which the color of reaction solutions might inform the dynamic coordination of ionic species. By understanding the speciation of monomers (Scheme 1), advances could be made in understanding NP reaction mechanisms.

3.2. Characterization for elucidating reaction pathway

3.2.1. X-ray diffraction (XRD)

X-ray diffraction provides a useful method for identifying crystal-line phases in reaction products which can especially be useful for gaining insight into the reaction pathway. Commonly, beyond simply examining end products, aliquots at various growth times may also be examined ex situ. However, each time an aliquot is taken, changing reaction conditions may possibly affect the reaction pathway. Experimental NP syntheses are normally done on a relatively small scale; therefore, the reaction concentrations may be altered even when small volumes are removed. These could lead to abnormal shifts in equilibria and generate misleading, incorrect identification of specific pathways. This is not to say that this occurs for every system, but we offer it as a precautionary note. To ensure results of ex situ XRD are representative of the reaction conditions, we suggest that aliquots removed are compared to individual reactions where the entirety of the flask is quenched at matching aliquot time intervals.

While residing as an iconic method for examining and understanding crystalline solids, a few complications arise due to the possible sizes and morphologies NPs allow. Described by the Scherrer equation, broadening of a reflection may correspond to the dimensions of the corresponding set of lattice planes in an inverse relationship [111]. The Scherrer equation, $D_{hkl} = K\lambda/B_{hkl}cos(\theta)$, describes this relationship between the crystallite size perpendicular to the direction identified by the Miller indices hkl (D_{hkl}) and the full width half maximum (FWHM) of the corresponding reflection (B_{hkl}), using K as the crystallite-shape factor, λ as the X-ray wavelength, and θ as the Bragg angle. For an

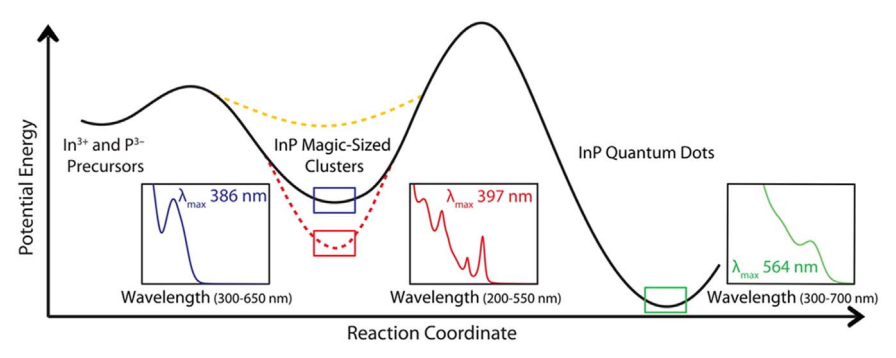


Fig. 27. Reaction coordinate plot of InP QDs rationalized by UV-Vis LEET experimental data. In violet, carboxylate-terminated InP MSCs and in red, phosphonate-terminated InP MSCs. Phosphonate-terminated InP MSCs are more thermally robust, confirmed by UV-Vis. Green indicates InP QDs and yellow indicates the direct formation of QDs due to the addition of an amine. Reprinted with permission from Ref. [93]. Copyright 2015 American Chemical Society. (For interpretation of the references to color in this figure legend, the reader is referred to the web version of this article.)

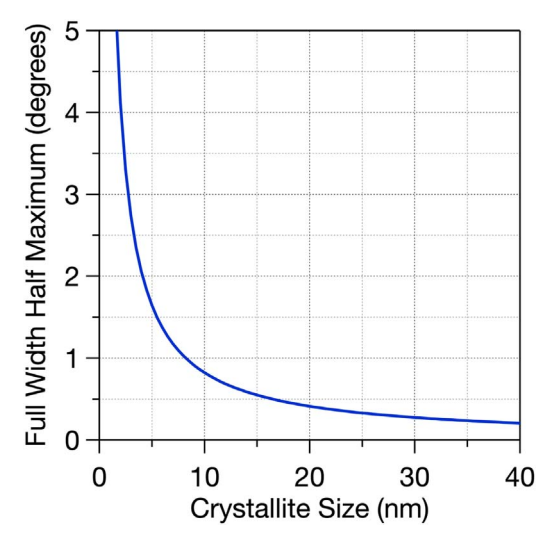


Fig. 28. For an example peak at 30° 2θ , the relation between crystallite size and peak broadening is plotted, using an X-ray wavelength for Cu K α (1.5406 Å) and a crystallite-shape factor of 0.9.

example reflection at 30° 2θ , the relation between crystallite size and peak broadening is plotted in Fig. 28, using the X-ray wavelength for Cu Ka (1.5406 Å) and a crystallite-shape factor of 0.9. As an example of the impact, it predicts reflections with crystallite sizes of 15 nm or smaller to show a FWHM of 0.5 degrees or greater, rapidly broadening with decreasing crystallite size.

Further, comparing PXRD patterns of NP samples with crystal structure reference patterns becomes complicated with possible morphological anisotropy, amorphous products, and overlapping patterns. In diffractograms from anisotropic nanoplates, planes parallel to the larger faces exist in smaller length scales than those perpendicular to the faces. Thus, reflections show variations in peak broadening within one pattern, which can obscure the identification of phases. One could imagine a possible impurity phase having few identifying reflections discriminating it from the majority phase. Should those reflections correspond to lattice planes of significantly small dimensions and be significantly broadened compared to other reflections, their signal could be difficult to discern from the noise. Additionally, varied peak broadening among reflections for one phase can complicate fitting analyses such as Rietveld refinement.

The formation of amorphous phases is also difficult to observe in a powder pattern especially if crystalline products are present. For example, a study done by Ahmadi et al. examined the reaction pathway of CIGSe using XRD and TEM [87]. They found XRD patterns of aliquots taken at various reaction times initially exhibited an unusual background that was not observed for the later samples (Fig. 29). The

use of a secondary technique, scanning transmission electron microscopy energy dispersive X-ray spectroscopy (STEM EDS), found that this odd background was due to the presence of amorphous $\rm In_2Se_3$. Without the use of a secondary technique, this amorphous phase would have been unidentified by XRD, and the study would have resulted in an incomplete and inaccurate reaction pathway determination.

Materials with similar crystal structures inherently have comparable, overlapping peaks, often with few distinguishing features due to XRD reflections resulting from lattice spacings within the crystalline products. In addition, commonality between patterns is an issue for binaries, ternaries, and quaternaries of the same elements. This is of utmost concern because the formation of permutations of constituent elements can easily occur in syntheses, and without control over these impurities, material properties could be detrimentally affected [112]. This is demonstrated by the CZTS system. In a review by Chen et al., a relationship between energies of formation and potential energies was used to calculate and plot the chemical potential energies of common constituent elemental, binary, and ternary materials possible for Cu, Zn, Sn, and S [113]. The resulting plot demonstrates the small potential energy window for the synthesis of CZTS, represented by the black shaded area in Fig. 30. In the represented Cu potential region, μ_{Cu} = -0.20 eV, the CZTS potential window is surrounded by CuS, ZnS, SnS, and Cu₂SnS₃, each accessible by slight changes of the Sn and Zn potentials. These potentials can be affected by deficiency or excess of Zn or Sn in the system. With Zn exhibiting the narrowest potential window (μ_{Zn}) for the existence of CZTS and the possible Cu_2SnS_3 and

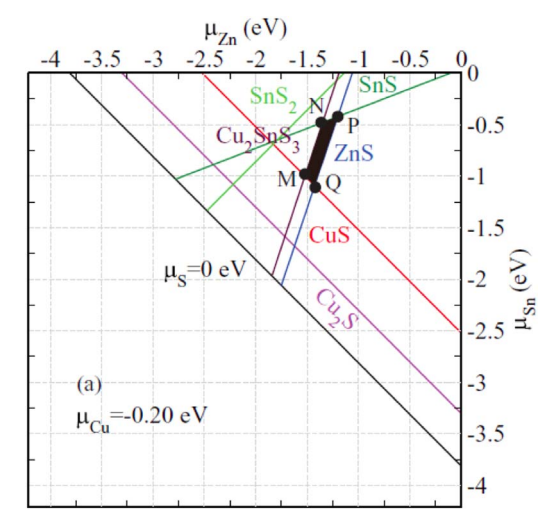
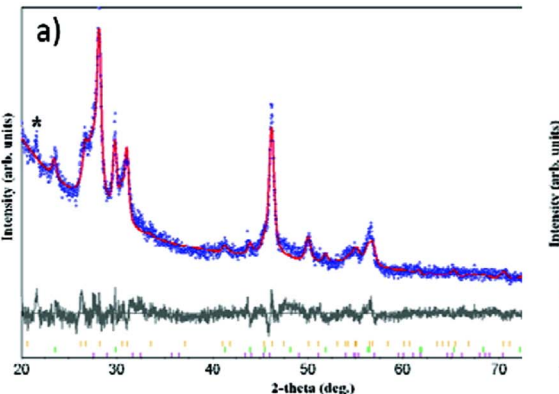


Fig. 30. Calculated stable chemical potential region of Cu_2ZnSnS_4 , black shaded area, in the $(\mu_{Zn}, \ \mu_{Sn})$ plane in the $\mu_{Cu} = -0.20 \, \text{eV}$ chemical potential space. Adapted with permission from Ref. [113]. Copyright 2013 John Wiley and Sons.



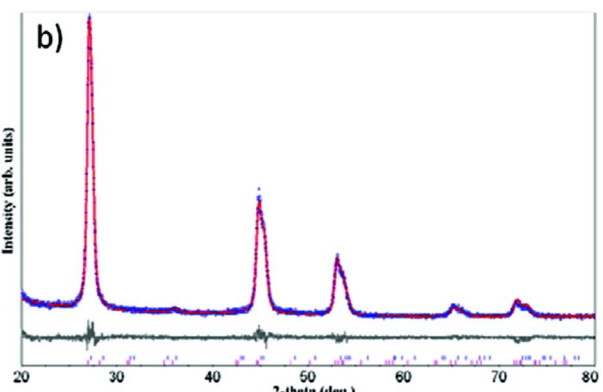


Fig. 29. PXRD patterns of aliquots taken at (a) 40 min at 200 °C and (b) 60 min at 230 °C of the CIGSe NP synthesis to exemplify the disappearance of an unusual background as the reaction progressed. Adapted with permission from Ref. [87]. Copyright 2012 American Chemical Society.

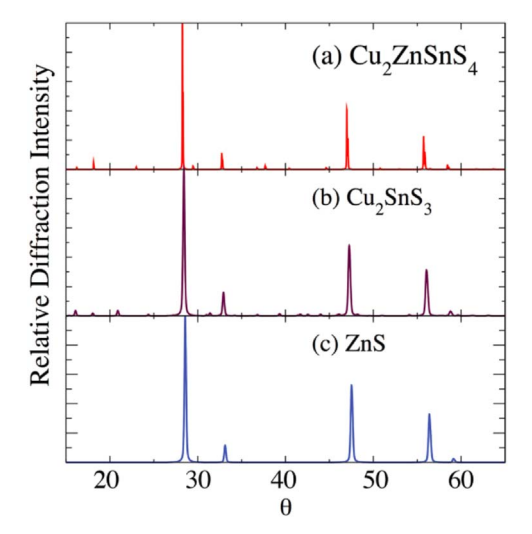


Fig. 31. Overlapping XRD peaks of kesterite Cu₂ZnSnS₄, Cu₂SnS₃, and ZnS. Reprinted with permission from Ref. [112]. Copyright 2012 John Wiley and Sons.

ZnS intermediates, the probabilities of these impurity phases appearing in a CZTS sample are high. Problematically, the major powder pattern reflections of ZnS and $\rm Cu_2SnS_3$ match those for $\rm Cu_2ZnSnS_4$, depicted in Fig. 31 [112], making the identification of these phases difficult without a secondary technique such as thermal analysis or Raman spectroscopy. Although these figures only depict the CZTS system, they display the ease of forming constituent binaries and ternaries, the possibility of overlapping XRD patterns of constituent materials, and, therefore, the importance of thorough characterization for all material systems.

Additionally, polymorphs can have overlapping diffraction reflections making it difficult to discern whether a single or a biphasic product is present. A study done by Kar et al. (Section 2.3.2.3.2) demonstrated the difficulty of correctly identifying present polymorph phases [89]. The formation pathway of CuInSe₂ was tracked and preliminary tests investigating injection order of the In and Se precursors were found to either result in the sphalerite or chalcopyrite phase of CuInSe₂. Although the chalcopyrite phase exhibits some low-intensity, unique reflections, the major peaks of the sphalerite and chalcopyrite phases overlap, as seen in Fig. 32. Thus, without further characterization, it is difficult to determine when chalcopyrite or sphalerite is the sole phase. Since the sphalerite pattern does not exhibit unique peaks, an existence of the sphalerite phase could go unnoticed. Even though chalcopyrite has unique peaks, the intensities are relatively low which could be indis-

tinguishable from the background of a mostly sphalerite-type NP sample. Complications due to peak broadening from NP dimensions further exacerbate this problem. Microscopy techniques such as HRTEM and selected area electron diffraction (SAED), among other techniques, might lend some support but the similar lattice spacings of the two polymorphs would pose the same problems. Possibly more conclusive could be Raman spectroscopy though further fundamental studies identifying distinguishing vibrational modes for the two polymorphs would be required.

3.2.2. Raman spectroscopy

In the development of NP syntheses, a recurring hurdle in the characterization of the end product lies in the difficulty of X-ray diffraction and electron microscopy to provide conclusive evidence of phase-purity. As discussed above, diffraction techniques may be limited by the possible presence of impurity phases exhibiting highly similar crystal structures and therefore overlapping Bragg peaks. Further evidence may be gained by electron microscopy techniques, especially in conjunction with energy-dispersive X-ray spectroscopy (EDS); however, measuring lattice spacings and performing electron diffraction may encounter similar difficulties with nondiscriminatory lattice spacings between possible phases. In some material systems, Raman spectroscopy has been identified as a valuable method for finding previously unidentified phases, both in terms of the signal arising from differences in chemical bonding, not lattice spacings, and the technique showing higher sensitivity to secondary phases of low concentration. In this section, we discuss Raman spectroscopy studies of three material systems to feature valuable information that can be garnered alongside some of the experimental design variations that can enhance detection of possible impurities.

3.2.2.1. Iron pyrite (FeS₂). Syntheses of iron pyrite (FeS₂) often cite Raman spectroscopy experiments as a conclusive method to verify the lack of secondary Fe-S phases, especially of possibly low concentrations [114,119]. Though the diffraction patterns of the many possible phases are distinct from one another, the possibility for small inclusions of other Fe-S phases has been postulated as a detrimental characteristic of some iron pyrite films. Summarized generally in Fig. 33 are peak locations for reported Raman spectra of some Fe-S phases and hematite, Fe₂O₃, a possible oxidation product of FeS₂. Iron pyrite shows its main A_{1g} peak at 341 cm⁻¹ with smaller peaks at 377 (E_g) and 425 cm⁻¹ (T_g(3)). The T_g(1) and T_g(2) modes of iron pyrite are reported to be unobserved due to light extinction by other modes and inefficient light scattering [115]. The orthorhombic FeS₂ polymorph, marcasite, is reported to have Raman peaks at 323 and 386 cm⁻¹ [116].

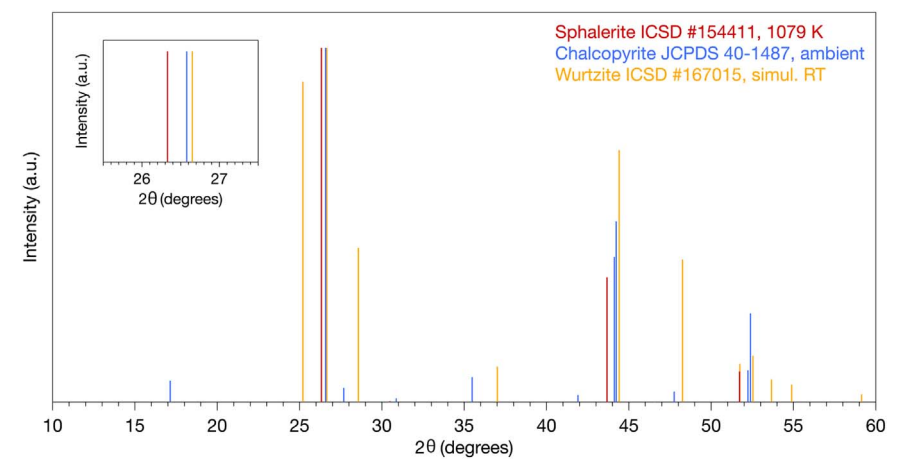


Fig. 32. Plotted reference patterns for CuInSe₂ crystalline polymorphs. In red is shown the sphalerite CuInSe₂ phase from ICSD #154411, in blue the chalcopyrite CuInSe₂ phase from JCPDS 40-1487, and in yellow the wurtzite CuInSe₂ from ICSD #167015. The wurtzite phase exhibits well-separated reflections, but the high-intensity peaks from the sphalerite and chalcopyrite phases overlap to a significant extent. (For interpretation of the references to color in this figure legend, the reader is referred to the web version of this article.)

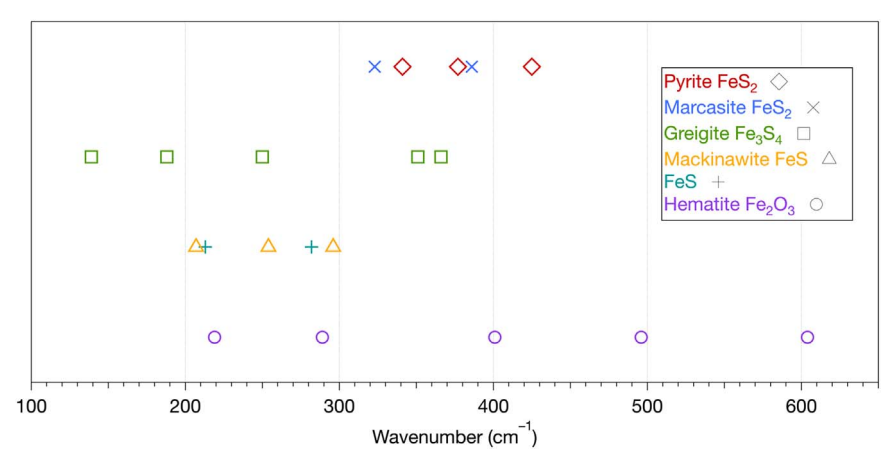


Fig. 33. Raman spectroscopic vibrational mode assignments for common impurity phases in iron-sulfide material systems. Data points were collected from the reports of Yu et al. (Ref. [114]), Shukla et al. (Ref. [115]), Cabán-Acevedo et al. (Ref. [116]), Boughriet et al. (Ref. [117]), and Bourdoiseau et al. (Ref. [118]).

An unidentified FeS phase was reported to show Raman peaks at 213 and $282 \, \mathrm{cm}^{-1}$ [114]. This phase may be an amorphous iron monosulfide because it is consistent with a study characterizing iron-containing surface sediments in which peaks at 214 and $282 \, \mathrm{cm}^{-1}$ were assigned to amorphous FeS [117]. The mackinawite phase (FeS) has been characterized to have smaller peaks at 207 and $254 \, \mathrm{cm}^{-1}$ with a main peak at $296 \, \mathrm{cm}^{-1}$. This study also reported the greigite phase (Fe₃S₄) to show peaks at 139, 188, 250, 351, and $366 \, \mathrm{cm}^{-1}$ [118].

Interestingly, Raman spectra of the pyrrhotite phase, Fe₇S₈, have not been reported. A Raman microprobe study by Mernagh et al. on various sulfide compounds determined both the hexagonal and monoclinic pyrrhotite polymorphs to lack Raman active vibrational modes, both by predictive factor group analysis and experimentally [120]. Additionally, experiments attempting to detect infrared bands for the compounds by Liese et al. were unfruitful [121]. This inapplicability of Raman spectroscopy to identify the possible presence of Fe₇S₈ polymorphs accentuates a weakness in using this technique to conclusively assert the phase-purity of an iron pyrite sample. In these cases, we might suggest complementary thermal analysis for possible signatures of secondary phases and the possibility of magnetic and Mössbauer spectroscopy to potentially identify iron oxidation states outside of the predicted low spin divalent state in iron pyrite. Further, this stands as an exemplary system portraying the possibility for confirmation bias in experimental results. Identification of spectroscopic signatures characteristic of the majority phase might not always indicate phase-purity if any possible secondary phase happens to lack Raman-active modes.

Additionally, another key aspect of Raman spectroscopy studies in the scope of studying iron sulfide phases is the importance of the laser power intensity during measurements. Shukla et al. provided supplemental data on the resulting oxidation of their iron pyrite films under 1.03 mW incident power [115]. Lowering the intensity to 0.14 mW gave data without destruction of the original film, as seen in Fig. 34. The possibility of this effect would be useful to keep in mind for Raman spectroscopy studies on other material systems.

3.2.2.2. Copper indium selenide (CuInSe₂). As discussed earlier in Section 3.2.1, the largely overlapping diffraction patterns of the chalcopyrite and sphalerite CuInSe₂ phases result in significant difficulty for identifying a possible mixture of products in NP syntheses. With the characteristic peaks of the chalcopyrite phase exhibiting low intensity, one could imagine diffraction techniques lacking the resolution to conclusively identify one of these compounds as an impurity phase of low concentration. In the NP field, Raman spectroscopy can be used as a complementary technique in order to characterize the composition and phase purity of the products.

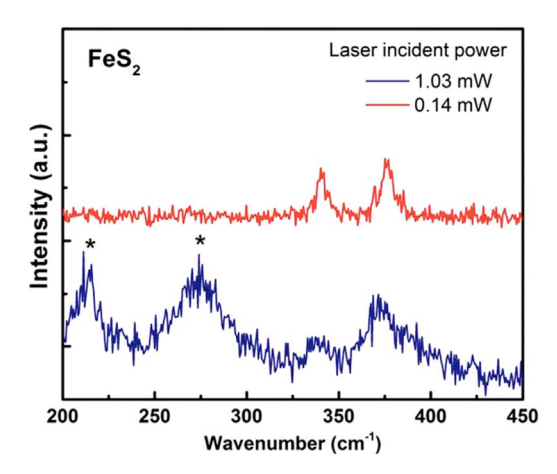


Fig. 34. Raman spectra of iron pyrite nanocubes using an excitation wavelength of 532 nm. At 1.03 mW of incident power, extra peaks (represented by an asterisk) are observed due to laser-induced oxidation. Reprinted with permission from Ref. [115]. Copyright 2016 American Chemical Society.

Raman spectroscopy studies in the CuInSe2 system have focused on the identification of the many Raman active modes of the chalcopyrite phase and on characterizing ordered vacancy compounds of alternative Cu-In-Se stoichiometries as well as the CuAu-ordered CuInSe₂ phase. A fundamental study by Tanino et al. identified the irreducible representation of the chalcopyrite space group and collected polarized Raman spectra to assign modes with respective frequencies [122]. The commonly observed, dominant A₁ peak was reported at 176 cm⁻¹ for the RT sample. The optical vibrational modes of the ordered vacancy compound CuIn₃Se₅ have been reported by Rincón et al. in which the dominant A1 mode was found to shift to smaller wavenumbers (155 cm⁻¹) [123]. Łażewski et al. compared first-principles calculations of the CuAu-ordered CuInSe₂ structure with previously published experimental results regarding the lattice dynamics of this polymorph [124]. Comparisons of the Raman spectroscopic data to the chalcopyrite CuInSe2 polymorph were made, and the main difference was said to lie in the higher frequency of the dominant A₁ peak in the CuAu-ordered CuInSe₂ at 195 cm⁻¹.

These collective results yield insight into possible impurity phases and polymorphs of the $CuInSe_2$ chalcopyrite system, but few reports discuss possible vibrational modes resulting from the high-temperature sphalerite $CuInSe_2$ structure. The lack of in-depth Raman spectroscopy studies likely stems from the difficult synthesis of this high temperature phase. Studies from Shirakata et al. in 1996 [125] and '97 [126] reported mixed-phase (chalcopyrite and sphalerite) $CuInSe_2$ films formed via chemical spray pyrolysis; the synthesis was tuned by

varying the pH of the spray solution and the temperature of the heated substrate. Sphalerite and chalcopyrite phases in the films were assigned by observing the presence or lack of small, characteristic diffraction peaks corresponding to chalcopyrite-CuInSe₂. These were then correlated with Raman spectra, and the authors noticed the commonly observed A₁ peak at 174 cm⁻¹ for those with a chalcopyrite assignment, while a Raman peak at 182 cm⁻¹ was noticed at higher intensity for films assigned as the sphalerite phase [125,126]. Further careful study of the vibrational modes for these polymorphs would benefit the NP synthetic community to expand the characterization set for identifying possible mixtures of CuInSe₂ phases.

3.2.2.3. Copper zinc tin sulfide (Cu₂ZnSnS₄, CZTS). The Cu₂ZnSnS₄ (CZTS) system, discussed above in Section 3.2.1, stands as a common example of the difficulty in identifying the possible common impurity phases: orthorhombic Cu₂SnS₃ and cubic ZnS. These structures embody such similar crystal structures that the dominant Bragg peaks overlap with that of the kesterite structure of CZTS. In this section, we highlight advances in the utility of Raman spectroscopy for identifying the many impurity phases of this quaternary system. One key aspect of these studies was the variation of the excitation laser

source wavelength in order to access different resonant conditions based on the differing vibrational modes of all possible phases.

In 2011, Fernandes et al. published a study of thin films composed of possible binary, ternary, and quaternary compounds in the Cu-Zn-Sn-S system formed by deposition of metallic precursors (dc-magnetron sputtering) followed by annealing and sulfurization [127]. Characterization of the films included EDS, inductively coupled plasma mass spectrometry (ICP-MS), XRD, SEM, electron backscatter diffraction (EBSD), and Raman spectroscopy.

Experimental Raman spectra for CZTS and the variety of possible impurity phases, all of which were measured with an excitation wavelength of 488 nm, are shown in Fig. 35. Fernandes et al. were not able to grow $\rm Sn_2S_3$ films but referenced literature assignments of peaks at 52, 60, and $\rm 307~cm^{-1}$, and though not depicted in the data, $\rm Cu_{2-x}S$ was reported to show a weaker, secondary peak at 264 cm $^{-1}$. Of note, $\rm MoS_2$ was studied because it can form when CZTS is grown on a Mo substrate. Notably, the shoulder peak in CZTS at 348 cm $^{-1}$ had a close overlap with the main peak of cubic ZnS at 350 cm $^{-1}$ and cubic Cu₂SnS₃ at 356 cm $^{-1}$. The authors suggested that detection of the 350 cm $^{-1}$ cubic ZnS peak could be enhanced by use of a UV laser but that this strategy would be limited by the shallower penetration depth [127].

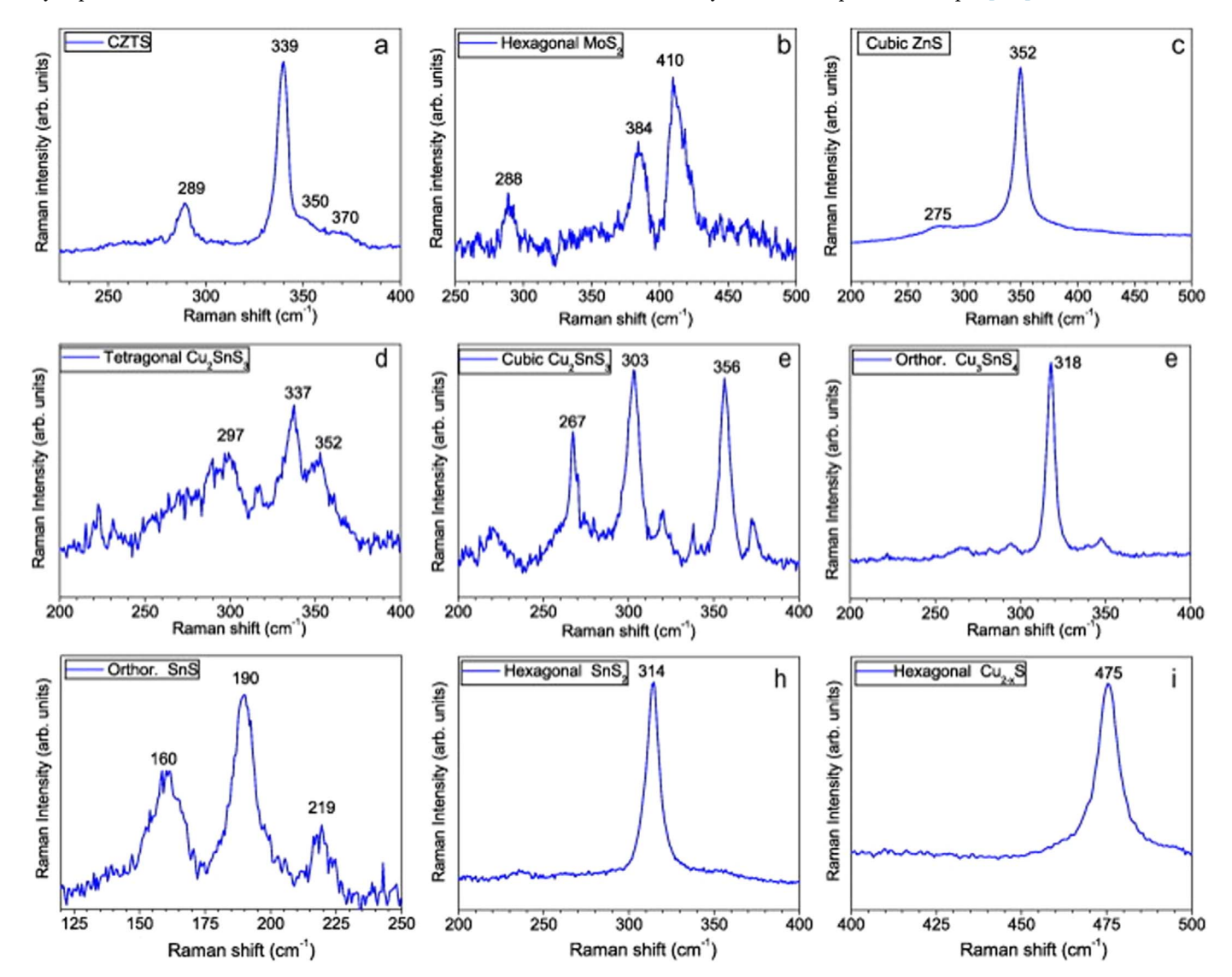


Fig. 35. Raman scattering spectra for different single phase reference compounds synthesized in the work by Fernandes et al. The excitation laser wavelength was 488 nm. Reprinted with permission from Ref. [127]. Copyright 2011 Elsevier B.V.

Dimitrievska et al. carried out Raman studies of polycrystalline CZTS films under different excitation laser energies [128]. Importantly, the authors determined that the detection of low concentrations of ZnS was possible as long as a sufficiently wide spectral range was measured. The authors also found that the CZTS vibrational modes fluctuated in intensity with respect to the excitation energy which was probed from UV to the near IR (NIR). Summarized in Fig. 36 are Raman spectra collected on polycrystalline CZTS, depicting the variation in peak intensities of vibrational modes as a function of the excitation wavelength. While it had been thought that higher intensity of a peak near 350 cm⁻¹ at UV excitation conditions indicated the presence of the ZnS vibrational mode at ~352 cm⁻¹, here Dimitrievska et al. claimed the growth of this spectral peak was due to higher resonance with an E mode of CZTS at 347 cm⁻¹. To support this, both the CZTS sample and a ZnS sample were tested with UV excitation (325 nm) over a greater spectral range. The inset of Fig. 36 showed second and third order peaks at 697 and 1045 cm⁻¹ for the ZnS control, while peaks at 671 and 1005 cm⁻¹ were reported to be second and third order peaks corresponding to CZTS itself. Thus, the importance of multiwavelength excitation has been shown for the characterization of CZTS and identification of possible secondary phases.

3.2.2.4. Outlook on Raman spectroscopy for NP identification. Overall, Raman spectroscopy is often suggested as a higher sensitivity supplementary technique for impurity detection in NP syntheses especially when related material systems exhibit similar diffraction patterns. However, these examples demonstrate the intricacy of experimentally assigning vibrational modes. Accurate understanding of Raman spectroscopy signatures is further complicated by the effects of various experimental parameters. For example, altering the wavelength of the excitation source may induce certain vibrational modes to fall in or out of resonant conditions. greatly affecting the intensities of observed peaks. In conjunction, manipulating this parameter may cause sample decomposition and affects the depth probed in the sample which may complicate assignments if the sample lacks compositional homogeneity. However, these effects may aid in the detection of impurity phases, allowing the possibility for measurement parameters to be tuned in order to enhance the resonance of signals characteristic of possible

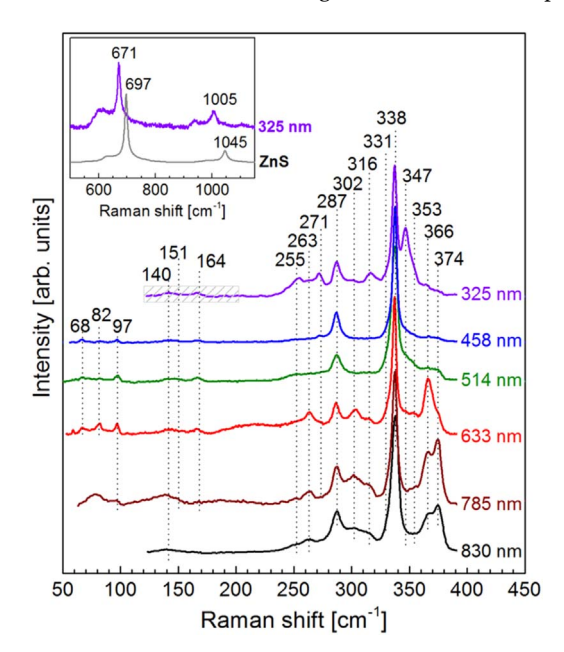


Fig. 36. Raman spectra of polycrystalline CZTS thin films measured with different excitation wavelengths with characteristic peaks labeled. The inset shows a wider spectral range of data collected for both the CZTS film as well as a ZnS control. Reprinted with permission from Ref. [128]. Copyright 2014 AIP Publishing.

impurity phases. Like all other characterization techniques, care must be taken to ensure possible impurities aren't being overlooked.

3.2.3. Thermal analysis

Thermal analysis presents simple techniques useful for probing the phase-purity of NP products. Employing methods such as thermogravimetric analysis (TGA), differential thermal analysis (DTA), or differential scanning calorimetry (DSC) may provide an indication of the number of phases present in a NP powder based on the number of transition temperatures observed upon heating. This method can be powerful when complemented with other elemental, phase, and imaging techniques. Due to the possible limitations of these standard methods, often resulting from possible impurity phases of similar structures and compositions relative to the desired product, thermal analysis may provide purity evidence the others cannot but does not yield specific compositional or phase evidence alone.

Data from this technique can be further strengthened with the characterization of NP powders of probable impurity compounds. If a NP impurity compound displays a transition temperature lower than the desired phase, and the desired phase only exhibits one transition temperature, the sample likely does not contain the impurity. Specifically, Riha et al. from our group employed this strategy in the characterization of one of the first solution-based syntheses for quaternary NPs, namely CZTS [129]. As identified in Section 3.2.1, possible impurities, Cu₂SnS₃ (CTS) and ZnS, display crystal structures with overlapping Bragg peaks with CZTS, complicating characterization. In the bulk, these three phases have high melting points with CTS exhibiting a phase transition at 775 °C from triclinic to cubic and melting at 850 °C [130,131], CZTS melting at 991 °C [131], and ZnS undergoing a phase transition from cubic to wurtzite at 1020 °C followed by melting at 1650 °C [132]. Due to size-dependent melting point depressions, these values could be lowered for these materials as NPs. This brings the melting points of many of these compounds within the range of common thermal analysis equipment. Fig. 37 displays DTA data of four samples tested: two CZTS samples, one CTS sample, and a mixture of CTS and ZnS [129]. The two CZTS samples each exhibited only one transition temperature, at 827 and 830 °C. The CTS similarly had one transition temperature but at a lower temperature (747 °C) while the CTS-ZnS mixture showed two transition temperatures (737 °C and 817 °C). The detection of transitions for the possible impurity phases at lower temperatures than that observed for the CZTS samples implies the lack of these byproducts in the CZTS samples.

Two CZTS NP synthetic reports have employed this method to bolster characterization of phase-pure products. In 2012, Shin et al. prepared CZTS nanoparticles by microwave irradiation of the constituent elemental precursors in aqueous solution to form precursor powders followed by annealing under H₂S [133]. Their thermal analysis by TGA and DTA exhibited mass loss and an endothermic peak at 840 °C, which the authors attributed to kesterite CZTS alone. In 2013, Chesman et al. reported a CZTS NP synthesis that targeted the in situ production of metal complexes coordinated by S-containing ligands followed by heating to cause decomposition and formation of the metal-sulfide solid phase components [134]. The progress of the reaction was characterized by in situ XRD on a small amount of reaction solution in a sample well. Thermal analysis (DTA) was carried out on the end product, showing one high temperature transition peak at 861 °C. These studies are not a fully comprehensive list of reports employing this method for characterization of the phase-purity of NP powders. However, they used unique synthetic methods for the production of CZTS NPs, and the reported transition temperatures as a collection gave a small, empirical range for the CZTS NP melting point (827-861 °C).

Of course, due to the melting point depression of small crystalline grains, variations in melting points of the same compound as a function of size differences might exist. We would encourage those using this characterization method to carry out control experiments on possible

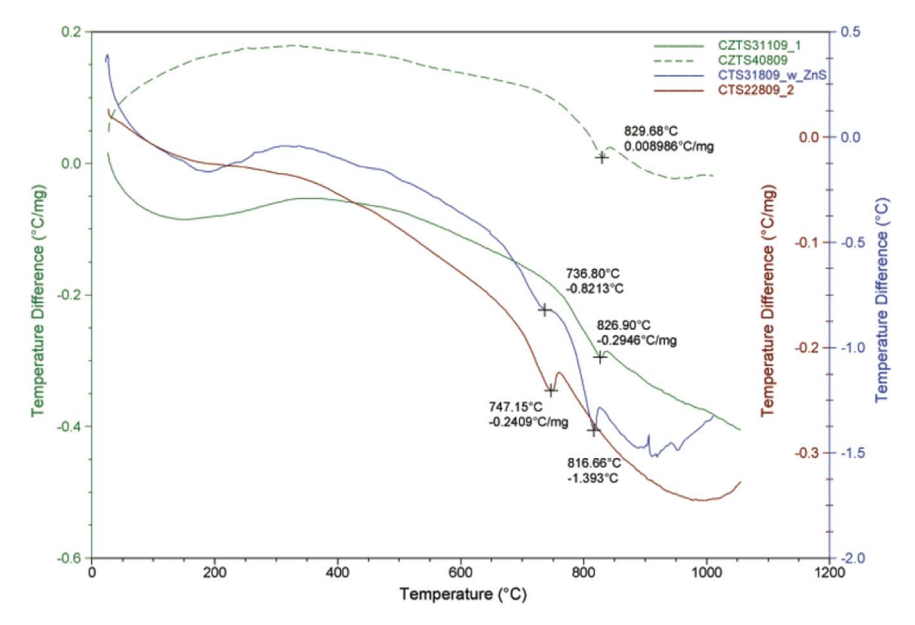


Fig. 37. Differential thermal analysis data of two CZTS NP samples (green solid and dashed lines), CTS NPs (maroon), and a mixture of CTS and ZnS NPs (blue). The CZTS samples show only one transition temperature at a higher value than either of the CTS or CTS+ZnS samples displayed, suggesting the phase-purity of CZTS. Reprinted with permission from Ref. [129]. Copyright 2009 American Chemical Society. (For interpretation of the references to color in this figure legend, the reader is referred to the web version of this article.)

impurity phases, synthesizing these compounds within similar synthetic methods employed for the desired product. Exemplified by this 34 °C range of transition temperatures reported for CZTS NPs prepared via only three different methods one might imagine melting point differences for impurity phases based on distinct synthetic methods, as well. A weakness of this method lies in the possibility of an impurity phase exhibiting a melting point overlapping with that of the desired end phase, making the data indecipherable between the presence of two phases or just one. Identifying likely impurity transitions would provide better evidence for eliminating possible alternative hypotheses and is especially important considering the sensitivity of NP synthetic systems.

3.2.4. X-ray photoelectron spectroscopy and X-ray absorption spectroscopy

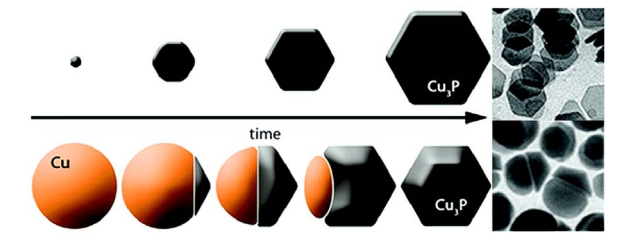
X-ray photoelectron spectroscopy (XPS) is a semi-quantitative, surface-sensitive technique that identifies the elemental composition of a sample and the elemental binding environments. This technique can be particularly useful for characterizing solid-phase intermediates and final products of NP syntheses especially for amorphous solids as long-range order is not required. For example, in the work by White et al., XPS on samples from the formation of h*-LiZnSb indicated the presence of an amorphous Sb⁰ intermediate [37]. This was suspected by PXRD because a very broad peak corresponding to the most intense reflection for elemental Sb was observed. XPS on early reaction samples showed three Sb 3d binding environments: Sb(0), Sb(III), and Sb(V). The +3 and +5 oxidation states were suggested to correspond to free (unreacted) and surface-bound forms of Sb precursor (triphenylstibine, Ph₃Sb), and the zero-valent species confirmed the amorphous Sb⁰ phase. The identification of elemental oxidation states highlights another advantage of XPS which exists as a complementary handle for characterizing solid-state intermediates in the pursuit of understanding reaction pathways.

Our group has used XPS to study the structure and the stability of NPs under air exposure [135–137]. For example, Riha et al. quantified the oxidation of Cu_2Se by tracking the Cu:Se ratio [135]. The ratio increased from 2:1–5.2:1 and complementary XRD data indicated the transformation of Cu_2Se to $\text{Cu}_{1.8}\text{Se}$. Both data sets suggested the solid-state diffusion of cationic Cu from the particle core to the surface. This finding was particularly useful for Korala et al. in a later study of $\text{Cu}_2\text{ZnSnS}_4$ (CZTS) NPs synthesized with a $\text{Cu}_{2\text{-x}}\text{Se}$ shell [136].

Copper(I) cations in stoichiometric Cu₂Se NPs generated Cu vacancies in the valence band ("self-doping" of Cu₂Se to Cu_{2-x}Se), increasing the mobile carrier concentration [135,138]. Thus, the authors hypothesized that a conductive shell of Cu₂Se grown on CZTS would induce self-doping and improve the conductivity of NP thin films upon exposure to air. XPS was used as a complementary technique to confirm the oxidation states of Cu in Cu_{2-x}Se. Finally, another oxidation study was done by Fredrick et al. on the surface reactivity of Fe₂GeS₄ [137]. As-synthesized NPs were studied with XPS, and oxidation of the surface was observed between 0 (several seconds of air exposure) and 24 h. The oxidation of Fe(II) to Fe(III) was observed alongside the transformation of the dominant Ge binding environment from that characteristic of Ge(IV) disulfide to that of GeO2. Because these changes are amorphous and could not be detected by PXRD, XPS gave unique information on this process. To alleviate the instability of the particles, ligand exchange was performed to cap the surface with S2-. Subsequent XPS spectra demonstrated the slowed oxidation of the Ge species.

XPS is a valuable resource for characterizing the intermediates and end products through the course of a reaction by elucidating elemental binding environments. Although the highlighted studies focused on identification of an amorphous intermediate phase and characterization of NP oxidation, we also believe XPS could be valuable for other investigations. For example, if crystalline and amorphous phases had distinct oxidation states of the same element, they could be identified simultaneously. Additionally, the measurement of elemental binding environments could inform bond transformations in the study of reaction mechanisms and pathways. However, XPS is limited to solids or samples that are not vulnerable to evacuation of the instrument. Further, due to the surface sensitivity of XPS, the binding environments are more representative of the surface rather than the ensemble. This can be used advantageously but must be kept in mind for all studies.

Another X-ray technique that provides similarly elemental-specific information but is more representative of the bulk of the sample is X-ray absorption spectroscopy. In particular, extended X-ray absorption fine structure (EXAFS) is used to analyze an element's specific local structure and gives a one-dimensional partial pair distribution function. Espinosa-Faller et al. used EXAFS to analyze the local structures of Cu, Zn, and Sn in CZTS NPs [139]. The authors discovered the presence of an aperiodic disorder on the



Scheme 15. Reaction pathway to Cu_3P by direct nucleation synthesized with the TOP:Cu molar ratio = 11:1 (top). Reaction pathway to Cu_3P by phosphorization of Cu particles synthesized with the TOP:Cu molar ratio = 5.6:1 (bottom). Reprinted with permission from Ref. [140]. Copyright 2012 American Chemical Society.

cation sites that diminished with annealing. Liakakos et al. studied the formation of various Co particle morphologies and used EXAFS as a complementary technique to PXRD and TEM [9]. The data confirmed the metallic nature of Co in all of the samples and provided evidence for well-defined local order despite variations in long-range order among the samples.

3.2.5. Ex situ transmission electron microscopy (TEM)

Imaging NP systems by transmission electron microscopy (TEM) is advantageous compared to other techniques because it reveals physical properties in high resolution at the atomic level (Å to nm). While inherently limited by the small sample size observed, it may provide highly detailed structural, morphological, and compositional information including but not limited to structure and defect properties as well as elemental analysis with use of STEM EDS. The combinatorial nature of the properties TEM can probe comes to great use in examining heterostructured NPs in which the spatial orientation of multiple phases is investigated. For example, core/shell NP syntheses benefit from elemental mapping by STEM EDS, identifying deposition of the shell material on the core rather than nucleation of the shell as NPs on its own.

Here, we highlight this methodology through work by De Trizio et al. in understanding the reaction pathway of Cu_3P NP formation

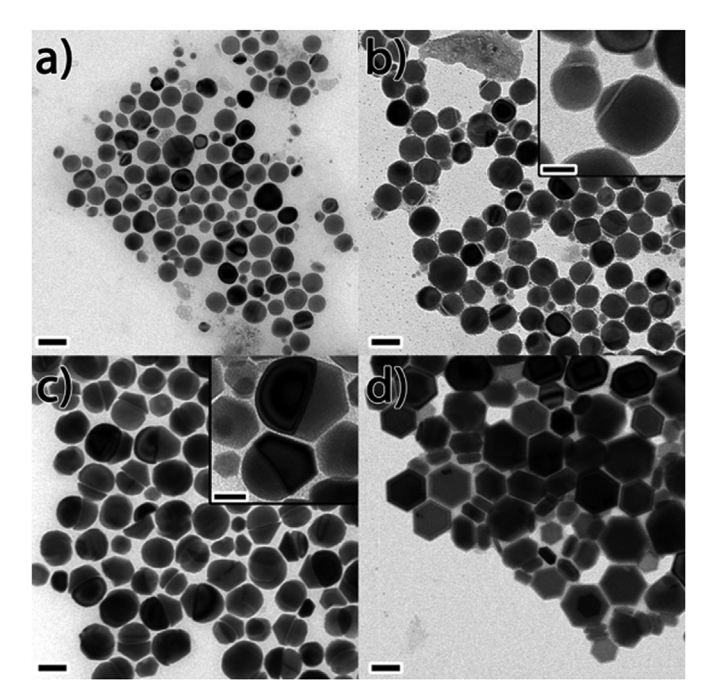


Fig. 38. TEM images documenting the formation of Cu particles and subsequent phosphorization (TOP:Cu molar ratio = 5.6:1). Aliquots collected after (a) 4 min, (b) 10 min, (c) 25 min, (d) 45 min reaction times. The scale bar is 50 nm for the panels and 20 nm for the insets. Reprinted with permission from Ref. [140]. Copyright 2012 American Chemical Society.

[140]. Images of reaction aliquots sampled throughout the reaction progress revealed two different reaction pathways depending on the TOP:Cu precursor ratio (Scheme 15): (1) Cu nucleation and subsequent phosphorization, termed a conversion pathway from Cu to Cu₃P NPs or (2) direct Cu₃P nucleation followed by growth, termed a consumption pathway by the authors. These conclusions were drawn by initially probing the roles and functions of the phosphorus precursor, TOP, and suggested capping ligand, TOPO. The concentrations of each were systematically changed and studied over time.

When the TOP:Cu molar ratio started at 5.6:1, Janus-type particles were synthesized in which a spherical *fcc*-Cu domain and a hexagonal *hcp*-Cu₃P domain co-existed (Fig. 38). Earlier reaction times revealed isolated Cu particles, and longer reaction times showed fully converted Cu₃P NPs. Thus, the authors hypothesized that phosphorization proceeded from a single site on the Cu particles which then extended into the whole NP. The possibility of inhomogeneous ligand coverage of the particles was offered due to the following hypothesis. If all sites were homogeneously available, the reaction likely would have proceeded more centrosymmetrically, leading to core-shell type structures.

When the TOP:Cu molar ratio was 11:1 or greater, the reaction pathway switched to direct Cu_3P nucleation as observed by ex situ TEM (Fig. 39). With increasing TOP:Cu ratios beyond 11:1, increasingly larger particles were observed for the same reaction times. Although it was difficult to discern by an ex situ method whether this was a

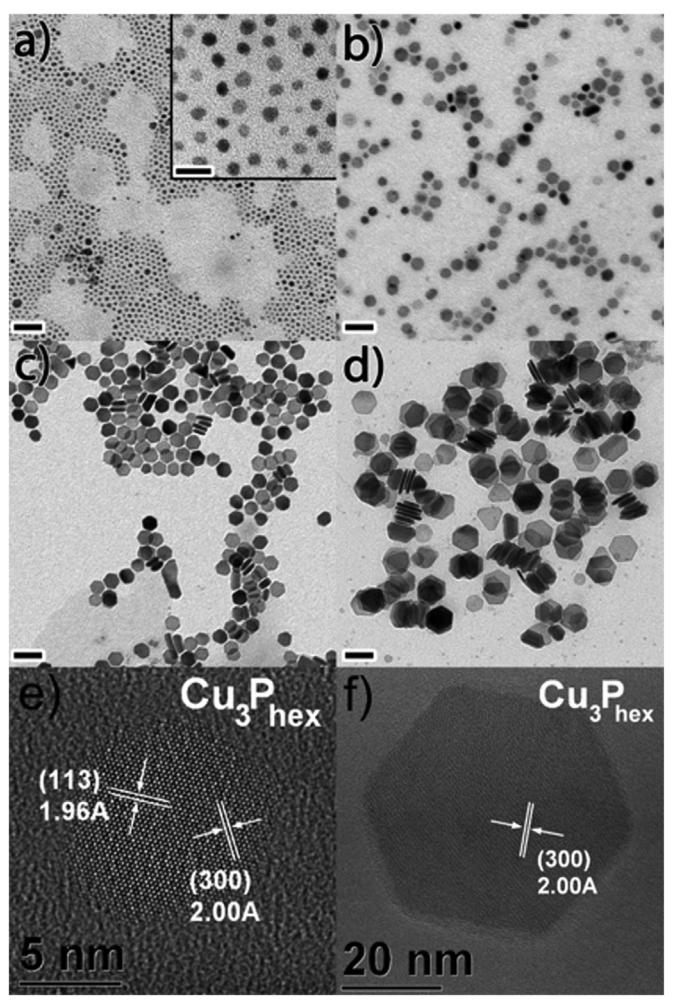


Fig. 39. TEM images tracking the direct formation of Cu_3P nanoplates (TOP:Cu molar ratio = 11:1). Aliquots collected after (a) 10 s, (b) 2 min, (c) 15 min, and (d) 25 min of reaction. The scale bar is 50 nm for the panels and 20 nm for the inset. (e,f) HRTEM images of Cu_3P nanoplates after 10 s and 25 min of reaction, respectively. Adapted with permission from Ref. [140]. Copyright 2012 American Chemical Society.

difference in reaction pathway or a result of faster nucleation and growth, the authors observed large differences in the morphologies and phases detected at various reaction times for the two synthetic conditions. Here, the 11:1 TOP:Cu molar ratio resulted in hexagonal plates comprised of only Cu₃P over the whole reaction time length.

In situ TEM could have provided higher temporal resolution of the reaction mechanism when compared to ex situ aliquots; however, it is limited by the difficulty in accurately replicating in-flask conditions. De Trizio et al. effectively depicted snapshots of the reaction progress through the use of ex situ aliquots. The reaction pathway interpretations were strengthened by the use of complementary techniques. In general, while electron microscopy (EM) has the benefits of elemental analysis by STEM EDS and identification of crystalline solids by SAED or HRTEM, it lacks the ability to inform on the organic portion of nanoparticles such as surface ligands or unreacted monomers. EDS could give qualitative insight on whether NP surfaces exhibit a constituent element-rich or -deficient composition, such as the P-rich Cu₃P NP surfaces reported by Sheets et al. [31], but more quantitative and accurate techniques describing the identity of these organic ligands such as NMR and IR are available.

3.3. Prospects in NP reaction characterization: understanding the complexity of NP syntheses

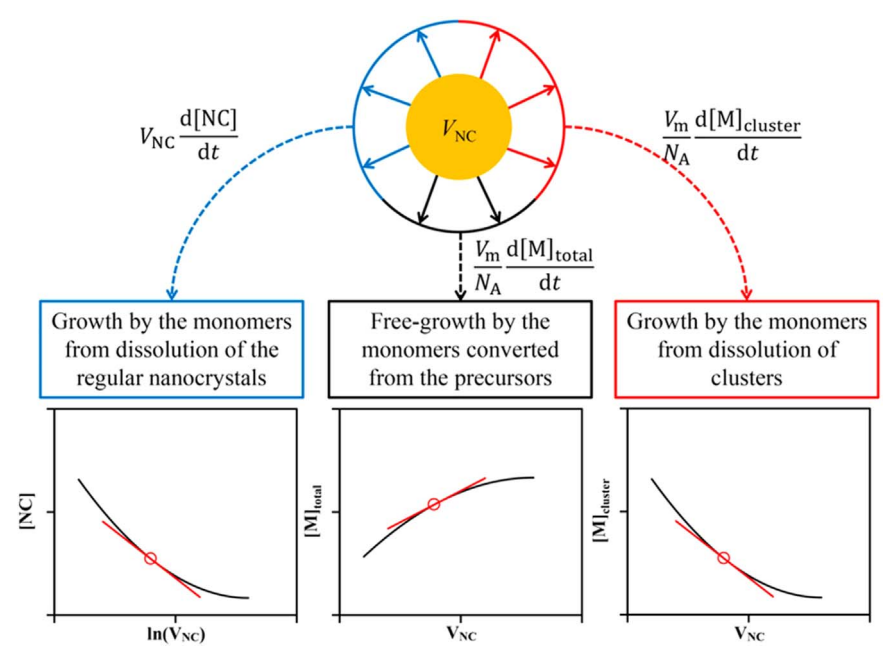
Nanoparticle synthesis is an interdisciplinary field and involves a wide variety of important components. Referencing Scheme 1, syntheses are inherently complex with pathways and mechanisms that could simultaneously occur. Many characterization methods are required to probe unique aspects such as molecular interactions or solid phase evolution. Traditionally this has been done through the use of ex situ complementary techniques. In this section, we describe studies advancing NP synthetic characterization in the development of in situ methods. This requires balancing the limitations of the characterization technique while accurately representing the NP reaction in the sample holder. The NP materials employed in these studies are highly-studied and well-behaved (e.g. Cd chalcogenides). These act as proof of concept systems, and development of their use should lead to progress in a wider range of NP materials.

3.3.1. Using mass conservation to rationalize NC growth via in situ FTIR and UV-Vis spectroscopy

Li et al. developed a model based on mass conservation to rationalize growth mechanisms of CdS quantum dots (QDs) [110]. The model defined the existence of CdS units to exist either as unreacted precursors, NCs, or clusters. Nanocrystals were defined as CdS species with defined crystal structures and lattice parameters corresponding to that of bulk CdS, while clusters encompassed CdS species generally less than 1.5 nm in diameter and potentially lacking periodic crystallinity. Three distinct NC growth channels were identified, all of which involved monomer incorporation in NCs but differed with regard to the origin of the monomer. The first channel was defined as incorporation of monomers converted directly from precursors and was termed "focusing of size distribution". The second and third channels described monomers originating from the dissolution of NCs and clusters, respectively. These channels were associated with the process of "self-focusing of size distribution". Experimentally, precursor conversion was tracked by liquid-phase Fourier transform infrared (FTIR) spectroscopy, and the NC size and concentration was measured by UV-Vis spectroscopy.

A major discovery from this work was the identification of multiple, simultaneous NC growth channels. This challenged the conventional understanding for NC size-focusing directly after a short burst of nucleation. Due to the inverse relationship of NC growth rate with its diameter, the size distribution of the NC ensemble should narrow. However, this assumes NCs do not dissolve back into solution once formed. Li et al. accounted for multiple monomer dissolution paths in the three growth channels identified and described the contribution of each channel to the total NC volume growth rate at any given time in the calculations depicted in Scheme 16. Under typical synthetic conditions for CdS, none of the three channels were observed to be dominant. Further, synthetic parameters ([Cd], [OA], [S], [Cd(oleate)₂], and temperature) were systematically probed in a high-throughput examination of their effect on the growth channels.

In order to track these processes, an automated microreactor system was designed (Fig. 40). This improved reproducibility, accuracy, and time resolution relative to standard solution-based NP synthetic characterization methods. The CdS synthesis had to be



Scheme 16. Three basic reaction channels for CdS growth and their mathematical models. The following terms are defined as: (V_{NC}) average volume of monodisperse NCs, ([NC]) concentration of nanocrystals, (t) time, (V_m) molar volume of nanocrystals, ([M]_{total}) total concentration of CdS composition units converted from precursors, (N_A) Avogadro's number, and ([M]_{cluster}) total concentration of composition unit in the form of clusters. Reprinted with permission from Ref. [110]. Copyright 2018 American Chemical Society.

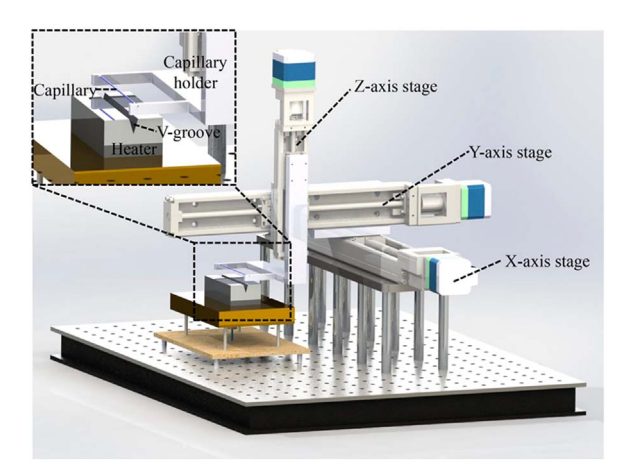


Fig. 40. Schematic of the microreactor system without instrumentation for clarity. Reprinted with permission from Ref. [110]. Copyright 2018 American Chemical Society.

adapted for capillaries, but the reduced volume increased heat transfer rates, eliminating some inherent irreproducibility of typical hot injection syntheses due to temperature variability upon injection of cold precursors. Additionally, NP growth studies typically require removing aliquots to study ex situ, which introduces variability by exposure of the reaction to a syringe and the washing of aliquots with cold solvents. Instead, simultaneous FTIR and UV–Vis spectroscopy measurements were collected in situ, achieving a time resolution on the order of milliseconds between data points. This provided a more accurate view of the reaction components.

Currently, this method is limited to the characterization of QDs of a sufficiently narrow size distribution. The synthesis of CdS QDs from Cd(oleate)2 and elemental S in ODE was studied because it is well reported and results in a well-defined growth stage with monodisperse QDs. The authors stated that these theoretical and experimental methods could be extended to polydisperse QD material systems should an experimental descriptor for size distribution be identified. Further extension of this methodology to other NP materials would present other limitations. First, Li et al. relied on the quantum-confinement of CdS NCs to measure their concentration and size by UV-Vis. Extension to non-quantum-confined NPs would require identification of a rapid measurement for their detection in solution. Second, it would be difficult to study a more complex, multinary system that could possibly undergo a higher number of simultaneous reaction channels due to a larger range of possible, unique intermediates. Identification of spectroscopic signatures for the conversion of precursors, the formation of all intermediates, and the growth of the end products would stand as a major challenge. However, this study has demonstrated an advancement in the in situ detection of concurrent reaction pathways and intermediates for a highly-studied CdS QD synthesis.

An example for a future direction of this instrumental technique could be in gaining insight on III-V InAs QDs. Although we recognize there are plenty of systems that are eligible to be studied by this microreactor system, the synthesis from Srivastava et al. [70] could be a significant next step. The properties of these InAs QDs meet the criteria of the microreactor system but also present an example from a class of materials that is often not considered as well-behaved as II-VI NC systems. Typical syntheses of III-V materials have resulted in broad size distributions due to the small library of pnictide precursors, many of which are highly reactive and exhibit uncontrolled formations of NPs. Srivastava et al. identified a reaction route to small, monodisperse InAs QDs as described in Section 2.2.3.3 [70]. The authors reported absorption spectra of InAs could be collected on dilute aliquots taken directly from the reaction solution, and well-resolved excitonic features could be observed for all sizes, allowing for the system to be probed by

UV—Vis. Additionally, the authors reported the ability to translate the hot injection synthesis to the heat-up method without sacrificing size distribution, encouraging for the potential adaption to capillary use. However, Li et al. argued that a "well-defined" growth stage was required to actually detect these different growth channels. The QD formation of InAs is reported to follow the LaMer model, but it would be interesting to test the sensitivity and capability of the microreactor methodology in this less-explored system.

3.3.2. In situ synchrotron X-ray scattering studies

Another prospective method is the use of synchrotron-based in situ small- and wide-angle X-ray scattering (SAXS and WAXS, respectively) to probe the formation of NPs. These methods provide insight into the mechanistic pathway of a reaction by examining the rate-limiting step as well as the reaction pathway by time-resolved identification of formed species. Preliminarily, well-behaved, well-understood CdSe NPs were examined by Abécassis et al. to differentiate between different growth pathways of the NPs (Fig. 41) [141]. The advantage of in situ measurements is the ability to have continuous data feedback and a consistent sample throughout the reaction. Removal of aliquots for ex situ studies may unexpectedly affect the concentration of reactants and species present in the reaction flask. Although the use of a capillary system raises concern on the accurate representation of a typical reaction volume, Abécassis et al. described how the in situ system can characterize on the order of 10^{17} NPs simultaneously.

The SAXS signal is sensitive to the size of NPs and its magnitude is directly proportional to the concentration. The complementary WAXS technique characterizes the phase and degree of crystallinity of a crystalline sample. By juxtaposing the data of temperature of the reaction system, mean radius, polydispersity, yield, and concentration of the NPs as a function of time, the authors were able to describe the nucleation and growth pathways for CdSe NPs synthesized with cadmium myristate (CdMyr), Se powder, and ODE (Scheme 17).

The strength of this protocol was the ability to track the nucleation event as a function of temperature, often a highly challenging step to observe and characterize due to its rapid occurrence. As the temperature ramped, the intensity of the low q profile in SAXS (corresponding to the dispersed CdMyr precursor in ODE) decreased. It was determined that Se powder dispersed in ODE did not have a measurable contribution, so this signified the dissolution of the Cd precursor into molecular monomers. After the SAXS profile briefly remained unchanged, the intensity of the low q scattering increased when the temperature was raised from 205 to 215 °C which the authors hypothesized to be the onset of NP formation. Nucleation stopped at the maximum reaction temperature of 240 °C. Moreover, the authors considered three different growth-limiting mechanisms: (1) diffusion-limited growth, (2) NP surface limited growth, and (3) precursor to monomer conversion limited growth. The observed growth rate was eight orders of magnitude lower than the expected theoretical diffusion-limited growth, and the experimental data did not fit calculations for growth limitation by reaction at the NP interface. Therefore, the authors suggested that monomer generation limited the NP growth and hypothesized this was due to the required reduction of Se in order to react with the Cd precursor.

3.3.3. Outlook of in situ X-ray diffraction for NP synthesis

Often, the difficulty in establishing in situ techniques is the robustness required from the method to accommodate the harsh environments at which many of these NP syntheses operate, such as chemically reducing environments, high temperature, and/or high pressure. Several in situ techniques for monitoring NP growth as well as chemical and structural transformations are reviewed by Kovalenko et al. [96] Other in situ techniques for studying the surface of NPs in reactive and corrosive environments (e.g. humid air, reactive gases, acidic solutions, etc.) are highlighted by Tao et al. [142].

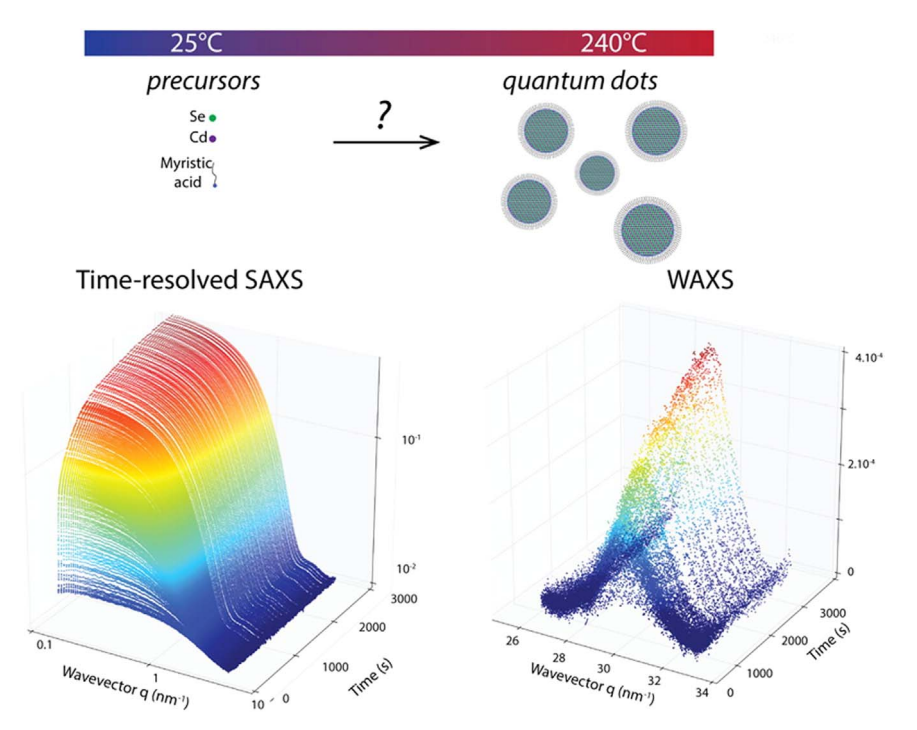
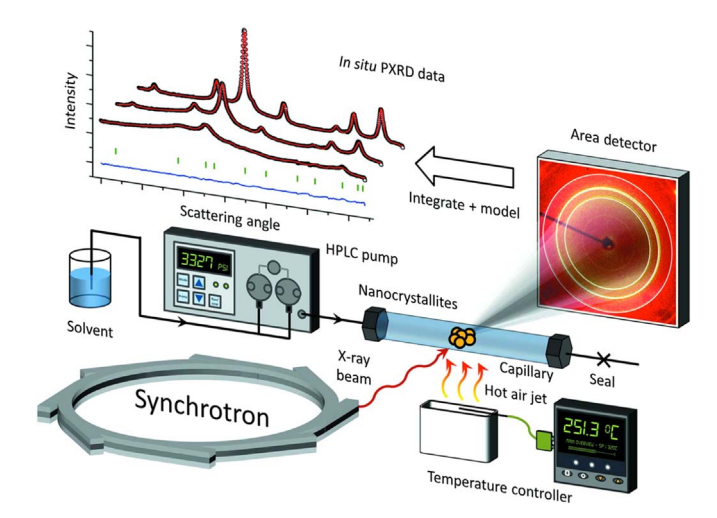


Fig. 41. Time-resolved SAXS and WAXS data used to elucidate the reaction steps from precursors to QDs. Reprinted with permission from Ref. [141]. Copyright 2015 American Chemical Society.

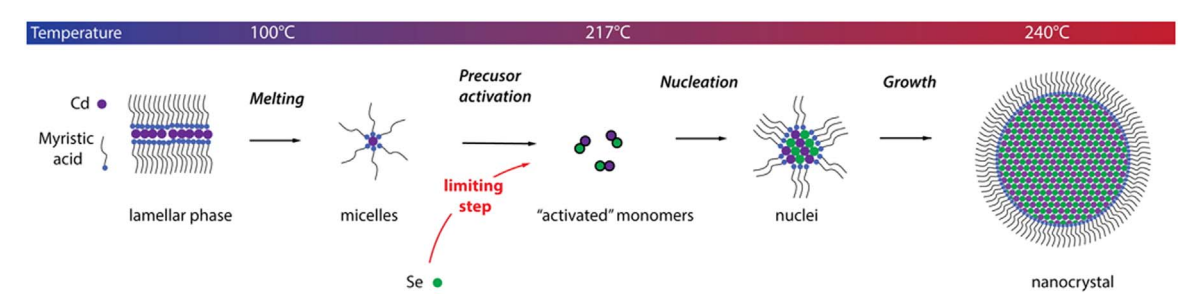
A method for in situ PXRD study of hydrothermal nanoparticle formation was developed by Andersen et al. in 2018 (Scheme 18) [143]. Specifically, a hydrothermal synthesis of $\gamma\text{-Fe}_2\text{O}_3$ was adapted for capillaries allowing second-scale time-resolved observation of the materials' crystallization and growth. The work provides an in-depth experimental approach highlighting the considerations necessary to conduct in situ PXRD experiments at a synchrotron beam source. For example, the group suggested maximizing precursor concentration to provide more diffracting material, resulting in better counting statistics. However, they cautioned this unavoidably sacrifices how the reaction is represented because precursor concentrations affect reaction mechanisms and pathways. Additionally, the authors examined the reproducibility of data collection and analysis by measuring 10 equivalent samples. Ultimately, the report reads as a standard operating procedure and is a unique compendium of detailed, practical experimental information.

These techniques, while innovative and pioneering for the field, still required complementary techniques to describe and support conclusions for well-behaved, well-characterized systems. The increased use of in situ characterization methods will require the development of standard techniques in the examination of more complex NP systems which involve unique considerations. More complex reaction mixtures may present species without straightforward, signatory properties for detection, and the addition of competing reaction pathways adds difficulty in deconvoluting the effects of various important parameters.

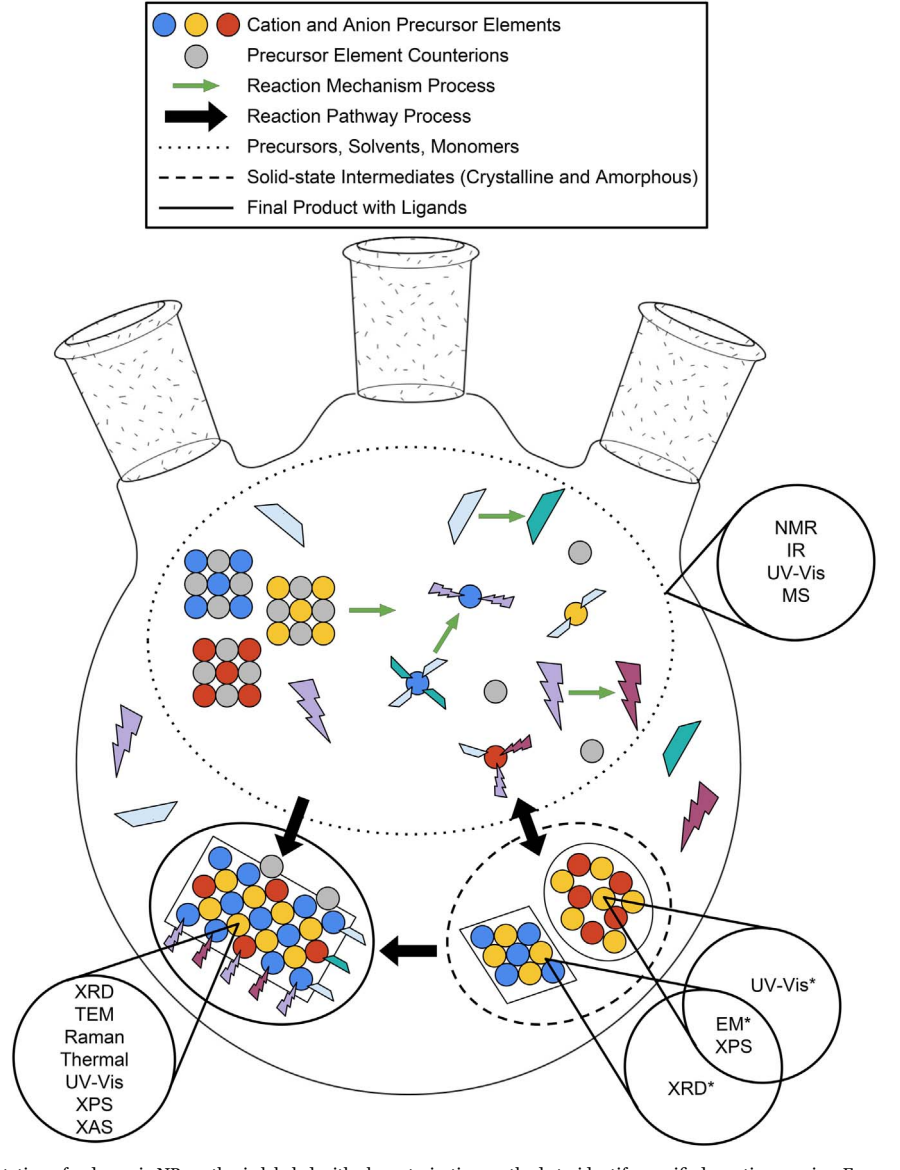


Scheme 18. Graphic representation of in situ synchrotron XRD methodology. Reproduced with permission of the International Union of Crystallography from Ref. [143].

Considering the often observed variability in size dispersion of more complex NP materials, this nonuniformity would open further variables in terms of possible reaction mechanisms and pathways.



Scheme 17. Summary of the reaction pathway to CdSe NPs enabled by in situ SAXS and WAXS. The authors hypothesized that the rate-limiting step was the generation of activated monomers. Reprinted with permission from Ref. [141]. Copyright 2015 American Chemical Society.



Scheme 19. A cartoon representation of a dynamic NP synthesis labeled with characterization methods to identify specified reaction species. For example, precursors, solvents, and monomers (encompassed within a dotted circle) can be characterized by NMR, IR, UV–Vis, and MS. Solvent molecules are represented with purple lightning bolts and light blue trapezoids. Subsequent transformations of these species are represented with a color hue change (e.g. purple to magenta and light blue to teal). (For interpretation of the references to color in this figure legend, the reader is referred to the web version of this article.)

3.4. Characterization summary and perspective

Represented in Scheme 19 are the techniques commonly utilized for characterization of solution-based NP syntheses. The components in the flask depict possible steps from precursors to end products, similarly represented in Scheme 1. The green arrows represent possible reaction mechanism transformations, and the black arrows are steps of reaction pathways. Many of these processes occur simultaneously, underscoring the inherent complexity of NP syntheses. However, characterization is commonly carried out on individual components and transformations, which are grouped by relevant techniques and are circled within the flask.

Reaction mechanism processes are typically described by NMR, IR, UV—Vis, and MS. These techniques are particularly useful in describing molecular species and are highly developed for describing the transformation of monomers and ligand coordination. However, their use does not typically extend to the solid-state components which are commonly characterized by XRD, TEM, Raman, thermal analysis, UV—Vis, and XPS. Traditional characterization is performed on isolated components of NP syntheses. The advancements outlined in this section provide temporal observations of processes via in situ methodology.

4. Conclusions

Consistent with the theme of solid-state chemistry over the past fifty years, the aim for NP synthesis is still understanding and designing reactions to ultimately achieve control over a range of thermodynamically and kinetically stable phases. We have highlighted examples here where new insights into reaction mechanisms and pathways and the roles of the various components of a synthesis provide new opportunities for elucidating understanding and control over the final products. This is a challenging but exciting area of chemistry because the perspectives on synthetic approaches draw from solid-state chemistry, organometallics, coordination chemistry, and organic chemistry. Developing new understanding so that we can move toward more predictive schemes continues to be the aspiration of the field and will lead to new opportunities for materials with novel structures and function, enabling a continually growing group of new technologies.

Traditionally, NP syntheses have involved the characterization of end processes. We challenge the community to characterize dynamic processes so that complete mechanisms and pathways can be proposed (including the identification and quantification of intermediates as well as complete balanced reactions). While a wide range of techniques are available for characterizing NP synthesis, they tend to be sensitive to single nuclei, solution species, or extended solids (but not necessarily clusters of varying sizes). This challenge then requires the expectation in the field be that multiple, complementary characterization methods be used. Moreover, many of the processes depicted here occur simultaneously in a reaction flask, but few characterization methods can describe or deconvolute these simultaneous processes. While some methods have been developed in order to address these limitations, such as the use of mass conservation with FTIR and UV-Vis to characterize growth mechanisms, these techniques are young and have not vet described more complicated systems such as the synthesis of multinary NPs. This leaves room for significant exploratory chemistry to not only develop techniques to answer the questions we pose and to challenge the limits of NP synthesis understanding but also to optimize these techniques to ensure they reproducibly answer the same questions across different NP systems. We close with challenges and important considerations for furthering NP synthetic strategies which we hope we have described well in this review.

- · adopt more uniform and specific diction
- characterize dynamic processes, not just final products
- know the limitations of the techniques used, both inherent to the technique and in relation to the materials studied
- use complementary techniques to find evidence in areas for which other techniques are blind
- examine reactions without compromising the replication accuracy of the components and processes as they exist in the original reaction (e.g. in situ capillary experiments, the use of control experiments)
- thoroughly consider all aspects and components present, even if something is traditionally regarded as benign

In particular, if we seek to collaborate with our theory colleagues, we must be able to describe transient species as well as failed reactions so as to contribute useful data for further developing computational methods that can help guide synthetic exploration.

Acknowledgements

There are no competing interests to declare. We thank Dr. Daniel Agocs and Prof. Gordon Miller (Iowa State University) for thoughtful comments. The work was supported by the NSF SSMC program (SSMC-1710672) and the W.M. Keck Foundation.

References

- [1] A. Stein, S.W. Keller, T.E. Mallouk, Science 259 (5101) (1993) 1558-1564.
- [2] R.E. Schaak, M.E. Williams, ACS Nano 6 (10) (2012) 8492-8497.
- [3] J.L. Fenton, B.C. Steimle, R.E. Schaak, Science 360 (6388) (2018) 513-517. [4] R. Ghosh Chaudhuri, S. Paria, Chem. Rev. 112 (4) (2012) 2373-2433.
- [5] L. De Trizio, L. Manna, Chem. Rev. 116 (18) (2016) 10852-10887.
- [6] C.B. Murray, D.J. Norris, M.G. Bawendi, J. Am. Chem. Soc. 115 (19) (1993) 8706-8715.
- Y. Yin, A.P. Alivisatos, Nature 437 (7059) (2005) 664-670.
- [8] D. Milliron, S.M. Hughes, Y. Cui, L. Manna, J. Li, L.W. Wang, A.P. Alivisatos, Nature 430 (6996) (2004) 190-195.
- N. Liakakos, B. Cormary, X. Li, P. Lecante, M. Respaud, L. Maron, A. Falqui, A. Genovese, L. Vendier, S. Koïnis, B. Chaudret, K.J. Soulantica, Am. Chem. Soc. 134 (43) (2012) 17922-17931.
- [10] C. Bullen, J. van Embden, J. Jasieniak, J.E. Cosgriff, R.J. Mulder, E. Rizzardo, M. Gu, C.L. Raston, Chem. Mater. 22 (14) (2010) 4135-4143.
- [11] R. García-Rodríguez, M.P. Hendricks, B.M. Cossairt, H. Liu, J.S. Owen, Chem. Mater. 25 (8) (2013) 1233-1249.
- [12] P. Reiss, M. Carrière, C. Lincheneau, L. Vaure, S. Tamang, Chem. Rev. 116 (18) 2016) 10731-10819.
- S.R. Alvarado, Y. Guo, T.P.A. Ruberu, E. Tavasoli, J. Vela, Coord. Chem. Rev. 263-264 (2014) 182-196
- [14] O. Yarema, M. Yarema, W.M.M. Lin, V. Wood, Chem. Commun. 52 (72) (2016)

- 10878-10881
- [15] J.S. Steckel, B.K.H. Yen, D.C. Oertel, M.G. Bawendi, J. Am. Chem. Soc. 128 (40) (2006) 13032-13033.
- H. Liu, J.S. Owen, A.P. Alivisatos, J. Am. Chem. Soc. 129 (2) (2007) 305-312.
- L.C. Frenette, T.D. Krauss, Nat. Commun. 8 (1) (2017) 2082.
- [18] T.P.A. Ruberu, H.R. Albright, B. Callis, B. Ward, J. Cisneros, H.-J. Fan, J. Vela, ACS Nano 6 (6) (2012) 5348-5359.
- Y. Guo, S.R. Alvarado, J.D. Barclay, J. Vela, ACS Nano 7 (4) (2013) 3616-3626.
- [20] B.A. Tappan, G. Barim, J.C. Kwok, R.L. Brutchey, Chem. Mater. 30 (16) (2018)
- [21] S. Mourdikoudis, L.M. Liz-Marzán, Chem. Mater. 25 (9) (2013) 1465-1476.
- J.W. Thomson, K. Nagashima, P.M. Macdonald, G.A. Ozin, J. Am. Chem. Soc. 133 (13) (2011) 5036-5041.
- [23] Y. Liu, D. Yao, L. Shen, H. Zhang, X. Zhang, B. Yang, J. Am. Chem. Soc. 134 (17) (2012) 7207-7210.
- Y. Wei, J. Yang, A.W.H. Lin, J.Y. Ying, Chem. Mater. 22 (20) (2010) 5672-5677.
- [25] S.C. Riha, B.A. Parkinson, A.L. Prieto, J. Am. Chem. Soc. 133 (39) (2011)
- [26] D. Aldakov, A. Lefrançois, P. Reiss, J. Mater. Chem. C 1 (24) (2013) 3756.
- K. Ramasamy, H. Sims, W.H. Butler, A. Gupta, Chem. Mater. 26 (9) (2014)
- [28] B.C. Walker, R. Agrawal, Chem. Commun. 50 (61) (2014) 8331.
- [29] M.P. Hendricks, M.P. Campos, G.T. Cleveland, I. Jen-La Plante, J.S. Owen, Science 348 (6240) (2015) 1226-1230.
- [30] M.P. Campos, M.P. Hendricks, A.N. Beecher, W. Walravens, R.A. Swain, G.T. Cleveland, Z. Hens, M.Y. Sfeir, J.S. Owen, J. Am. Chem. Soc. 139 (6) (2017) 2296-2305.
- [31] E.J. Sheets, W.-C. Yang, R.B. Balow, Y. Wang, B.C. Walker, E.A. Stach, R. Agrawal, J. Mater. Res. 30 (23) (2015) 3710-3716.
- [32] G.G. Yordanov, H. Yoshimura, C.D. Dushkin, Colloid Polym. Sci. 286 (6-7) (2008) 813-817.
- [33] Z. Li, Y. Ji, R. Xie, S.Y. Grisham, X. Peng, J. Am. Chem. Soc. 133 (43) (2011) 17248-17256.
- [34] Z. Deng, L. Cao, F. Tang, B. Zou, J. Phys. Chem. B 109 (35) (2005) 16671-16675. [35] C. Pu, J. Zhou, R. Lai, Y. Niu, W. Nan, X. Peng, Nano Res. 6 (9) (2013) 652–670.
- [36] R. Xie, Z. Li, X. Peng, J. Am. Chem. Soc. 131 (42) (2009) 15457-15466.
- [37] M.A. White, K.J. Baumler, Y. Chen, A. Venkatesh, A.M. Medina-Gonzalez, A.J. Rossini, J.V. Zaikina, E.M. Chan, J. Vela, Chem. Mater. 30 (17) (2018) 6173-6182.
- [38] Z.A. Peng, X. Peng, J. Am. Chem. Soc. 123 (1) (2001) 183-184.
- [39] M. Yarema, R. Caputo, M.V. Kovalenko, Nanoscale 5 (18) (2013) 8398–8410.
- [40] R.G. Pearson, J. Am. Chem. Soc. 85 (22) (1963) 3533-3539.
- R.G. Parr, R.G. Pearson, J. Am. Chem. Soc. 105 (26) (1983) 7512-7516.
- [42] R.G. Pearson, Chemical Hardness, Wiley-VCH Verlag GmbH, Weinheim, Germany, 1997.
- C. Nayral, T. Ould-Ely, A. Maisonnat, B. Chaudret, P. Fau, L. Lescouzères, A. Pevre-Lavigne, Adv. Mater. 4 (1) (1999) 61-63.
- N. Cordente, M. Respaud, F. Senocq, M.-J. Casanove, C. Amiens, B. Chaudret, Nano Lett. 1 (10) (2001) 565–568.
- C. Pan, K. Pelzer, K. Philippot, B. Chaudret, F. Dassenoy, P. Lecante, M.J. Casanove, J. Am. Chem. Soc. 123 (31) (2001) 7584-7593.
- [46] F. Dumestre, B. Chaudret, C. Amiens, M.C. Fromen, M.J. Casanove, P. Renaud, P. Zurcher, Angew. Chemie - Int. Ed. 41 (22) (2002) 4286-4289.
- C. Desvaux, C. Amiens, P. Fejes, P. Renaud, M. Respaud, P. Lecante, E. Snoeck, B. Chaudret, Nat. Mater. 4 (10) (2005) 750-753.
- A. Meffre, S. Lachaize, C. Gatel, M. Respaud, B. Chaudret, J. Mater. Chem. 21 (35) (2011) 13464-13469
- [49] M. Monge, M.L. Kahn, A. Maisonnat, B. Chaudret, Angew. Chemie Int. Ed 42 (43) (2003) 5321-5324.
- [50] A. Glaria, M.L. Kahn, T. Cardinal, F. Senocq, V. Jubera, B. Chaudret, New J. Chem. 32 (4) (2008) 662-669.
- M.L. Kahn, A. Glaria, C. Pages, M. Monge, L. Saint Macary, A. Maisonnat, B. Chaudret, J. Mater. Chem. 19 (24) (2009) 4044-4060.
- M.L. Kahn, M. Monge, V. Collière, F. Senocq, A. Maisonnat, B. Chaudret, Adv. Funct. Mater. 15 (3) (2005) 458-468.
- C. Amiens, B. Chaudret, D. Ciuculescu-Pradines, V. Collière, K. Fajerwerg, P. Fau, M. Kahn, A. Maisonnat, K. Soulantica, K. Philippot, New J. Chem. 37 (11) (2013) 3374-3401.
- H. Yu, J. Li, R.A. Loomis, P.C. Gibbons, L.W. Wang, W.E. Buhro, J. Am. Chem. Soc. 125 (52) (2003) 16168-16169.
- [55] H. Yu, P.C. Gibbons, W.E. Buhro, J. Mater. Chem. 14 (2004) 595-602.
- F. Wang, W.E. Buhro, Small 6 (4) (2010) 573-581.
- [57] M.V. Kovalenko, W. Heiss, E.V. Shevchenko, J.-S. Lee, H. Schwinghammer, A.P. Alivisatos, D.V. Talapin, J. Am. Chem. Soc. 129 (37) (2007) 11354-11355.
- [58] S.G. Hickey, C. Waurisch, B. Rellinghaus, A. Eychmüller, J. Am. Chem. Soc. 130 (45) (2008) 14978-14980.
- W.J. Baumgardner, J.J. Choi, Y.-F. Lim, T. Hanrath, J. Am. Chem. Soc. 132 (28) (2010) 9519-9521. M.J. Polking, H. Zheng, R. Ramesh, A.P. Alivisatos, J. Am. Chem. Soc. 133 (7)
- (2011) 2044-2047. P.D. Antunez, J.J. Buckley, R.L. Brutchey, Nanoscale 3 (6) (2011) 2399-2411.
- M.V. Kovalenko, D.V. Talapin, M.A. Loi, F. Cordella, G. Hesser, M.I. Bodnarchuk, W. Heiss, Angew. Chemie - Int. Ed. 47 (16) (2008) 3029-3033.

- [63] M. Yarema, S. Pichler, M. Sytnyk, R. Seyrkammer, R.T. Lechner, G. Fritz-Popovski, D. Jarzab, K. Szendrei, R. Resel, O. Korovyanko, M.A. Loi, O. Paris, G. Hesser, W. Heiss, ACS Nano 5 (5) (2011) 3758-3765.
- [64] K. Kravchyk, L. Protesescu, M.I. Bodnarchuk, F. Krumeich, M. Yarema, M. Walter, C. Guntlin, M.V. Kovalenko, J. Am. Chem. Soc. 135 (11) (2013) 4199-4202.
- [65] M. He, L. Protesescu, R. Caputo, F. Krumeich, M.V. Kovalenko, Chem. Mater. 27 (2) (2015) 635-647.
- [66] O. Yarema, D. Bozyigit, I. Rousseau, L. Nowack, M. Yarema, W. Heiss, V. Wood, Chem. Mater. 25 (18) (2013) 3753-3757.
- [67] H. Zhong, Z. Wang, E. Bovero, Z. Lu, F.C.J.M. Van Veggel, G.D. Scholes, J. Phys. Chem. C 115 (25) (2011) 12396-12402.
- O. Yarema, M. Yarema, D. Bozyigit, W.M.M. Lin, V. Wood, ACS Nano 9 (11) (2015) 11134–11142.
- [69] O. Yarema, M. Yarema, V. Wood, Chem. Mater. 30 (5) (2018) 1446-1461.
- [70] V. Srivastava, E. Dunietz, V. Kamysbayev, J.S. Anderson, D.V. Talapin, Chem. Mater. 30 (11) (2018) 3623-3627.
- [71] S.D. Dingman, N.P. Rath, P.D. Markowitz, P.C. Gibbons, W.E. Buhro, Angew. Chemie - Int. Ed. 39 (8) (2000) 1470-1472.
- [72] N.S. Karan, Y. Chen, Z. Liu, R. Beaulac, Chem. Mater. 28 (16) (2016) 5601-5605.
- [73] F. Wang, A. Dong, W.E. Buhro, Chem. Rev. 116 (18) (2016) 10888-10933.
- [74] Y. Chen, N.T. Landes, D.J. Little, R. Beaulac, J. Am. Chem. Soc. 140 (33) (2018) 10421-10424.
- [75] P. Zolotavin, P. Guyot-Sionnest, ACS Nano 4 (10) (2010) 5599-5608.
- [76] A. Das, A. Shamirian, P.T. Snee, Chem. Mater. 28 (11) (2016) 4058-4064.
- [77] A. Das, B. Hsu, A. Shamirian, Z. Yang, P.T. Snee, Chem. Mater. 29 (10) (2017) 4597-4602.
- [78] D.P. Shoemaker, Y.-J. Hu, D.Y. Chung, G.J. Halder, P.J. Chupas, L. Soderholm, J.F. Mitchell, M.G. Kanatzidis, Proc. Natl. Acad. Sci. USA 111 (30) (2014) 10922-10927.
- [79] A. Bhutani, J.A. Schiller, J.L. Zuo, J.N. Eckstein, L.H. Greene, S. Chaudhuri, D.P. Shoemaker, Chem. Mater. 29 (14) (2017) 5841-5849.
- [80] Z. Jiang, A. Ramanathan, D.P. Shoemaker, J. Mater. Chem. C 5 (23) (2017) 5709-5717
- [81] A.J. Martinolich, J.A. Kurzman, J.R. Neilson, J. Am. Chem. Soc. 138 (34) (2016) 11031-11037.
- [82] A.J. Martinolich, J.R. Neilson, Chem. Mater. 29 (2) (2017) 479-489.
- [83] S.G. Kwon, T. Hyeon, Small 7 (19) (2011) 2685-2702.
- [84] J. van Embden, A.S.R. Chesman, J.J. Jasieniak, Chem. Mater. 27 (7) (2015) 2246-2285.
- [85] C. de Mello Donegá, P. Liljeroth, D. Vanmaekelbergh, Small 1 (12) (2005) 1152-1162.
- [86] J. Wang, P. Liu, C.C. Seaton, K.M. Ryan, J. Am. Chem. Soc. 136 (22) (2014) 7954-7960
- [87] M. Ahmadi, S.S. Pramana, L. Xi, C. Boothroyd, Y.M. Lam, S. Mhaisalkar, J. Phys. Chem. C 116 (14) (2012) 8202-8209.
- [88] L.N. Hutfluss, P.V. Radovanovic, J. Am. Chem. Soc. 137 (3) (2015) 1101-1108.
- [89] M. Kar, R. Agrawal, H.W. Hillhouse, J. Am. Chem. Soc. 133 (43) (2011) 17239-17247
- [90] D.B. Agocs, A.L. Prieto, Hot Injection Synthesis and Characterization of Copper Antimony Selenide Non-Canonical Nanomaterials Toward Earth-Abundant Renewable Energy Conversion, Colorado State University, 2018.
- [91] E.M. Chan, C. Xu, A.W. Mao, G. Han, J.S. Owen, B.E. Cohen, D.J. Milliron, Nano Lett. 10 (5) (2010) 1874-1885.
- [92] D.C. Gary, B.A. Glassy, B.M. Cossairt, Chem. Mater. 26 (4) (2014) 1734–1744.
- [93] D.C. Gary, M.W. Terban, S.J.L. Billinge, B.M. Cossairt, Chem. Mater. 27 (4) (2015) 1432 - 1441.
- [94] C.J. Murphy, J.M. Buriak, Chem. Mater. 27 (14) (2015) 4911–4913.
- [95] K.L. Sowers, B. Swartz, T.D. Krauss, Chem. Mater. 25 (8) (2013) 1351-1362.
- [96] M.V. Kovalenko, L. Manna, A. Cabot, Z. Hens, D.V. Talapin, C.R. Kagan, V.I. Klimov, A.L. Rogach, P. Reiss, D.J. Milliron, P. Guyot-Sionnnest G. Konstantatos, W.J. Parak, T. Hyeon, B.A. Korgel, C.B. Murray, W. Heiss, ACS Nano 9 (2) (2015) 1012-1057.
- [97] Z. Hens, J.C. Martins, Chem. Mater. 25 (8) (2013) 1211–1221.
- [98] M.A. Boles, D. Ling, T. Hyeon, D.V. Talapin, Nat. Mater. 15 (2) (2016) 141-153.
- [99] N.C. Anderson, J.S. Owen, Chem. Mater. 25 (1) (2013) 69-76.
- [100] N.C. Anderson, M.P. Hendricks, J.J. Choi, J.S. Owen, J. Am. Chem. Soc. 135 (49) (2013) 18536-18548.
- [101] K. De Keukeleere, S. Coucke, E. De Canck, P. Van Der Voort, F. Delpech, Y. Coppel, Z. Hens, I. Van Driessche, J.S. Owen, J. De Roo, Chem. Mater. 29 (23) (2017) 10233-10242.
- [102] R. García-Rodríguez, H. Liu, J. Am. Chem. Soc. 136 (5) (2014) 1968-1975.
- [103] W. Schoefberger, J. Schlagnitweit, N. Müller, Annu. Rep. NMR Spectrosc. 72 (2011) 1-60.

- [104] D.J. Norris, N. Yao, F.T. Charnock, T.A. Kennedy, Nano Lett. 1 (1) (2001) 3-7.
- [105] F. Wang, R. Tang, W.E. Buhro, Nano Lett. 8 (10) (2008) 3521-3524.
- [106] J.T. Kopping, T.E. Patten, J. Am. Chem. Soc. 130 (17) (2008) 5689-5698.
- G. Socrates, Infrared and Raman Characteristic Group Frequencies: Tables and Charts, John Wiley & Sons, 2004.
- [108] P.E. Chen, N.C. Anderson, Z.M. Norman, J.S. Owen, J. Am. Chem. Soc. 139 (8) (2017) 3227-3236.
- [109] J.M. Pietryga, Y.-S. Park, J. Lim, A.F. Fidler, W.K. Bae, S. Brovelli, V.I. Klimov, Chem. Rev. 116 (18) (2016) 10513-10622.
- [110] J. Li, H. Wang, L. Lin, Q. Fang, X. Peng, J. Am. Chem. Soc. 140 (16) (2018) 5474-5484.
- [111] P. Scherrer, Nachr. Ges. Wiss. Gött. (1918) 96-100.
- [112] A. Walsh, S. Chen, S.H. Wei, X.G. Gong, Adv. Energy Mater. 2 (4) (2012)
- [113] S. Chen, A. Walsh, X.-G. Gong, S.-H. Wei, Adv. Mater. 25 (11) (2013) 1522-1539.
- [114] B.-B. Yu, X. Zhang, Y. Jiang, J. Liu, L. Gu, J.S. Hu, L.J. Wan, J. Am. Chem. Soc. 137 (6) (2015) 2211–2214.
- [115] S. Shukla, G. Xing, H. Ge, R.R. Prabhakar, S. Mathew, Z. Su, V. Nalla, T. Venkatesan, N. Mathews, T. Sritharan, T.C. Sum, Q. Xiong, ACS Nano 10 (4) (2016) 4431-4440
- [116] M. Cabán-Acevedo, M.S. Faber, Y.Z. Tan, R.J. Hamers, S. Jin, Nano Lett. 12 (4) (2012) 1977-1982.
- [117] A. Boughriet, R.S. Figueiredo, J. Laureyns, P. Recourt, J. Chem. Soc. Faraday Trans. 93 (17) (1997) 3209-3215.
- [118] J.A. Bourdoiseau, M. Jeannin, C. Rémazeilles, R. Sabot, P. Refait, J. Raman Spectrosc. 42 (3) (2011) 496-504.
- [119] C. Steinhagen, T.B. Harvey, C.J. Stolle, J. Harris, B.A. Korgel, J. Phys. Chem. Lett. 3 (17) (2012) 2352-2356.
- [120] T.P. Mernagh, A.G. Trudu, Chem. Geol. 103 (1993) 113-127.
- [121] H.C. Liese, Appl. Spectrosc. 28 (2) (1974) 135–139.
- [122] H. Tanino, T. Maeda, H. Fujikake, H. Nakanishi, S. Endo, T. Irie, Phys. Rev. B 45 (23) (1992) 13323-13330.
- [123] C. Rincón, S.M. Wasim, G. Marín, J.M. Delgado, J.R. Huntzinger, A. Zwick, J. Galibert, Appl. Phys. Lett. 73 (4) (1998) 441-443.
- [124] J. Łażewski, H. Neumann, K. Parlinski, G. Lippold, J. Stanbery, Phys. Rev. B -Condens. Matter Mater. Phys. 68 (14) (2003) 1-8.
- [125] S. Shirakata, T. Murakami, T. Kariya, S. Isomura, Jpn. J. Appl. Phys. 35 (Part 1, 1A) (1996) 191-199.
- [126] S. Shirakata, H. Kubo, C. Hamaguchi, S. Isomura, Jpn. J. Appl. Phys. 36 (Part 2, 10B) (1997) L1394–L1396.
- [127] P.A. Fernandes, P.M.P. Salomé, A.F. Da Cunha, J. Alloy. Compd. 509 (28) (2011) 7600-7606
- [128] M. Dimitrievska, A. Fairbrother, X. Fontané, T. Jawhari, V. Izquierdo-Roca,
- E. Saucedo, A. Pérez-Rodríguez, Appl. Phys. Lett. 104 (2) (2014) 021901. [129] S.C. Riha, B.A. Parkinson, A.L. Prieto, J. Am. Chem. Soc. 131 (34) (2009) 12054-12055.
- [130] S. Fiechter, M. Martinez, G. Schmidt, W. Henrion, Y. Tomm, J. Phys. Chem. Solids 64 (2003) 1859-1862.
- [131] G.H. Moh. Chem. Erde 34 (1) (1975) 1-61.
- [132] S.B. Qadri, E.F. Skelton, D. Hsu, A.D. Dinsmore, J. Yang, H.F. Gray, B.R. Ratna, Phys. Rev. B - Condens. Matter Mater. Phys. 60 (13) (1999) 9191-9193.
- [133] S.W. Shin, J.H. Han, C.Y. Park, A.V. Moholkar, J.Y. Lee, J.H. Kim, J. Alloy. Compd. 516 (2012) 96-101.
- [134] A.S.R. Chesman, J. van Embden, N.W. Duffy, N.A.S. Webster, J.J. Jasieniak, Cryst. Growth Des. 13 (4) (2013) 1712-1720.
- [135] S.C. Riha, D.C. Johnson, A.L. Prieto, J. Am. Chem. Soc. 133 (5) (2011) 1383-1390
- [136] L. Korala, J.T. McGoffin, A.L. Prieto, ACS Appl. Mater. Interfaces 8 (7) (2016) 4911_4917
- [137] S.J. Fredrick, A.L. Prieto, J. Am. Chem. Soc. 135 (49) (2013) 18256-18259.
- I. Kriegel, C. Jiang, J. Rodríguez-Fernández, R.D. Schaller, D.V. Talapin, E. da Como, J. Feldmann, J. Am. Chem. Soc. 134 (3) (2012) 1583-1590.
- [139] F.J. Espinosa-Faller, D.R. Conradson, S.C. Riha, M.B. Martucci, S.J. Fredrick, S. Vogel, A.L. Prieto, S.D. Conradson, J. Phys. Chem. C 118 (45) (2014) 26292-26303.
- [140] L. De Trizio, A. Figuerola, L. Manna, A. Genovese, C. George, R. Brescia, Z. Saghi, R. Simonutti, M. Van Huis, A. Falqui, ACS Nano 6 (1) (2012) 32-41.
- [141] B. Abécassis, C. Bouet, C. Garnero, D. Constantin, N. Lequeux, S. Ithurria, B. Dubertret, B.R. Pauw, D. Pontoni, Nano Lett. 15 (4) (2015) 2620-2626.
- F.F. Tao, M. Salmeron, Science 331 (6014) (2011) 171-174.
- H.L. Andersen, E.D. Bøjesen, S. Birgisson, M. Christensen, B.B. Iversen, J. Appl. [143] Crystallogr. 51 (2) (2018) 526-540.